I.C. Gerritsma | 4261976

NATURAL COASTAL STRUCTURES TO RESTORE ERODING MANGROVE-MUD COASTS

Faculty of Civil Engineering
Hydraulic Engineering
November 2020

TUDelft Deltares

Natural coastal structures to restore eroding mangrove-mud coasts

by

I.C. (Isabella) Gerritsma

in partial fulfillment of the requirements for the degree of

Master of Science
in Civil Engineering

at the Delft University of Technology (TU Delft)

Student number:	4261976	
Thesis committee:	Prof. dr. ir. S.G.J. Aarninkhof,	Delft University of Technology
	Prof. dr. P.M.J. Herman,	Delft University of Technology, Deltares
	A.G.M. Gijón Mancheño MSc,	Delft University of Technology
	Ir. B.P. Smits,	Deltares
	Dr. B.K. van Wesenbeeck,	Delft University of Technology, Deltares

An electronic version of this thesis is available at http://repository.tudelft.nl/.

'Hell and Flood' by Hieronymus Bosch (1514)

"The audience, in common with western society at large, believes that the world, if not the universe, consists of dialogue between men, or between men and an anthropomorphic God: the result of this view is that man, exclusively, is thought divine—given dominion over all life, enjoined among all creatures to subdue the earth. Nature is then an irrelevant backdrop to the human play called Progress, or Profit. If nature is brought to the foreground, it is only to be conquered—man versus nature."

— Ian McHarg, 1969

Abstract

Degrading mangrove forests and coinciding erosive coastlines is an urgent global concern. Mangroves are essential for their interaction with hydrodynamic and sediment processes at mangrove-mud coasts. The sediment trapping capability of mangroves and their ability to strengthen the bed are crucial to the morphodynamics of mangrove-mud coasts and their dynamic equilibrium. Disrupting the feedback loops between coastal processes by direct or indirect anthropogenic influence, can be disastrous on both a local and global scale. Earlier on, solutions were sought in building 'hard' structures, such as concrete sea walls, to lower incoming wave energy and enhance sedimentation to restabilize erosive coastlines and bring back mangroves. As these approaches proved to be counterproductive and even accelerate destabilization of the coastline, nature-based solutions might provide a new path to a durable solution.

A pilot project was initiated in Demak, Indonesia, where several permeable brushwood and bamboo dams were constructed near the receding coastline. The dams function by mimicking mangrove capabilities of wave attenuation and sediment trapping. The open structure of the dams allows sediment to flow through, while they decrease wave heights by dissipation. This creates calmer conditions behind the dams and allows mud to settle. The deposition of fine sediments enhances a rise in nearshore bedlevel and provides nursery ground for mangroves to reestablish, realising a first step towards rehabilitation of the mangrove ecosystem and restabilizing the coastline. Although results of the pilot project in Demak show sedimentation behind the structures, several things remain unknown about their functioning. Other pilot projects were performed in, amongst others, Vietnam, Thailand and Surinam. The large variety of coastal system characteristics encountered in these pilot projects, complicates the process of linking dam performance and environmental factors significantly.

This research aims to connect the dots between different coastal characteristics and dam performance. A conceptual 2DH process-based model, using Delft3D FM, was created to analyse the effect of permeable structures under changing boundary conditions at various shorelines. The two dimensions enable the modelling of flow and sediment transport around coastal structures and longshore currents and processes. The rectangular flow grid includes an offshore tidal boundary condition and two lateral Neumann boundary conditions. A wave model is "online" coupled to the flow model and uses a time-varying wind and wave input. Both models use an alongshore uniform bedlevel with a concave profile shape. Three dams are modelled with each a length of 50 m. A gap of 10 in between each dam allows for flow around the structures as the structures can only be modelled with zero permeability in Delft3D FM. The dams are located on the horizontal area of the profile, close to the land boundary. The model setup was tested for the coastline at Demak and validated with the model of Smits (2019).

The input profile is not an equilibrium profile. A change in wave height, wave direction and sediment supply was applied independently, to study the effect on dam performance if one condition would change or is altered at a coastal site. The dam effect is modelled for two years, to study the short-term effects.
A decrease or increase in wave height resulted in similar rise in bedlevel elevation behind the dams. Without the dams, an increase in wave height increased the tidal flat elevation and steepened the foreshore, inducing a concave profile shape. Placing the dams on the tidal flat induces extra rise in elevation, but won't mitigate the erosion of the foreshore. Smaller wave heights tend to reshape the profile towards a more convex profile. When dams are implemented on, an increase in bedlevel behind the dams occurs. The waves stir up sediment at the tidal flat boundary which are redistributed by the tidal currents forming a more convex profile. The dams could be placed best close to the shoreline to allow for the natural redistribution of the sediment when at the same time induce a rise in bedlevel for mangroves to reestablish.
Altering the nearshore sediment supply affects the dam performance significantly. The dam performance increases for lower sediment supplies. Dams reduce erosion due to decreased sediment input, but it is likely a short-term solution. For higher sediment supplies, the coastline can more effectively restore by itself and the dams reduce in efficacy.
A change in wind and wave direction won't represent a situation at a real coastline, but rather implies a hypothetical change. The model results show an increase in dam performance for increasing wave angles (shore-normal

to shore-parallel). The bed shear stress is decreased more effectively for smaller wave angles, but also reduce the sediment concentration behind the dams.

With the many distinctive boundary conditions at mangrove-mud coasts in mind, the simplified model setup is made easily adaptable to enable future use of the model. Based on the model setup for Demak and the model results in this research, an improvement on the computational grid is suggested before applying the model to other coastal sites.

Preface

This thesis represents the final work for my masters Hydraulic Engineering at the Delft University of Technology. The research project was carried out at Deltares, an independent, renowned research institute in Delft. It was part of the "Building with Nature" pilot project in Indonesia, with nature restoration as its objective. An attractive and interesting subject which I really enjoyed working on.

I would like to thank Deltares for offering this opportunity to conduct my graduation research at their office and to join the Demak project team. Special thanks to the people from the Demak team for offering me valuable insight into this interesting Building with Nature project.

Along the course of my project, Bob Smits has always been at my side offering his extensive and useful knowledge on numerical modelling and guidance in exploring the many directions of my research. His enthusiasm for modelling really sparked my interest even more. I would like to thank my graduation committee enormously for their involvement, their inspiration, broad spectrum of knowledge and of course their super useful feedback during the project. I would like to grant special thanks to Bob for all the weekly talks and his extensive feedback every time. Thanks for all the times you helped me interpret model results and decide on possible next steps. I would like to thank Stefan Aarninkhof, the chair of my committee, for taking time to really understand my project and for the many helpful suggestions. Your ability to identify key points in my research project really helped me stay on track. Thanks to Peter Herman for the inspiring and helpful insights in the field of numerical modelling. Your critical questions and practical recommendations during the meetings were very much appreciated. I would like to thank Bregje van Wesenbeeck for sharing her ecological expertise and for challenging me to remain focused on the main objective of this research. Your extensive knowledge on the subject of mangrove coasts really added to my project. Thanks to Alejandra Gijón Mancheño for all the useful and extensive feedback on my work during the project. I am really grateful for all your shared knowledge on dam modelling and the project in Demak.

Isabel Gerritsma
Delft, November 2020

Contents

List of Figures

List of Tables

1 Introduction

1.1 Context

Rising sea levels and growing pressure on ecosystems by anthropogenic influences are creating a need for revision of 'traditional' mono-functional hydraulic engineering practices. The last decades have seen an increase in research on nature-based solutions. The Netherlands specifically, follow the 'Building with Nature' philosophy. This philosophy, explained by de Vriend et al. (2015), reassesses 'traditional' engineering practice and is not about fighting nature but establishing a collaboration with nature. The essence of nature-based engineering is understanding the natural and societal system in which infrastructural changes need to be made. These include physical processes (e.g. sediment dynamics, hydrodynamics, vegetation dynamics), ecological aspects, biological aspects and the socioeconomic and governance aspects. A complete understanding of all variables empowers solutions benefiting both nature and humans. It enables optimal use of the system but also gives something back. When people learn how to sustain the ecosystems they live and construct in and offer their preservation services in return, symbiosis could be the result. Humans can use ecosystem services, but must sustain the ecosystem in return.

Understanding the need for nature-based solutions and adopting this more profound mindset, could help bringing valuable ecosystems back that are vulnerable at this moment. For this research project the focus is on mangrove forests as globally endangered ecosystems. Mangrove forests are present at coastlines or at saline to fresh water transitions (estuaries, deltas, lagoons) all around the (sub) tropics and are essential ecosystems. For the civilised world they also provide many ecosystem services (Spencer and Möller, 2013). Wave attenuation decreases flood risk (McIvor et al., 2012) and the ability of trapping sediment enables the coast to keep up (to some extent) with sea level rise (McIvor et al., 2013), protecting the coast in the long run. People near the forests live from fishery and extract fuel wood, but the forest itself also facilitates water filtration and carbon storage (Ewel et al., 1998). Understanding that these forests mean so much to the tropical coastal systems, it is devastating to know they are degrading in a considerable number of coastal regions around the world (Luther and Greenberg, 2009; Polidoro et al., 2010).

One example of endangered mangrove forests is the coastline near Demak (Java, Indonesia), which has a rapidly retreating coastline for several years (Winterwerp et al., 2014). Figure 1.1 shows the retreat of the coastline in the past decade. This is likely triggered by the exorbitant subsidence rate of Java (Wilms et al., 2019) but also the limitation of sediment input by dammed rivers and the construction of many fish ponds at the coastline by local fishermen which replaced most of the previous mangrove forests and confined the intertidal range (Winterwerp et al., 2014). To mitigate the erosion, local authorities have build parallel "traditional" hard structures. This increased the erosion rate even more, as the wave attack became larger in front of the structures and eroded the really soft, muddy bed, causing the structure to fail eventually (Winterwerp et al., 2013). At the same time the structures blocked the onshore sediment flux, decreasing the sediment availability at the nearshore. The attempt showed the need for other, more innovative, alternatives. Currently, Deltares, among others from the Ecoshape consortium, is studying the effect of bamboo/wooden permeable dams which attenuate wave action and allow sediments to pass and settle in the calmer region behind the dams (Wilms et al., 2019; Ecoshape, 2015). The sedimentation provides nursery ground for mangroves to propagate in order to rehabilitate the mangrove ecosystem (Lewis, 2005), which in turn helps restore the older coastal bed profile and the coastal processes of a healthy dynamic mangrove-mud coast. Restoring the mangrove ecosystem and the coastal profile can stop the ongoing erosion eventually (Winterwerp et al., 2014, 2013). Using the permeable dams, which are made of natural materials, to alter the coastal processes in order to restore an ecosystem in the natural system, is a perfect example

of a nature-based solution. A current modelling study by Deltares (Smits, 2019) has some promising results and sedimentation does indeed occur behind those dams; a first step in restoring mangrove forests. Though, comparing the sedimentation rates with the current land subsidence rates and sea level rise in that region show higher relative sea level rise rates than sedimentation rates, meaning that the coastline will keep retreating (Wilms et al., 2019; Smits, 2019).

As stated previously, Demak is not the only region with a retreating coastline and degrading mangrove forests, since other mangrove-mud coasts suffer from similar circumstances as well. Implementation of nature-based solutions like the permeable coastal structures could help restore their natural coastal system and prevent drowning of valuable urban or rural areas. Since the permeable dams show positive sedimentation results in Demak at first glance it might be a good idea to implement the dams in other coastal regions, some with less extreme subsidence rates perhaps.

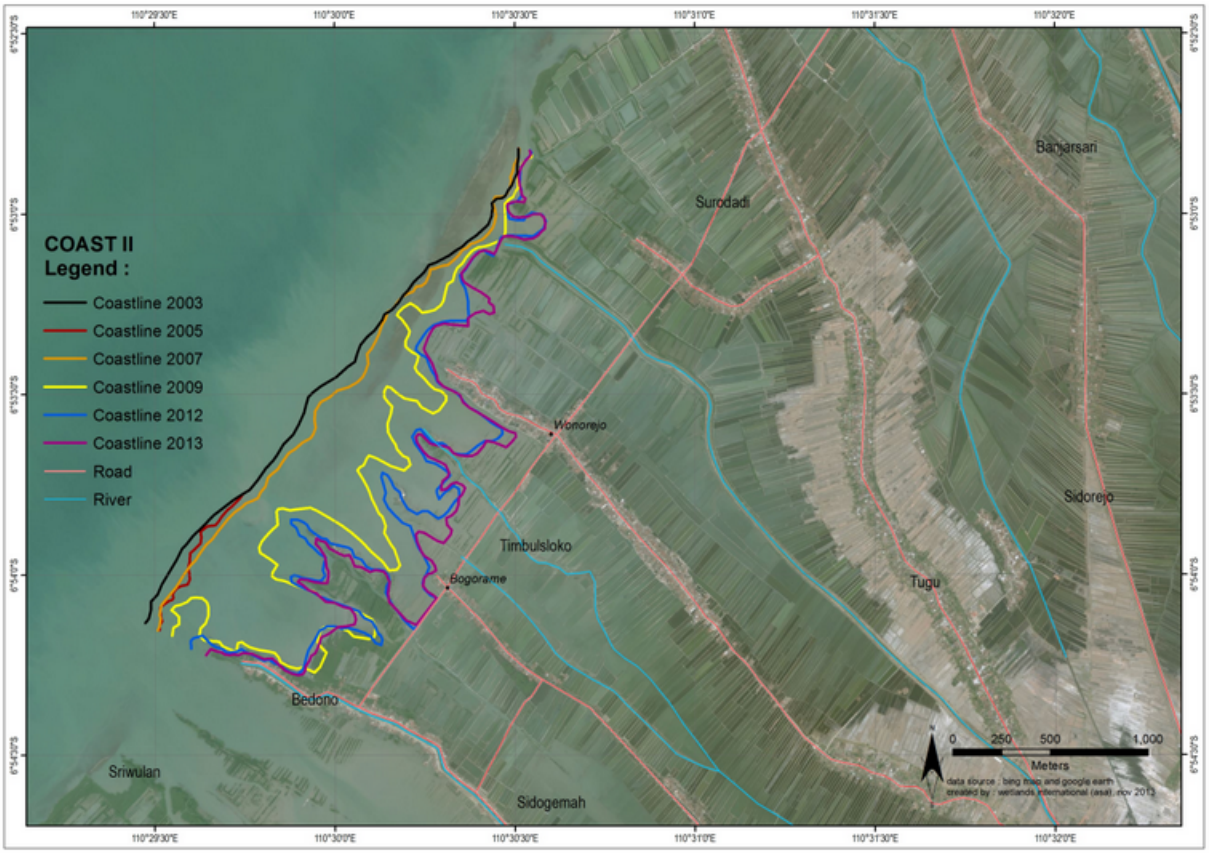

Figure 1.1: Coastline retreat from 2003 to 2013 at the Demak coastline in Indonesia. (Winterwerp et al., 2014).

1.2 Problem statement

Alongside the current pilot project in Demak, pilot projects in other mangrove-mud coast areas have been performed as well, giving information on the implementation of natural permeable coastal structures and their effect on the sedimentation at the coastline. In the Netherlands, Switzerland, Thailand and Vietnam, for instance, the permeable dams were constructed and monitored, providing data to evaluate the performance of permeable dams (Dijkema et al., 2007; Schleiss, 2006; Winterwerp et al., 2005; Albers et al., 2013). However, as other coastal regions have different environmental conditions (e.g. sediment availability, wave conditions, tidal range), a thorough understanding of the relation and differences between coastal system parameters and the impact of those differences on dam functioning is essential. The specific coastal processes related to successful functioning of the dams are not readily understood, hindering a good local assessment of permeable dam implementation in coastal regions globally.

1.3 Research questions and objectives

Following the problem statement, this research focuses on finding a quick assessment model to determine the effect of different boundary conditions on the performance of permeable coastal structures in mangrove-degrading, erosive coastlines. This simplified model is used to evaluate the effects of a change in boundary conditions on the short term performance of permeable dams constructed in Demak.
This objective translates into the main research question:

> *Which erosive mangrove-mud coasts could benefit from permeable coastal structures?*

To attain a satisfying answer to this research question, the project follows a structural, step-wise approach and is subdivided into three smaller project phases with related objectives and sub-research questions.

Phase I - Site evaluation

1. *How do other erosive mangrove-mud coasts differ in local boundary conditions from the pilot project in Demak?*
   (a) Analyse the current situation in Demak to understand how the boundary conditions affect sedimentation behind the permeable dams.
   (b) Collect information on the boundary conditions of different coastal sites suffering from coastline erosion and mangrove degradation and compare these conditions to the conditions in Demak.

Phase II - Conceptual 2D-model setup and testing

2. *How can the coastal characteristics of Demak and other evaluated sites be schematized in a general process-based model setup?*
   (a) Analyze different ways to schematize the various coastal characteristics in a general model setup in order to obtain results in the same order of magnitude as for other, existing (modelling) studies.

Phase III - Conceptual 2D-model application

3. *How does a change in boundary conditions influence sedimentation rates behind the dams?*
   (a) Describe the short term influence of a change in boundary conditions on the sedimentation behind the dams by using the reference model of Demak. The morphological timescale is 2 years.

1.4 Research approach

The first phase considers a literature review on the physical processes at a mangrove-mud coast, together with a more thorough study on the mangrove environment and its rehabilitation. Phase I also evaluates the differences between coastal characteristics worldwide, especially in comparison to the coastal characteristics of Demak's coastline. Phase II uses the boundary conditions of the different coastal sites evaluated in Phase I to setup an idealized process-based 2D-model. The coastal characteristics of Demak enable testing and validation of the model. This provides insight in simplifications that can be made, without losing accuracy. Once a simplified model setup is determined, tested and validated using data from Demak, the boundary conditions of the reference model setup are varied independently to determine their influence on sedimentation behind the dams. The varying boundary conditions are based on data from other evaluated coastlines, to allow for an initial prognosis on the dam functioning at other locations.

1.5 Thesis outline

The thesis structure follows the same structure as the three research phases, with a discussion, conclusions and recommendations lastly. Phase I comprises a project introduction, site analysis and literature review, in which Chapter 1 gives an introduction on the topic and the actual problem. This chapter also elaborates on the objectives and related research questions. Chapter 2 gives an overview of the underlying theoretical framework for this research. Phase II explains the analysis on various erosive coastlines and the grouping of accompanying coastal

system data. Chapter 3 envelopes this second phase. An elaborated site analysis of the coastline of Demak is part of this chapter. Subsequently, Phase III describes the model setup, testing and application. The input selection and model setup are described in Chapter 4, as well as the validation results for Demak to test the model applicability. Chapter 5 includes the application of the model to investigate the influences of different boundary conditions on the sedimentation behind the dams. The results are discussed in Chapter 6 and the conclusions and recommendations in Chapter 7.

2

Theoretical background

This chapter presents the important theoretical concepts related to the erosion of mangrove-mud coasts. The problems of erosive coastlines are complex and show varying underlying causes for the disturbance of the mangrove-mud coast dynamics. In Section 2.1 the mangrove environment and its classifications are explained briefly, together with the ecosystem services that are important to restore on erosive mangrove-mud coasts. Section 2.2 explains the physical processes composing the dynamics of mangrove-mud coasts. The last section, Section 2.3 describes the requirements for mangrove rehabilitation.

2.1 The mangrove environment

Mangrove forests are found in tropical and subtropical intertidal areas around the world and cover around 60 - 75 % of the (sub)tropical coastlines (R.J. Reimold, 1974; Mitra, 2013). Figure 2.1 shows the mangrove distribution on earth, with mangrove forests indicated with green. Mangroves exist between the 25^{th} parallel north and the 25^{th} parallel south.

Figure 2.1: Global mangrove distribution (Giri et al., 2011)

Since mangrove forests are thriving on shorelines and riverbanks where tidal inundation occurs around 30% of the time, they have to manage the salinity of the water. Mangroves can withstand fairly high levels of salinity, thanks to three processes: salt excretion, salt exclusion and salt accumulation (Mitra, 2013). The process the mangroves use primarily, differs per species. Besides salinity, also extreme conditions of tides, winds and temperature can

be withstood by mangroves. A deconstructed mangrove forest due to a tsunami or hurricane often completely restores itself within a few years/decades.
Figure 2.2 shows a classification system that groups mangroves on their structure and function. They are classified by their global distribution, geomorhpological type and their ecological type (Spencer and Möller, 2013). The classification on geomorphological setting results in four different type of coastal sites where mangroves can flourish: deltas, oceanic islands, lagoons and estuaries.
This illustrates itself in the different systems where mangroves appear: deltas, oceanic islands, lagoons and estuaries (Spencer and Möller, 2013). Between these three functional groups significant differences are encountered in hydrology, nutrient cycling and ecological productivity, which causes each kind of mangrove forest to provide different goods and services (Ewel et al., 1998).

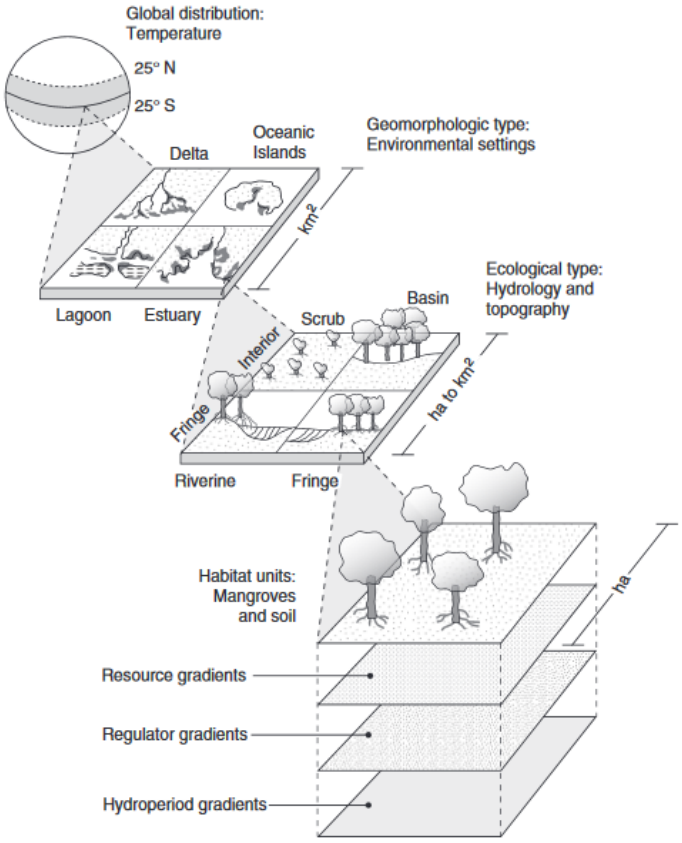

Figure 2.2: Classifying mangroves by their structure and function based on different factors: global, geomorphological and ecological. From Spencer and Möller (2013), reproduced from Twilley and Rivera-Monroy (2009).

2.1.1 Ecosystem services

Mangrove forests can offer a lot of ecosystem services such as flood protection (by wave attenuation), stabilizing the nearshore coastal profile by trapping sediments (even up to some extent of sea level rise), carbon sequestration, minimization of carbon dioxide at the regional level, enrichment of coastal waters (nutrient supply and regeneration), maintenance of biodiversity (e.g. the provision of nursery and breeding grounds), coastal fisheries and the supply of commercial forest products (timber, firewood) (Ruitenbeek, 1992; Mitra, 2013). For this research project, flood protection and stabilization of the nearshore environment by sediment trapping are most relevant and are elaborated on.

Flood protection Waves approaching the coast can, when large in height, cause flooding and damage to coastal communities living near the shoreline. Often mangroves grow on muddy coasts with mild wave climates, but during storm conditions or large tidal effects they attenuate wave energy, decreasing the risk of flooding (McIvor et al., 2012). For example Kathiresan and Rajendran (2005), Vermaat and Thampanya (2006), argue that mangrove forests decreased loss of lives and coastal infrastructure in case of a tsunami by attenuating the wave height. Or, according to Kathiresan (2015), the cyclone 'Nargis' in 2008, causing more than 30,000 deaths, where the mortality rates were worse in areas with damaged or diminished mangrove forests.

It is already shown by previous laboratory and field measurements that mangroves dissipate wave energy, governed by both canopy traits and incident wave conditions. McIvor et al. (2012) state that most notably the physical structure of the trees affect the wave energy dissipation. A higher density leads to a larger reduction in wave height. In shallow water the aerial roots of mangroves increase wave energy dissipation, whereas in deep water, the lower branches perform this function. Besides this, Hu et al. (2014) investigated the influence of currents on wave energy dissipation by vegetation. Especially a flooding tide during storm conditions could create a critical situation.

Bedlevel elevation Tidal currents transport cohesive sediment flocs into the mangrove forest where they stay in suspension, due to turbulence induced by flow around mangrove roots. During high water slack (HWS) the sediment settles, as lower ebb currents are not strong enough to re-entrain it (Furukawa and Wolanski, 1996). In this way, mangroves enhance onshore sediment flux and improve settling conditions in the nearshore mangrove area. Additionally, attenuation of waves decreases erosion of sediments. A system which imports and accumulates external sediments is called allochthonous system. Systems that are characterized as autochtonous, experience bedlevel elevation through local plant productivity (e.g. development of roots in the soil) (Spencer and Möller, 2013). Roots increase the shear strength of soil and prevents washing away of the soil layer (Scoffin, 1970).
The study by McIvor et al. (2013) uses historical evidence to suggest that, over thousands of years, some mangrove forests were able to keep up with sea level rise. Sediment supply and sub-surface root growth rate were noted as important factors. The ability of mangroves to keep up with sea level rise is an important subject for ongoing research, as it might offer solutions for current anthropogenic induced sea level rise.

2.2 Mangrove-mud coast dynamics

This section describes the physical processes at open mangrove-mud coasts. First, the nearshore hydrodynamic processes that are important for sediment transport at open coasts are described, whereupon cohesive sediment properties and related small-scale sediment processes are explained. The effect of vegetation on hydrodynamics and sediment dynamics is discussed in the final subsection, which links all processes on a larger scale; the morphodynamics of a mangrove-mud coast.

2.2.1 Hydrodynamics

Important nearshore hydrodynamics for fine sediment transport at muddy coasts are addressed here, by explaining tides and waves. Tides affect flow, create a bed boundary layer and instigate turbulence in the water column. Waves also affect the boundary layer, as well as flow in the water column through radiation stresses. Waves and wave-induced currents play a major role in transporting sediment in the surf zone; Waves stir up sediment, while (tidal/wave-induced) currents are responsible for transporting sediment. The book by Bosboom and Stive (2015) provides most of the information for this subsection; it is stated when other material is used. A short description on the large-scale relationship between tidal influence and wave influence on coastal morphology is given first, followed by Subsection 2.2.1.2 which explains important tidal processes for fine sediment transport at open coasts. Lastly, Subsection 2.2.1.3 explains wave propagation at open coasts.

2.2.1.1 Relative dominance of tides and waves

Coastal areas experience fluctuation in relative dominance of tide and waves, which is defined by Davis and Hayes (1984) as the ratio between the tidal range and wave energy (Figure 2.3). The morphology of coasts is largely dependent on such relative dominance. Wave-dominance exhibits offshore fining of sediments as the influence of waves decreases offshore. A more stormy wave climate results in bars and wide sandy beaches, whereas swell waves tend to narrow the sandy littoral zone and create finer sediment zones in deeper water. Tide-dominant coasts are characterized by large tidal flats and tidal ridges (wide, low in height parallel or sub-parallel bars). Tidal currents sort sediment; Fine sediments are deposited onshore while coarser sediment is taken offshore. Intermediate ranges exhibit wave-shaped beaches alongside characteristics caused by tidal influence.

2.2.1.2 Tides

Waterlevel and flow velocity both vary throughout the tidal cycle and encompass the tidal motion of water. Variation in the rising and falling waterlevel is called vertical tide, where high water levels are called *high tide* and low water levels *low tide*. Horizontal tide -the horizontal movement of the tide-,is defined by the variation of flow velocity. Ebb currents (flow velocity directed against the direction of propagation) and flood currents (flow velocity directed along the direction of propagation) also have maximum and minimum values. Maximum ebb or flood currents do not necessarily coincide with low- and high tide respectively. Minimum values for flow velocity occur when tidal flow reverses from ebb to flood or vice versa. Reversal of the tidal flow is called slack water. Slack water

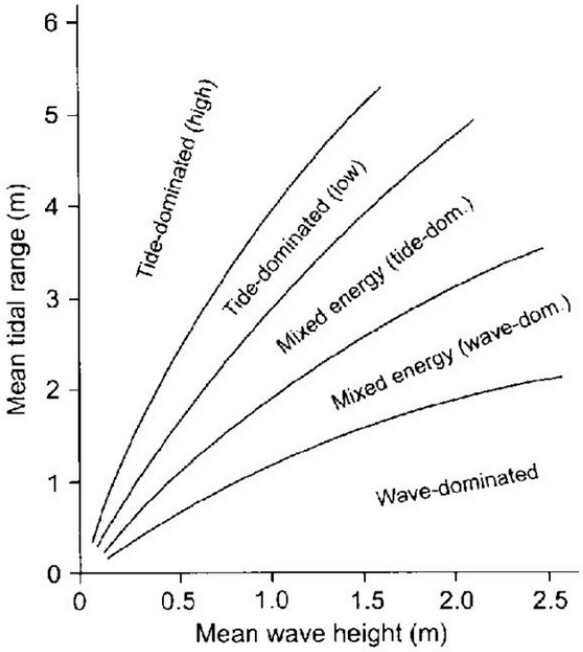

Figure 2.3: The dominance of tides and waves based on the ratio between the tidal range and the wave energy. From Masselink and Hughes (2003), adjusted from Davis and Hayes (1984).

around low water is called low water slack (LWS) and slack water at the time the waterlevel is high is called high water slack (HWS).

Tidal propagation As the tidal wave propagates towards the coast, the phase difference between the vertical tide (waterlevel) and the horizontal tide (flow velocity) can determine if the wave is progressive, standing or something in between (Figure 2.4). A progressive wave is defined by a zero phase difference between the vertical and horizontal tide; high/low tides coincide with maximum flood/ebb velocities. When slack water occurs at the same time as high/low tide, a standing tidal wave occurs. The upper plot in Figure 2.4 shows maximum ebb and flood velocities leading the waterlevel by a quarter period, i.e. a phase difference of -90°. Along coasts, velocity normally leads the waterlevel with a phase difference between 0 and -90°. The phase difference between velocity and elevation is caused by (bottom) friction and (partial) reflections of the tide. Progressive tidal waves occur when the water is deep and bottom friction does not affect propagation significantly.

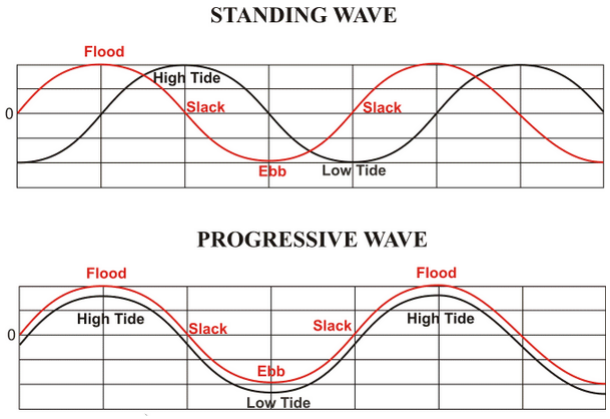

Figure 2.4: The phase difference between the horizontal and vertical tide determines whether the tidal wave is called progressive or standing. Intermediate tidal wave states exist, with velocity leading the waterlevel. From NOAA (2020).

Tidal asymmetry Besides a possible phase difference, both horizontal and vertical tide may experience asymmetry. This asymmetry can be about both the vertical (i.e. asymmetry) and the horizontal axis (skewness)(Bosboom

and Stive (2015)).

Tidal asymmetry of the vertical tide
Skewness of the waterlevel means a difference in amplitude of the waterlevel in upward and downward direction; the absolute difference between MSL and high/low tide is not the same. Friction causes more amplitude damping during low water than during high water; resulting in a skewed signal. A low water depth means a shorter distance to the bed for settling fine particles, enhancing sedimentation.
When there is a difference between the falling and rising period, an asymmetrical shape of the tidal curve can be noticed. A rising period that is shorter than the falling period can be explained with the propagation velocity (without friction): $c = \sqrt{gh} = \sqrt{g(h_0 + \eta)}$. This velocity is larger during high tide than low tide, resulting in a shorter rising period than falling period. Friction can enhance this phenomenon as it affects low tide more than it does high tide. Moreover, using the influence of the waterlevel on the propagation velocity shows that a skewed signal also affects vertical asymmetry.

Tidal asymmetry of the horizontal tide
The peak current velocity for ebb and flood can differ throughout the tidal cycle, resulting in a difference in ebb/flood duration. This is referred to as peak flow asymmetry. Peak flow asymmetry (skewness of the velocity signal) influences fine sediment transport in case of alluvial systems of fine sediment (Van Maren and Winterwerp, 2013). When fine sediment is abundantly present, the impact of peak flow asymmetry on the asymmetry of vertical mixing (internal asymmetry) within the water column can be significant, impacting transport of fine sediment.
Asymmetry in the slack water period shows differences in duration for high water slack (HWS) and low water slack (LWS). This slack water asymmetry is especially important for fine sediments (as opposed to coarse sediments, which have an instantaneous response to flow velocity), as most of the relevant fine sediment processes scale non-linearly to flow velocity (J.C. Winterwerp, 2015b). For instance, when the HWS period is longer than the LWS period, particles have more time to settle and remain longer on the bed than during LWS, which creates a net landward sediment transport.

2.2.1.3 Waves
Surface waves play an important role in both the modification of the bed boundary layer and the flow field by generation of radiation stresses. These non-linear effects are both of great importance to fine sediment transport processes (Winterwerp and van Kesteren, 2004). This section first describes linear wave transformation towards the coast, followed by an explanation of the wave boundary layer. The last part consists of an explanation of the wave-induced set-up and currents.

Linear and non-linear wave transformation The seabed affects waves by *shoaling, refraction, bottom friction and wave-breaking*. Coastal structures cause wave *diffraction*. Shoaling is the increase of wave height due to a concentration of wave energy when waves propagate into shallower water. Refraction occurs when the trajectory of a wave is bent towards shore-normal incidence, as oblique waves in shallow water decrease in velocity along the wave crest, due to the difference in water depth. The breaking of a wave occurs when particle velocity exceeds the velocity of the wave crest and is expressed in exceedance of the wave steepness limit. Wave steepness is equal to wave height divided by wave length: $S = \frac{H}{L}$ and Miche (1944) expressed the steepness limits by a deep water limit and a shallow water limit. Exceedance of the shallow water steepness limit results in depth-induced breaking, the exceedance of the deep water steepness limit results in white-capping.
Non-linear wave transformation towards the coastline is related to asymmetry of the wave signal along the horizontal axis (skewness) and along the vertical axis (asymmetry). A skewed surface elevation shows a difference in height of the crests and troughs. Along the vertical axis, a wave signal can show asymmetry as a result of velocity difference between the wave crest and the wave trough in shallow water. Since the wave crest travels faster than the wave trough, a steepening of the wave occurs and results in a pitched-forward signal. Traveling towards the coast, a shoaling wave will increase in skewness. As the wave comes closer to the surf zone, skewness will decrease and asymmetry will increase. The resulting pitched-forward wave will break eventually. Together with surface elevation, orbital velocities become both skewed and asymmetric, which affects sediment transport.

Wave boundary layer Waves drive a fluid motion underneath the wave surface where particles follow an orbital path -and thus are subject to orbital velocities. These orbital velocities decrease towards the bottom. Orbital paths change when waves transition from deep water waves to shallow water waves. In deep water, when waves do not feel the bed, orbital paths are circular and velocities decrease linearly towards the bottom. In shallow water, orbital paths are elliptical with decreasing vertical orbital velocities towards the bed. Horizontal particle displacement, however, remains almost constant.
Since the water-bed boundary forces flow velocity to zero, a boundary layer forms in which the flow velocity diminishes to the no-slip condition at the seabed (Winterwerp and van Kesteren, 2004). The decrease in velocity

results in shear stresses in the boundary layer and can extend over the entire water column. Besides the development of a boundary layer by the current velocity, a wave boundary layer develops as it propagates through shallow water. The orbital velocity limits the thickness of the wave boundary layer as the velocity reverses, restricting the layer to expand vertically. Due to this restricted boundary layer, large shear stresses can occur, which cause sediment to stir up. These stresses are often larger than current-induced shear stresses. Bed friction in the boundary layer also causes wave energy dissipation (or energy from the flow above in general).
As calculation of the bed shear stresses involves complex turbulence modelling, bed shear stress is often determined by using (empirical) friction laws. In general, a friction factor related to the current boundary layer, couples bed shear stress to current velocity (depth-averaged), while a friction factor for waves couples bed shear stress to free stream velocity (velocity at the top of the boundary layer). Determination of the friction factor for rough beds and turbulent flows is complex and is frequently based on the bed material and bed forms.

Wave-induced set-up and currents Waves can generate a momentum flux (a depth-integrated and wave-averaged flow of momentum), defined by Longuet-Higgins and Stewart (1964) as radiation stress. Gradients in radiation stresses generate wave forces acting on the water in a specific direction. These wave forces can cause set-down in the shoaling zone, set-up in the surf zone and development of a longshore current (when waves approach the shore under an angle). Set-down in the shoaling zone is the lowering of the waterlevel due to an offshore directed wave force. Set-up in the surf zone is the heightening of the waterlevel due to an onshore directed wave force. Both instances explain the compensation of wave force by a hydraulic pressure gradient. In the case of a longshore current, cross-shore variation in the shear component of radiation stress is compensated by the bed shear stress. Wave breaking in the breaker zone drives the longshore current, often an important factor for sediment transport.

2.2.2 Fine sediment dynamics

This section concerns sediment dynamics on a muddy coast, which is different from that of a sandy shoreline. Mud is the encompassing name for clay, silt, organic matter and fine sand and often has cohesive characteristics, depending on the clay fraction of the sediment. The cohesiveness of fine sediment determines distinctive behaviour of the soil, in comparison to non-cohesive material. Cohesive material is studied in much more detail the last decades thanks to its ability to adhere contaminants and to contain a lot of organic material (Dankers and Winterwerp, 2007). This subsection is divided in a part about the characteristics and properties of fine (cohesive) sediment and a part explaining the physical processes of cohesive sediment (settling, flocculation, erosion, deposition, consolidation). Although it is known that non-physical effects (e.g. biological effects, chemistry) are of major importance to sediment dynamics (Montserrat et al., 2008; Winterwerp and van Kesteren, 2004), they are outside the scope of this research. Information in this subsection is derived from Winterwerp and van Kesteren (2004), unless stated otherwise.

2.2.2.1 Sediment characteristics and properties

Cohesive sediment is comprised of fine sediments like clay and silt (and sometimes small quantities of fine sand particles), which have, according to the Dutch grading system, a particle grain size smaller than 2 μm and between 2 - 63 μm , respectively. Although mud can consist of clay particles, normally a clay fraction of 10% or more is considered to be cohesive as the clay particles are attributing to the cohesiveness of the soil (Shrestha and Blumberg, 2005). Clay particles are not, like sand, Euclidean particles, but are small and can also have a plate-like shape. Negative charge on clay particles can be neutralised through cations, such as sodium ions, in seawater. Polymeric effects and/or Van der Waals forces bind the clay particles together, resulting in cohesive behaviour.
The open structure of cohesive sediment consists of approximately 80 - 95% water filling the pores. This large water content makes the soil bearing capacity less than that of more coarse sediment and decreases permeability of the soil significantly, which, in turn, increases risk for liquefaction. The Atterberg, or plasticity limits, characterize behaviour of sediment as a liquid or as a solid by describing water content of a soil sample. They make a distinction between inorganic and organic-rich soils, various levels of plasticity and cohesive or non-cohesive behaviour.

2.2.2.2 Physical processes

The physical processes of fine sediments are different from coarse sediments due to their cohesive behaviour. Figure 2.5 shows the processes related to fine sediment that is transported in the water column. The following paragraphs explain the processes displayed in Figure 2.5.

Flocculation Three processes in the water column govern flocculation: 1) collision due to Brownian motions 2) particles that settle faster collide vertically with slower particles and 3) collision due to turbulent motion. If particles collide through one of these processes, the attractive forces cause particles to form flocs, which can

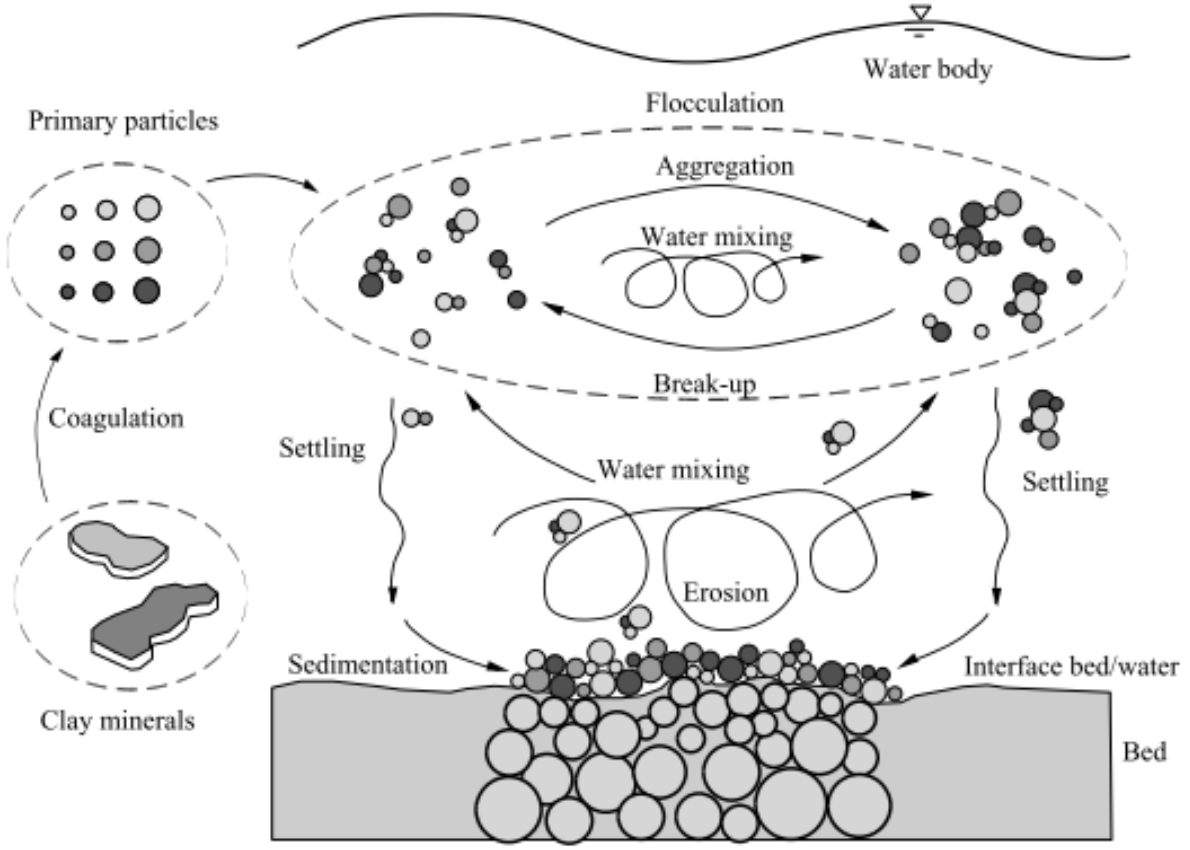

Figure 2.5: Small-scale cohesive sediment processes. From Maggi (2005).

aggregate with other flocs to form large flocs. Aggregation of flocs is limited by turbulent energy as turbulent forces can cause flocs to break up again. This ongoing process of aggregating and breaking up, called flocculation, is one of the most important characteristics for fine, cohesive sediment. The majority of distinctive sediment dynamics at coasts is determined by this process. Settling, deposition and consolidation processes are affected by flocculation.

Settling The suspended sediment concentration affects the settling velocity of the sediment, together with the sizes of the flocs. Mehta (1986) shows that when the suspended sediment concentration is low (0.1 - 0.3 g/L), the settling velocity is independent from the concentration level. A high suspended sediment concentration, in the range of 1 - 10 g/L, increases settling velocity as larger and denser flocs are formed. This increase of settling velocity has an upper concentration limit due to hindered settling. Dankers and Winterwerp (2007) describe this phenomenon occurring in high mud concentrations. Large flocs have a larger settling velocity, however, higher up in the water column, slower settling small flocs can reduce settling speeds significantly. The settling velocity is thus a dynamic parameter.

Deposition Settling particles deposited on the bed are subject to near-bed turbulence. If near-bed turbulence is critical, the flocs are broken up and re-entrained into the water column. Near-bed turbulence is expressed as a function of bed shear stress and a critical shear stress. A bed shear stress lower than the critical shear stress allows flocs to form a soft soil on the bed.

Consolidation When deposited soil is not re-suspended into the water column, flocs are partly destructed and move closer together. Consolidation occurs as water is squeezed out of the pores, decreasing the pore water content and increasing strength of the soil. Consolidation of soil is important for the sensitivity to erosion, which is described in the next subsection.

Erosion A bed can be characterised as starved or alluvial. An alluvial bed has abundant sediment to bring into suspension, whereas a starved bed has limited sediment availability. In case of an alluvial bed, a sediment trans-

port formula for coarse sediment can be used, e.g. van Rijn or Engelund-Hansen, which relates the flow velocity to sediment transport. In a starved bed (non equilibrium) condition, the water-bed exchange process has to be described explicitly by a pick-up function, following the entrainment approach. Entrainment is re-suspension of sediment particles through turbulent mixing over the vertical of the water column. It occurs if a critical value of the bed shear stress is exceeded, i.e. the threshold of erosion. This threshold is dependent on the strength of the bed.

As erosion of a fine sediment bed has different stages -or modes-, entrainment can be characterized as induced by the lowest bed shear stress. Increasing bed shear stress will lead to floc erosion, surface erosion and mass erosion respectively. Floc erosion is the suspension of flocs from the bed. Increasing bed shear stress will increase erosion rate and floc erosion will become surface erosion, where each eroding particle is replaced by water. This erosion process is gradual as layers of consolidated flocs are removed. For this type of erosion an erosion rate can be determined, as it is related to the rate in which water can enter the soil. Moreover, the critical bed shear stress for erosion is equal to the drained strength of the material at the sediment-water surface. Lastly, mass erosion occurs when bed shear stresses are high, due to a strongly varying or accelerating flow, e.g. in strong tidal currents or under storm conditions. In this case clumps of material are removed "*when the bed shear stress exceeds the critical shear strength of the bed at some depth below the sediment-water interface*", according to Shrestha and Blumberg (2005).

2.2.3 Morphodynamics of a mangrove-mud coast

The information in this section is derived from J.C. Winterwerp (2015a); Winterwerp and van Kesteren (2004), unless stated otherwise. Muddy coasts exhibit fine cohesive sediments which are transported along the coast under mild hydrodynamic conditions. The foreshore slopes are mild, with slopes of 1/1000 to 1/1500. Subsequently, longshore tidal- or wave-induced currents are small. Tidal current is directed perpendicular to the coast and waves refract towards the coast, reaching the shoreline perpendicularly. Wave dissipation mainly occurs through viscous damping by the soft mud and hardly any breaking occurs. Sediment transport is, due to the cross-shore current directions, primarily perpendicular to the coast. Locally generated waves and wind-induced currents disperse the fine sediments nearshore.

Mangrove-mud coasts are generally dynamic areas. Gross sediment transport at coasts with an abundance of fine sediments can be large, especially in relation to the net sediment transport. Small changes in gross sediment transport can thus result in a relatively large change in the net sediment transport and sometimes reverse the direction of the net transport. The cross-shore profile of a mud coast is dynamic, since the tidal currents carry a net sediment transport towards the coast by tidal filling, while the waves erode the bed by stirring up the sediment. However, when large waves erode the foreshore, tidal currents bring sediment back onshore; so besides erosion of the bed, larger waves also contribute to a net onshore sediment flux. Small waves, however, only take sediment. This difference between the tidal influence and the influence of waves can be recognized in dynamic equilibrium profiles for mud coasts. Wave-dominated mud coasts show a concave coastal profile, while tide-dominated mud coasts have a convex coastal profile. Sediment supply is also an important factor in the development of the equilibrium profile of a mud coast (Friedrichs, 2012), as the asymmetry of the waves and tide have different influences on an alluvial bed versus a starved bed. So much so, that the direction of net sediment transport can be opposite.

The importance of tidal asymmetry on the net fine sediment flux was explained in Subsection 2.2.1.2. Asymmetry in slack water gives a net sediment transport in ebb/flood direction when LWS/HWS is longer than HWS/LWS, on a starved bed. In case of an alluvial bed, asymmetry in the peak flow velocity results in an asymmetry in vertical mixing within the water column and influences the transport fine sediment. Higher peak flood velocities than peak ebb velocities enhance net landward sediment transport. Asymmetry in waterlevel can also result in asymmetry in time needed for particles to settle. Tidal flats are influenced by sediment supply, tide- and wave forcing. However, the morphology of tidal flats also affect wave- and tide-induced velocities over the flat (Friedrichs, 2012). An example of this feedback between the morphology and forcing on a tidal flat is the effect of the flat on net sediment transport. A large prism to be stored on the tidal flat can result in a short HWS duration but can also enhance strong settling due to the small water depth. The relative dominance of the two determines net direction of fines (Bosboom and Stive, 2015).

Mud coasts are often defined by extensive mangrove forests fringing the coastline. Subsection 2.1.1 explains the ability of these forests to attenuate incoming waves and bedlevel development due to the trapping ability of mangroves. Both processes show the effect of vegetation on hydrodynamics and morphodynamics. Healthy mangrove-mud coasts show convex profiles, but when the equilibrium at the coast gets disturbed, a concave profile can emerge. An example is the construction of fish ponds at mangrove-mud coasts. Fish ponds require partial removal of mangroves and at the same time decreases landward sediment flux. The decrease in net transport of fine sediment towards the coast triggers erosion of the coastline in front of the fish ponds. Due to the decrease in net onshore sediment flux, the waves are reflected by the fish pond structures and create additional erosion in front of the fish ponds. As the erosion continues, a concave profile develops and the reflection of wave energy

increases even more; creating a positive feedback loop. Figure 2.6 shows the convex and concave profiles for a mangrove-mud coast. The concave profile can occur due to the construction of fish ponds, but other causes are possible.

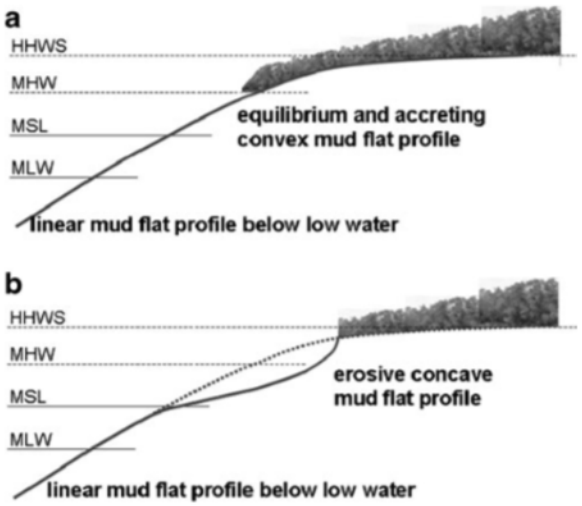

Figure 2.6: Convex and concave profiles for a mangrove-mud coast. A healthy mangrove-mud coast exhibits a convex profile, while concave profiles are the result of erosive mangrove-mud coasts. From Winterwerp et al. (2013).

Chapter 1 explained the need for different solutions than traditional "hard" structures. Constructing a breakwater to decrease the wave energy, will increase the reflection of the waves in front of the structure. This, in turn, increases the wave energy in that location, triggering erosion of the soft muddy bed. Together with instability of the fine sediment bed (liquefaction), the structure will fail in the long run. Thus, this structure decreases the onshore sediment flux as well.

2.3 Mangrove rehabilitation

Mangrove forests are one of the most important ecosystems in the world and can offer humans numerous benefits; ecosystem services. Though, instead of solely using these ecosystem services, humans can also offer human services to maintain a healthy ecosystem. Instead of the human-centered perspective, a symbiosis of humans and (mangrove) ecosystems can be established. This section explains the requirements for mangrove rehabilitation as a way to restore erosive coastlines and a healthy ecosystem. The previous section (Section 2.2) mentioned the failure related to the use of "hard" structures. Another measure that sees low success rates, is planting of mangroves. This is done at wrong bedlevel elevations, or in mud that is too soft to root newly planted mangroves, washing them away (Lewis, 2005).

The requirements for mangrove rehabilitation are classified as ecological requirements, hydrological (and socio-economic) requirements and morphological requirements. This research concerns the morphological requirements. However, the other requirements are of equal importance for mangrove replanting or restoring projects.

The strategy proposed by (Winterwerp et al., 2013), based on all types of requirements and also incorporating morphological requirements, consists of 5 separate steps. The first step is to restore the fine sediment balance which maintained a net onshore sediment flux. This is done by bringing back intertidal area, offering storage space (increase of the tidal prism). The removal of fish ponds could create a buffer zone for the tide to flow freely again. Step 2 involves the trapping of sediment on the mudflat in a way that does not involve any "hard" engineering. Natural permeable structures could be used to enhance sedimentation in the nearshore. Also, excavation of ditches improves drainage and stimulates plant productivity (Bakker et al., 2002). As a third step, reduction of wave height is advised. Step 4 includes the restoration of hydrological conditions, e.g. tidal inundation and fresh water flows (Lewis, 2005). When deemed necessary, the fifth step is the planting of mangroves within the right "Window of Opportunity" (Balke et al., 2011). However, propagules will also spread themselves when the conditions are restored.

3

Mangrove-mud coasts

In order to create a generalized model setup where boundary conditions can vary in relation to several coastal sites, the coastline near Demak is used as a case study for initial data input. This chapter provides insight in other coastal site characteristics than those that are present in Demak. Section 3.1 investigates the different coastal sites and their boundary conditions, Section 3.2 offers an elaborate description of the coastal system of Demak. As a summary of this chapter, Section 3.3 gives an overview of the coastal characteristics of Demak and two other selected coastal sites.

3.1 Coastal sites

Degrading mangrove forests Hamilton and Casey (2016) created a global database of a continuous mangrove forest cover. This cover was evaluated from 2000 to 2014 and the results show the increase or decrease in mangrove cover per country. Indonesia has the largest mangrove cover in the world; Its coastlines were fringed by 23143 km^2 of mangrove forest in 2014. Compared to 2000, when 24073 km^2 of mangroves covered the coastline, Indonesia suffered a mangrove loss of 3.86%. Although this is a big loss, other countries experienced even greater losses. From the research paper by Hamilton and Casey (2016) the first 30 countries are selected that together make up for approximately 85-90% of the worlds mangrove cover. From these countries the ones with a big loss (>0.60%) in mangrove cover are Indonesia, Malaysia, Myanmar, Mexico, Brazil, USA, Cuba, Philippines, India, Thailand, Vietnam and Suriname. Appendix .. states the mangrove cover loss, estimated by Hamilton and Casey (2016), for 2000 - 2014.

Erosive coastlines In a recent paper by Luijendijk et al. (2018), sandy beaches worldwide are evaluated and their erosive or accretion behaviour is determined. The Shoreline Monitor, developed by Deltares and TU Delft (2018), collects erosion and accretion rates of sandy beaches worldwide, but data for muddy beaches also appears. As for Demak, its muddy coastline shows an unsurprising high erosion rate, as shown in Figure 3.1. The countries suffering from mangrove degradation, selected earlier from Hamilton and Casey (2016), can be checked with Shoreline Monitor, Deltares and TU Delft (2018), at what locations their shoreline is most erosive. For this project, the shoreline position for all coastlines around the world between 1984 and 2016, have been used to create a map of erosive and accreting coastlines. Red lines indicate long-term erosion and green lines show coastline accretion. The erosive spots are potentially suitable for bamboo dams to mitigate mud erosion.

Data availability Often, in countries where mangroves fringe the coastline, little data is available. No measurements have been carried out or there is no funding for preservation of mangrove forests. Nowadays, the body of data is growing, as awareness of the value of mangroves spreads. In some coastal sites pilot projects have been set up to test the effects of bamboo fences are. Vietnam, Thailand and Suriname are examples of countries in which pilot projects have started. Especially at the southern coastline of Vietnam, close to the Mekong river, quite some measurements have been carried out. In the Soc Trang province a pilot project was set up with bamboo T-fences. This site could prove interesting for validation of the model concept.

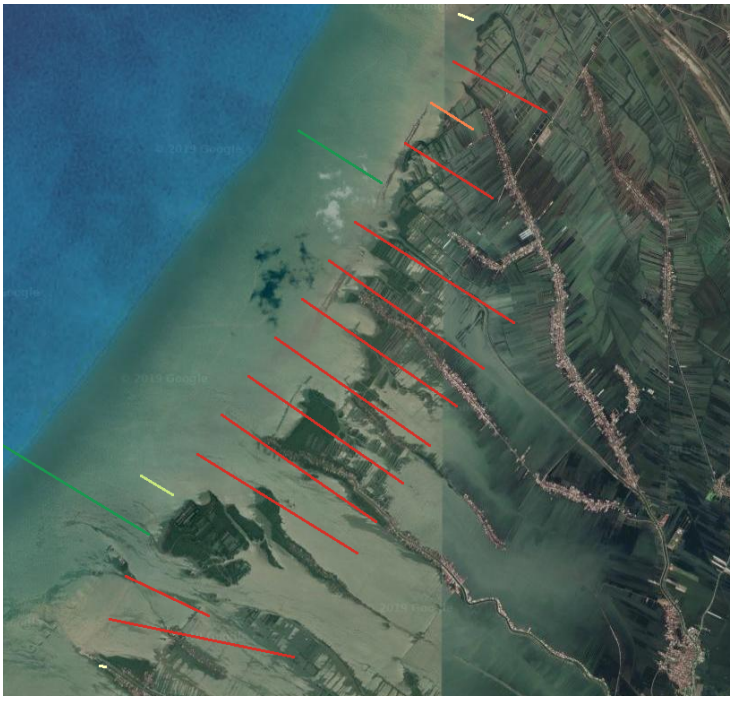

Figure 3.1: Demak erosion rate. (Deltares and TU Delft, 2018).

3.1.1 Selection of coastal sites

The previous section explained different criteria for site selection. Vietnam and Surinam have already initiated pilot studies on mangrove rehabilitation, making them suitable for their data availability. Both countries experienced, and are experiencing still, losses in mangrove cover, as concluded in Subsection 3.1. Besides these factors, both sites offer very different coastal characteristics from Demak, providing a varied set of boundary conditions that influence sedimentation behind the dams. The following paragraphs describe two specific coastal sites in Surinam and Vietnam, suffering from erosion and mangrove degradation.

Vinh Tan (Soc Trang), Vietnam In the Soc Trang Province in southern Vietnam, at Vinh Tan, research for dam placement and monitoring have been carried out, resulting in useful data. Near Vinh Tan, coastline retreat and mangrove degradation are endangering dykes and the people living behind them (Albers and Von Lieberman, 2011). Data from Deltares and TU Delft (2018) also shows long-term erosion in the area. In Section A.1 the coastal characteristics of this coastline part of Vietnam are described in more detail. Figure 3.7 gives an overview of the coastal characteristics as described in Section 3.3.

Weg naar Zee (Paramaribo), Suriname The coastline of Surinam experiences an erosion/sedimentation cycle of around 30 years, due to the extensive mudbanks that migrate along the coastline from east to west. Abundant sediment supply from the Amazon river is distributed along the coast towards the Northwest. Although a lot of sediment is available near the coast, human activities affect the coastal ecosystems. At Weg naar Zee, near Paramaribo, erosion is becoming a growing concern, specifically with communities living behind the coastline. An interest in sustainable solutions has formed, as hard sea dykes appear to only worsen the problem (Winterwerp et al., 2013). Section A.2 delves deeper in the coastal system of Weg naar Zee, which is summarized in an overview in Figure 3.8 (Section 3.3).

3.2 Environmental conditions of the Demak coastal area

The environmental conditions and an understanding of the coastal system of Demak give an idea about the required model setup: its input and boundary conditions. The information on the project site at Demak is derived from the discussion paper by Winterwerp et al. (2013) and from the two theses of Smits (2016) and van Domburg (2018). Their theses already enclose an extensive site analysis, found rather useful for the current project.

3.2.1 Meteorology

The island of Java is located in the South-East of Asia and has a strong seasonal climate determined by two monsoons. This section elaborates on the two monsoons and its effect on the coastal area of Demak in terms of wind and rainfall. The island experiences the interchange of two monsoons every year: the northwest monsoon from November to April and the southeast monsoon from June to September. Around May and October the dominant wind direction and rainfall intensity changes, indicating the transition of the northwest to the southeast monsoon and vice versa.

Northwest monsoon

Between November and April the wind blows from mainly from the west over the Java Sea. During December, January and February these winds are strongest and can reach 10-15 m/s. Moreover, during these months the most rainfall is experienced (an average rainfall of 4 to 5 m/year) and therefore this monsoon is often referred to as 'the monsoon', with the southeast monsoon being the dry season.

Southeast monsoon

During May the wind direction changes from west to south, starting the southeast monsoon with its prevailing southerly winds. In July and August the wind speeds are largest, but less compared to the northwest monsoon. The southeast monsoon does not provide much rain and with just 1 m/year on average.

3.2.2 Hydrodynamics

The Demak coastal site experiences a mild wave climate and fairly low tidal ranges. This is accompanied by mild currents. The three hydrodynamic aspects that influence the sediment dynamics and vegetation dynamics are elaborated in this section.

Tide

The tide at this coastline has a mixed tidal signal, but is mainly diurnal with small semi-diurnal components. This classification is made by deriving the form factor F with the tidal constituents at Demak, see Eq. 3.1. Using Eq. 3.1 gives a form factor F of 2.4.

$$F = \frac{K_1 + O_1}{M_2 + S_2} \tag{3.1}$$

Table 3.1 includes these tidal constituents, derived from Smits (2019). Daily inequality and monthly variations in the spring-neap cycle are prominent and determine an irregular periodicity. This clearly visible in Figure 3.2, which also indicates a tidal range at spring tide of approximately 0.60 m and at neap tide of 0.40 m. When semi-diurnal components are in synergy with diurnal components the tidal range at spring tide can be larger. According to Bosboom and Stive (2015) this tidal signal characterizes a micro-tidal regime.

Tidal constituents	**Amplitude [cm]**	**Phase [°]**
M_2	9.14	69.21
S_2	5.58	314.73
N_2	3.52	24.47
K_2	2.26	339.57
K_1	21.29	254.04
O_1	5.36	149.74
P_1	6.88	257.03
Q_1	0.46	25.74
MF	0.84	67.52
MM	0.65	39.50
M_4	0.22	206.57
MS_4	0.10	352.99
MN_4	0.13	305.7

Table 3.1: Tidal constituents at Demak, Smits (2019).

Although Java is located on the southern hemisphere, the rotation of two main constituents in the Java Sea is counterclockwise, so these propagates westward through the Java Sea. Since Java is close to more than one tidal node, the tidal propagation near Demak is rather complex and there is not just one tidal propagation direction. The tidal currents at the coastline are in the order of 0.15 m/s, Ecoshape (2015).

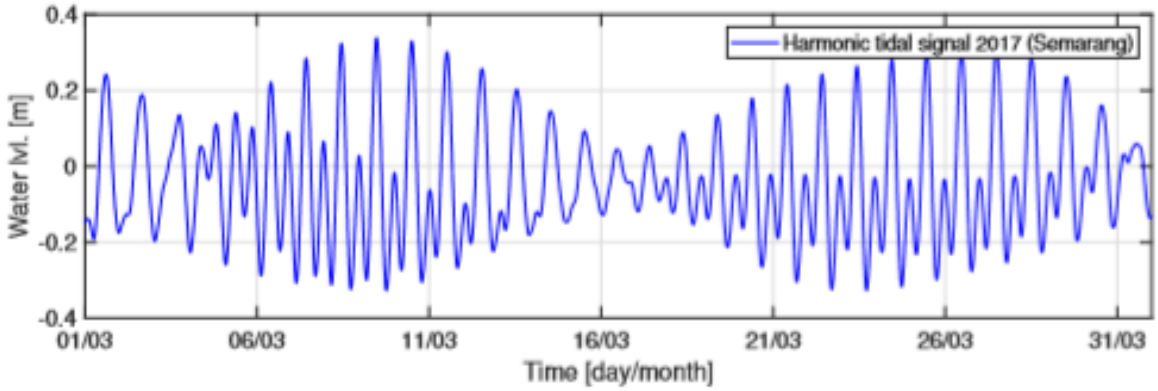

Figure 3.2: Tidal signal at the tidal station in Semarang, van Domburg (2018).

Water level variation

Besides the tidal water level variation some seasonal average water level variation is also present at Demak. When the harmonic tidal signal measured at Semarang is plotted for various years, see Figure 3.3a, on a monthly scale the mean shifts throughout the year. The amplitude of this shift is around 5 cm in a year. (van Domburg, 2018). Besides the harmonic tidal signal at Semarang, there are also absolute measured values, shown in Figure 3.3b. This plot shows a yearly varying average water level as well, but especially two peaks (highest average water level) are visible: between October - January and May - July/August. Interpreting the plot, the highest average water levels occur at different moments each year and the difference between the lowest average water level and the highest average water level is not a yearly constant either.

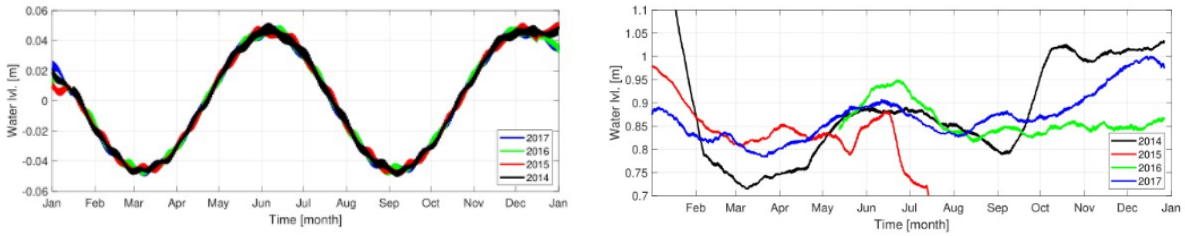

(a) Harmonic tidal signal

(b) Measured tidal signal

Figure 3.3: Tidal signal at the tidal station in Semarang for 2014 - 2017, van Domburg (2018).

Wave climate

As expected by evaluating the wind directions and speeds during the year, the northwest monsoon causes the largest waves to develop. During this period a predominant northwestern offshore wave direction and a maximum wave height around 2.5 m are experienced. The southeast monsoon delivers different wave conditions, with an eastern predominant offshore wave direction and a maximum wave height of 2 m.

Due to wave transformation the offshore waves differ in direction and height from the nearshore waves. Although refraction is not accounted as having a large influence (the coastal slope is really mild) waves are transformed from the offshore northwest/east direction to a nearshore northern direction. Moreover, the mean wave height near the shoreline was measured as 0.46 m. This was documented by Wyrtki (1961) and also provided maximum offshore wave heights between 2.6-3.0 m with a period of 5.5 s.

Currents

The mild slope and relatively low energy wave climate do not exert high wave-induced currents at the nearshore. The nearshore wave-induced currents are reckoned to be in the order of 0.1 m/s.

According to Wyrtki (1961) the larger ocean currents follow the same wind patterns, as the winds during the monsoons are very steady. This means a transition in current direction twice a year. During the northwest monsoon the residual ocean currents are driven towards the east and during the southeast monsoon the residual currents flow towards the west. The currents at the nearshore are fairly small and do not significantly influence the sediment transport, however, the large rainfall during the northwest monsoon and its residual ocean current towards

the east induce a gravitational circulation keeping fine sediments near the coast Ecoshape (2015). This is not the case during the southeast monsoon, and large scale sediment transport near the coast is not induced.

3.2.3 Morphology

Bathymetry

The shallow mud coast at Demak experiences a slope of 1:600, but in earlier times this slope used to be much milder and between 1:1000 or 1:1500. Cheniers, small lenses of sand, are situated parallel to the coastline at a distance of tens to hundreds of meters away from the shoreline. They attenuate incoming waves, creating a milder wave climate for the mangroves at the shoreline. BioManCo (2018) did fieldwork in the Demak coastal waters and discovered fluid mud effects on the hydrodynamic conditions, but more measurements and research has to be done on the stratigraphy and mud state. They also did measurements on the bed level for two transects at the Demak coastline, which is analysed in the thesis by van Domburg (2018). Appendix .. shows the location of the transects and the bathymetry data. The resulting bathymetry is visualised in Figure **??**. These transects extend for 400 to 600 meters into the sea, where the permeable dams are located 150 meters out of the coast so they are still in the range of this profile. What is remarkable is that the average slopes of these two cross-shore .. are 1:300 and 1:450 approximately: a rather steep profile. Neglecting the steep part of the profile (part D in the eroding transect and part A in the accreting transect) gives slopes of 1:500 and 1:2000 respectively.

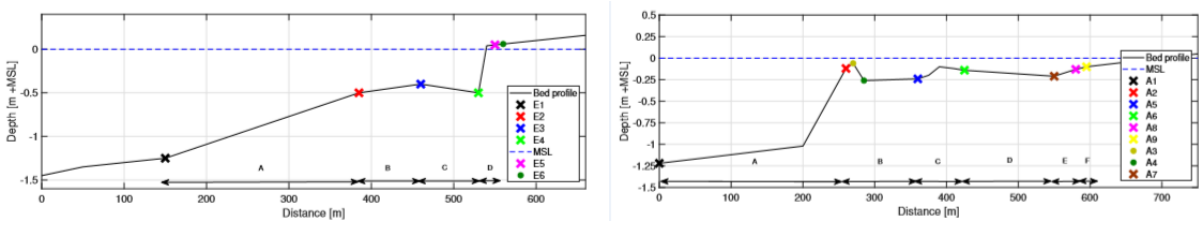

(a) Eroding transect

(b) Accreting transect

Figure 3.4: Coastline profile for two transects at Demak, van Domburg (2018).

Sediment composition

BioManCo (2018) did research on the sediment distribution at the coast of Demak. They performed several measurements. Results of these measurements were a bulk density of 1390 kg/m^3 for a regular mud sample and a dry density of 585 kg/m^3. For the cheniers a bulk density of 1580 kg/m^3 was found and a dry density of 1080 kg/m^3. Besides the density of the soil, grain size diameters were determined. On average the mud content of the soil was 80%, so 80% of the mass had a particle diameter less than 63 μm. Around 20 - 30 % consists of fine sand.

Sediment sources/sinks

Not much is known about the exact sediment sources or sinks in this coastal area. Erosion of land due to clearance of forests in the mainland had increased the sediment discharge from rivers towards the coast, but according to Ecoshape (2015) approximately half of the sediment distributed by the rivers towards the coast must have been drifted to deeper water and is lost from the coastal system.

3.2.4 Mangroves

Different mangrove species show different behaviour in terms of seedling dispersal, growth, pioneering etc. According to Ecoshape (2015) *Avicennia marina* and *Rhizophora mucronata* are most prominent in the Demak area, of which the *Avicennia marina* is the most important pioneer species.

3.2.5 Human pressure

Sea level rise is a common threat to almost all coastal regions in the world. More specific for this area is the exorbitant subsidence rate due to extensive groundwater extraction. Besides these aspects, the replacement of the mangroves by many fish ponds does have a tremendous effect on the coastline and its ecosystem.

Relative sea level rise

The rising sea level is a topic much talked about these years. A lot is uncertain, leading to many sea level rise scenarios. For the Demak area Smits (2019) derived three sea level rise scenarios; 0.42 cm/year, 0.50 cm/year

and 0.60 cm/year. These correspond with the global sea level rise predictions for this particular area. Besides the rising sea level, land subsidence also contributes to a relative sea level rise and in Demak this is an extensive contribution. This is mainly caused by huge amounts of groundwater extraction and natural alluvium soil consolidation. Near Semarang values for subsidence rates reached 8 cm/year, but this is not certain to be valid for the Demak coastal system. In the report by Smits (2019) the best, intermediate and worst case (just as for the sea level rise) comprised 7.8 cm/year, 10 cm/year and 13 cm/year.
The sea level rise and land subsidence together sum up to a relative sea level rise of 8.22, 10.5 and 13.6 cm/year for the three scenarios respectively.

Aquaculture

Along the shoreline of Java many mangrove forests have been replaced by fish and shrimp ponds. In the 1980's inhabitants saw financial possibilities in this fish farming, but did not know the consequences of the substitution yet. Now the ponds do not provide well enough anymore, due to previous outbreak of diseases and accumulated pesticides residues, Winterwerp et al. (2013). Sediment dynamics have changed since the mangroves were removed and the intertidal range confined. The IKI-project includes restoring the mangroves, but at the same time finding a way in which the local community can still .. their aquaculture. With Mixed-Mangrove Aquaculture fish ponds continue to exist but mangroves are restored around to filtrate the water and prevent too much salt intrusion. Mangrove bloom and aquaculture will be simultaneous.

3.3 Overview of the coastal sites

The three coastal sites have similarities, e.g. cheniers, but the differences mainly dominate. An overview of the three sites enables a quick comparison of the main coastal characteristics influencing the morphology of the defined area. The three Figures 3.6, 3.7 and 3.8 summarize the coastal parameters and Figure 3.5 shows the specific weather conditions during the year for the three sites.

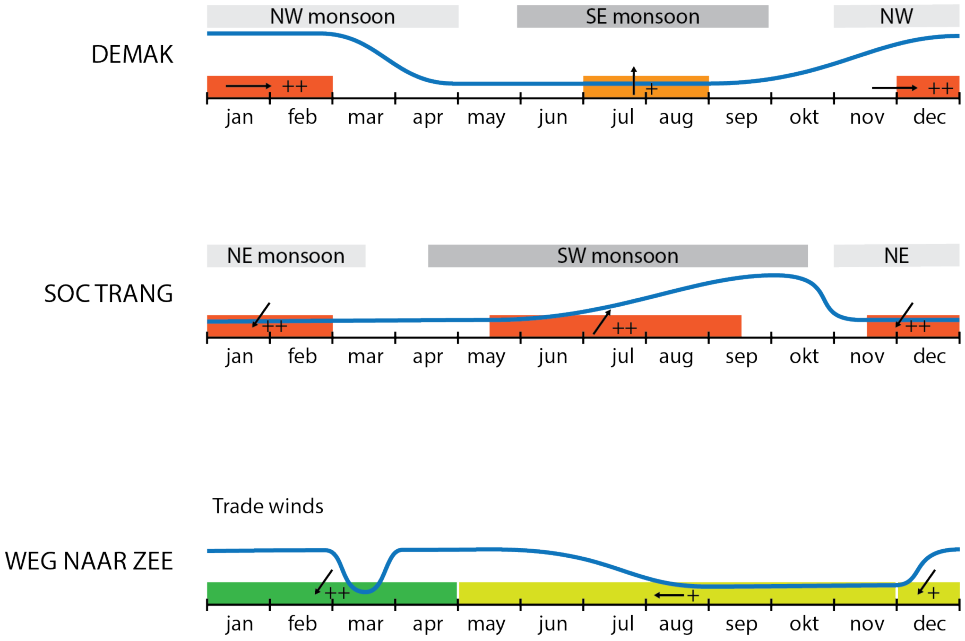

Figure 3.5: Seasonal variability in terms of wind speed, wind direction and the annual rainfall. The blue line represents the annual rainfall, the color bars indicate periods of higher wind speeds with arrows indicating the wind direction.

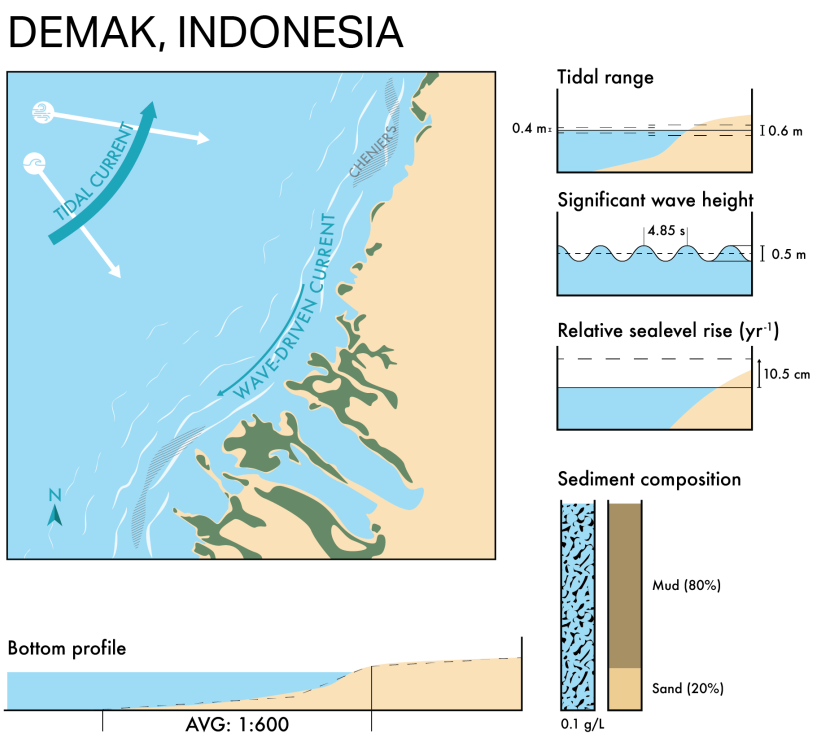

Figure 3.6: The coastal system at Demak.

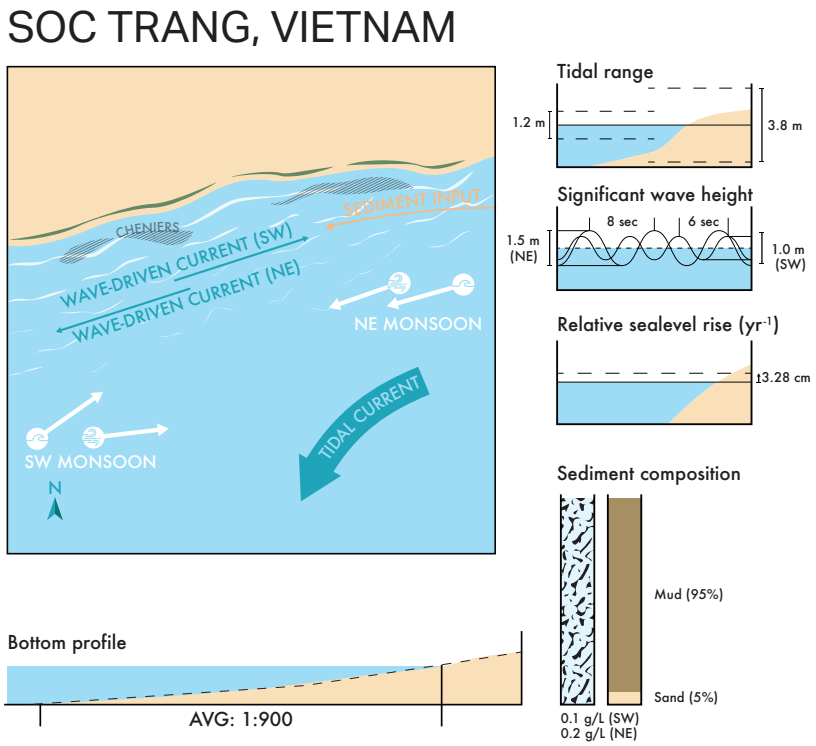

Figure 3.7: The coastal system at Vinh Tan.

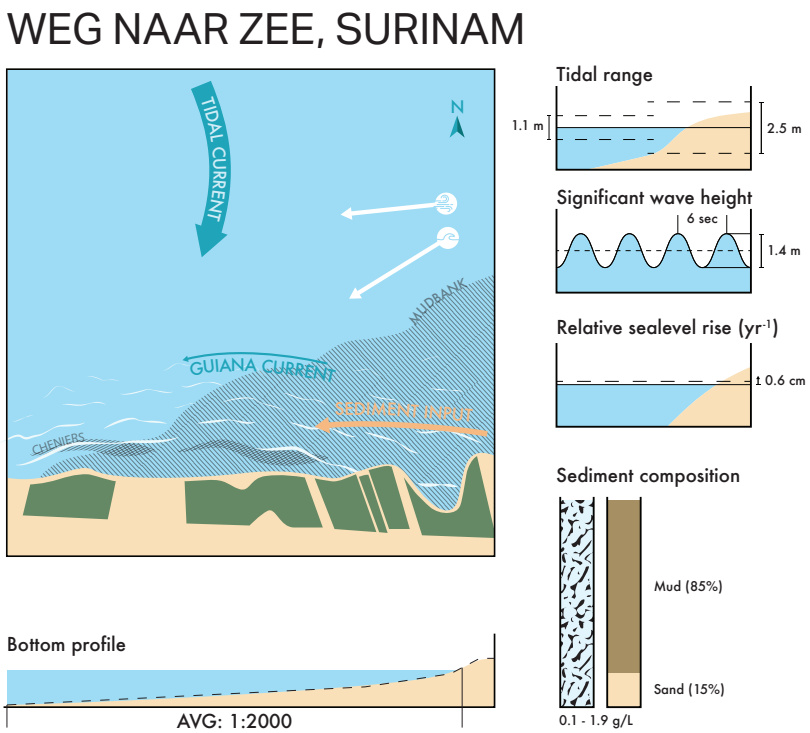

Figure 3.8: The coastal system at Weg naar Zee.

4

Permeable dam model setup

In order to create a simple model setup for various sites, one idealised model has been created where the input parameters of the different sites can be tweaked easily. The basis for the model design choices comprise Section 4.1, followed by a detailed model setup description in Section 4.2. The model setup is made compatible for different sites and Section 4.3 includes the input variation according to Demak's coastal system. The concluding section of this chapter, Section 4.4, includes the validation of the model.

4.1 Morphodynamic model: Delft3D FM

To study the effect of different coastal system parameters on the dam performance a numerical model is set up. By altering the hydrodynamic forcing and sediment input, the effect of the dams can be studied in more detail. Although several numerical models are available to use, Deltares has developed, amongst others, Delft3D FM; a fully integrated computer software suite comprising different modules able to simulate different processes in coastal, river and estuary environments. The different modules can be used 'stand alone' or coupled to simulate the interactions between different processes. Delft3D FM is process-based and its key component is the Flow engine "D-Flow FM", which calculates non-steady flow and transport phenomena to simulate the hydrodynamics on structured and unstructured, boundary fitted grids in 1D, 2D and 3D (Deltares, 2020a). Delft3D FM is well suited to study the effect of different forcing conditions or parameter settings in morphodynamic simulations on open coasts. The next two subsections elaborate on the various design considerations related to the use of Delft3D FM. This includes the dimensional space for the simulations and the use of different modules to include the necessary coastal processes.

4.1.1 Dimensional space

In reality the bamboo dams are permeable and allow sediment transport through the brushwood, but in Delft3D FM there is no option to model permeable structures yet. An option would be to model the bamboo dams as vegetation with a certain density exerting the same drag force and permeability as the permeable bamboo dams. This would then enable 1D modelling. Another option is to model the bamboo dams as 'thin dams' in Delft3D FM. These structures are not permeable and sediment transport through the gaps in between the dams is assumed. Smits (2016) validated the assumption of sediment inflow through the gaps in between the dams, but this requires a 2D modelling approach. Another consideration is the modelling of the longshore currents driven by wind, waves and tides. Other coastal sites than Demak, e.g. Soc Trang and Weg naar Zee (see Chapter 3), experience strong longshore currents transporting sediment along the shoreline. This requires a 2D model setup as well.
Modelling 3D processes in a cohesive sediment environment results in computationally very expensive simulations. It is desired to work with a depth-averaged approach to regain a 2DH model as the study is focused on the larger scale processes in the coastal areas, leaving the computation times within acceptable limits.

4.1.2 Delft3D FM modules

Simulating the effect of the dams on the morphodynamics in Demak requires different modules of Delft3D FM. Firstly, the core component D-Flow FM is used for the hydrodynamic simulations where the flow itself is simulated. Coupling flow to sediment transport requires the flow module coupled to D-Morphology to simulate the

sediment transport and update the bathymetry. As the mangrove coasts are muddy environments, formulas for cohesive sediment transport are used, which differ substantially from the sediment transport formulas for coarse grains. The wave forcing is simulated with D-Waves, which is coupled with D-Flow FM by means of 'online coupling'. This section writes the key points of each module, where Appendix B gives a more technical explanation of each module, with its governing equations.

D-Flow FM

D-Flow FM solves the Navier-Stokes equations with use of several assumptions simplifying these equations. The fluid is assumed to be incompressible and the Boussinesq assumption is used by assuming constant density. Moreover, the shallow water assumption neglects vertical accelerations in the vertical momentum equation resulting in a hydrostatic pressure equation. The remaining set of partial differential equations are solved by the input of an appropriate set of initial conditions and boundary conditions. All on an unstructured finite volume grid (Deltares, 2020a).

D-Waves

The module D-Waves is based on the spectral module SWAN, developed by the Delft University of Technology. It computes the non-steady propagation of short-crested waves over a variable bottom. The waves are described by a two-dimensional wave action density spectrum since the action density is conserved in the presence of currents where energy is not. The wave spectrum evolution is described by the spectral action balance where the source term includes the following processes: generation by wind, dissipation by white-capping, bottom friction and depth-induced breaking and non-linear wave-wave interaction (quadruplets and triads). Also, refraction, shoaling and directional spreading is considered (Deltares, 2020c).

D-Morphology

The sediment transport for both suspended and bed total load resulting from the flow and wave conditions are computed with D-Morphology. As a dynamic feedback system exists between D-Morphology and D-Flow Fm the resulting morphological change serves as an update for the bathymetry used in the hydrodynamic computations. The module both handles cohesive and non-cohesive sediment fraction, with different formulations for both. Simulating muddy environments requires cohesive sediment formulations (Deltares, 2020a).

4.2 General model setup

The three coastal sites have very different characteristics specified. Including just the larger scale processes enables the use of one model for the three sites. The simplifications in time and spatial scales were described in Section 4.1 where the current section translates these simplifications into the setup for an idealized model to study the effect of permeable dams in different mangrove-mud systems. To easily follow the explanation of the Delft3D model setup, Figure 4.1 gives an overview. This overview illustrates the coupled wave and flow domain. As explained in Section 4.1, the wave domain calculates the wave input for the flow domain whereas the flow domain, coupled to the sediment module, updates the bathymetry recurrently influencing the hydrodynamic forcing. The following subsections elaborate further on the different model components and conditions displayed in Figure 4.1.

4.2.1 Computational grid

For the wave and flow module a computational grid is created. These are illustrated in Figure 4.2. Figure 4.2a shows the wave domain incorporating three nested grids. The outer grid has a grid cell size of 500 by 500 m. Then the nested, smaller grid has a grid cell size of 100 by 100 m and the smallest grid cell size is 10 by 10 m. The refining of the wave grid by means of nested grids enables wave computations on a smaller scale at the dam locations where an increase in accuracy is desired when at the same time minimizing the computation time. Grid refinement is also used for the computational grid in the flow domain, where in Figure 4.2b the decrease in grid cell size from the seaward boundary towards the landward boundary is visible. The flow module includes an unstructured grid and there is no need for nested grids, seen in the wave module. Refinement of the grid can be done locally by using triangular grid cells.

As the input wave conditions are based on deep water conditions, i.e. the waves are not yet affected by the water depth, the length of the wave grid should be large enough to ensure deep water conditions for a particular bathymetry. With the length of the wave domain on 20 km, the water depth for the various bathymetries (Subsection 4.2.2) exceeds the deep water limit of $h > 0.5 \cdot L_0$. Besides the length of the wave grid, the width is susceptible to a numerical criterion. As the exact wave input is not known along the wave boundaries, errors in the wave boundary conditions cause errors travelling through the wave domain. To ensure that these 'shadow

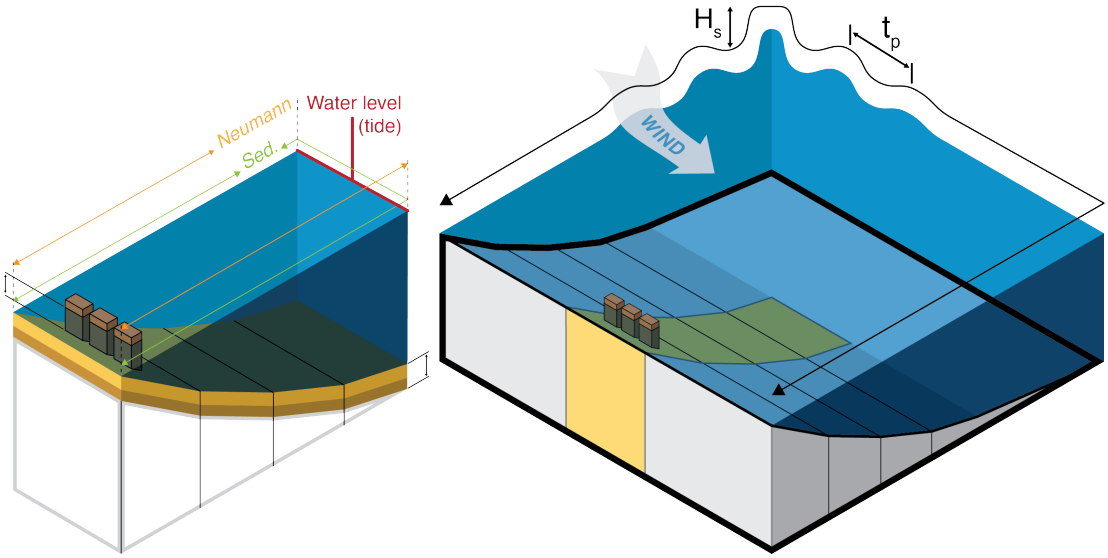

(a) Flow domain **(b)** Coupled wave and flow domain

Figure 4.1: Morphological model including the three modules D-Flow FM, D-Waves and D-Morphology, all coupled.

effects' do not occur near the dams, the width of the wave grid is based on the mean wave direction. (Delft University of Technology, 2020). With the mean wave direction of the incoming waves equal to 0°, but a directional spreading of 15°, the necessary width of the wave grid is 20 km.

4.2.2 Bathymetry

An important simplification in the model is the use of an alongshore uniform coast. The dams are placed parallel to the coastline to study cross-shore sedimentation/erosion patterns. Two dimensions, instead of one dimension, enable the flow around the structures and wind and wave directions that are not solely cross-shore.

4.2.3 Boundary conditions

Reducing the input highly decreases the computation time. For example reducing the wave climate to just a few significant wave heights and related wave periods for one dominant wave direction, simplifies the simulations. However, in dynamic muddy environments where seasonal variability is high, input reduction can become difficult by the major differences in wind and wave conditions between seasons. For example the wave direction between the two monsoons in Vietnam changes to its opposite, causing a wind-driven longshore current in the exact opposite direction, see Figure 3.7 again. Therefore, the wave boundary conditions and the sediment boundary conditions are set up per season. The following paragraphs elaborate on the boundary conditions for the different modules in Delft3D FM.

Waves The wave module requires three boundary conditions. The same time-varying wave boundary condition is applied on all three open boundaries. The significant wave height and wave period vary in time, while the wave direction and directional spreading are kept constant.

Flow Like the wave module, the flow module needs three boundary conditions; one for each open boundary. The offshore boundary is assigned a waterlevel boundary where the waterlevel is prescribed by tidal constituents. The amplitude and phase of different constituents serves as input for the waterlevel boundary. Additionally, in case of a relative sea level rise, another waterlevel boundary at the offshore boundary prescribes a rise in sea level. The two lateral boundaries will be assigned Neumann boundary conditions. Here the waterlevel gradient is equal to zero.

Morphology Using the morphology module, the three open boundaries of the flow domain require sediment boundary conditions additional to the flow boundary conditions. The lateral inflow boundaries, however, are close to the area of interest causing a higher sensitivity of the model to the lateral sediment inflow boundaries. In case of insufficiently known boundary conditions this can lead to a insert word. Therefore the inflow boundaries

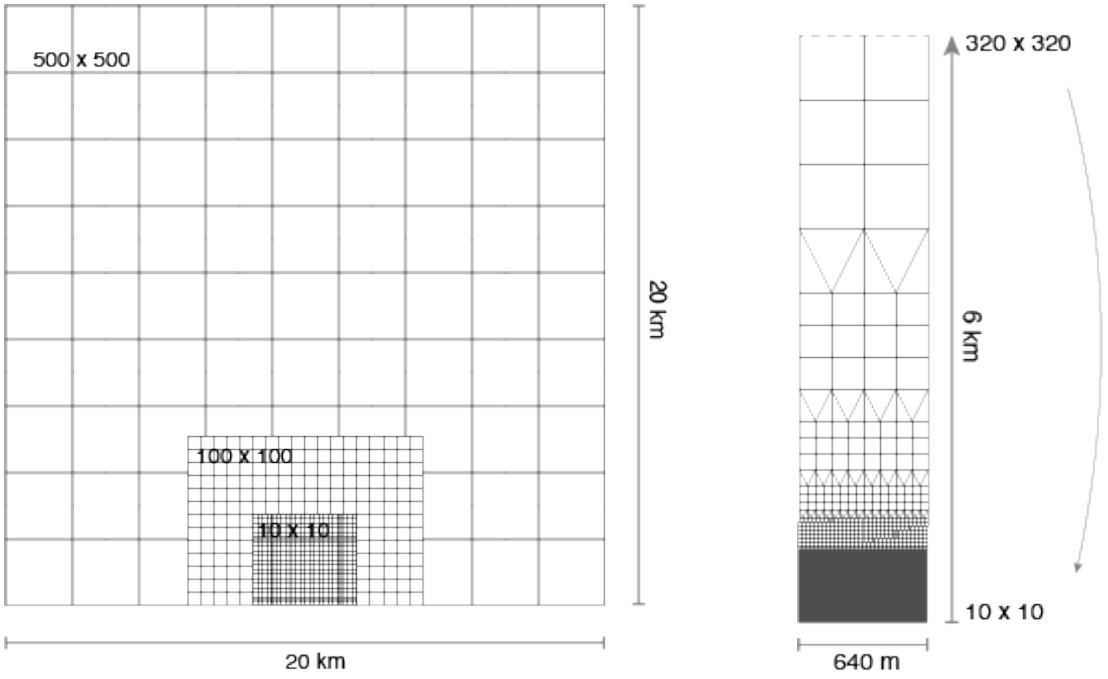

(a) Nested wave grids

(b) Unstructured flow grid

Figure 4.2: Computational grids

use a Neumann boundary condition. For cohesive sediment this means that the mud concentrations computed inside of the model domain are applied at the inflow boundaries.

4.2.4 Dams

As explained in Section 4.1 two options are considered for modelling the permeable coastal structures. The 2DH modelling approach enables the use of thin dams in the flow module, which is an easier method than the substitution of the permeable structures by vegetation. Thin dams are a suitable option to model the permeable dams and are used in the current model as well.

In D-Waves the dams can be modeled as obstacles with certain reflection and transmission coefficients. For the model setup, the reflection coefficient is set equal to zero, disabling reflection by the obstacles. The dam height is set at 2.0 m +MSL.

4.3 Case study: Demak

The model setup described in the previous Section 4.2 is tested firstly with the situation at the Demak coastline. The Demak model setup is a reference model to see 1) the working of the general model setup and 2) by varying coastal characteristics dam functioning in Demak is related to the dam functioning at other coastlines.

Figure 4.3 renders the model setup for Demak, where the components are explained separately in the following subsections. This model setup is referred to as the reference simulation (excluding and including dams). Subsection 4.5 elaborates on the forcing parameters that are varied to study the effect of wave conditions and suspended sediment concentration (SSC) on the sedimentation behind the dams. These simulations are slightly altered from the reference simulation.

4.3.1 Seasonal variability

Smits (2016) studied the trapping of sediment by permeable dams in Demak and concluded that most of the morphological change happened during the more energetic NE monsoon, which makes it easier to reduce the input for the modelling of the dams in Demak. At the same time, it is much less computationally expensive to simulate longer time scales, as three months of morphological change during the NE monsoon actually represents what happens in one year. Therefore, Demak is set up for just one seasonal condition: the NE monsoon.

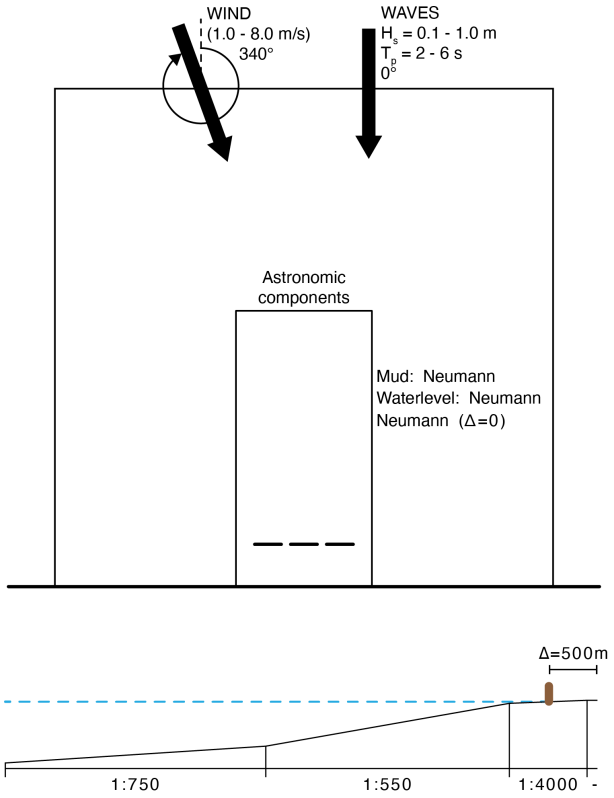

Figure 4.3: Model setup for Demak

4.3.2 Bathymetry

The bathymetric input for the model setup is highly schematized and does not represent an equilibrium profile. To leave out any unrelated bedlevel changes, some spin up time is necessary before the actual start of the model run. Ideally, the spin up includes the simulation of an equilibrium profile where the bathymetry is fully adapted to the forcing. Section C.2 includes an analysis of the equilibrium profile with the setup of the model for Demak. The resulting profile after the spin up time of 2 years is given in Figure 4.4. The nearly horizontal part at the land boundary is referred to as the 'tidal flat' in the rest of the project.

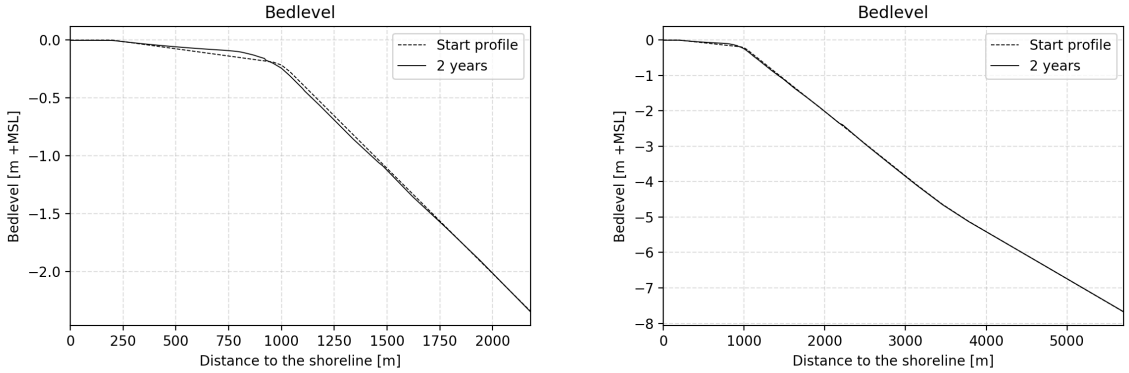

Figure 4.4: The average bedlevel profile after a spin up time of 2 years. The left graph shows the profile with a length of 2 km and the right graph the profile along the entire length of the model, 6 km.

4.3.3 Boundary conditions

Waves The boundary conditions for the wave module are based on the wave data analysis by Smits (2016) and BioManCo (2018), as is the case for the wind input. The wind velocity and wave heights are varied in time. Both (the ranges for) the conditions are given in Table 4.1 and Figure4.5 shows the wave significant wave height and

wind velocity through time.
The wave period is calculated using the assumption that non-breaking waves in deep water will not exceed a steepness S of 0.02. The steepness S is defined as the wave height over the wave length: $S = \frac{H}{L}$. The simplified dispersion equation for deep water gives the wave period related to the wave height: $T = \sqrt{\frac{2\pi \cdot L_0}{g}}$. Then combining the steepness formulation and the deep water dispersion equation gives the wave period related to the wave height, resulting in a peak wave period range of 2 - 6 s with waves of height 0.1 - 1.0 m.

$$T = \sqrt{\frac{2\pi \cdot H}{g \cdot S}} \tag{4.1}$$

With:

T	=	wave period	$[s]$
H	=	wave height	$[m]$
g	=	gravitational acceleration	$[m/s^2]$
S	=	steepness	$[-]$

Wave				**Wind**	
H_s $[m]$	T_p $[s]$	Dir. [°]	Spreading [°]	Velocity $[m/s]$	Dir. [°]
0.1 - 1.0	2 - 6	0	15	0.8 - 8.0	340

Table 4.1: Wind and wave conditions used as input for the wave model.

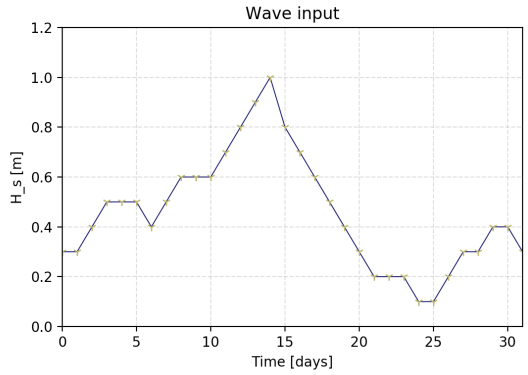

(a) The significant wave height ranging from 0.1 m to 1.0 m.

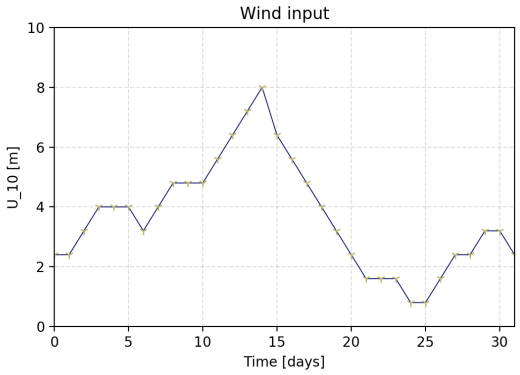

(b) The wind velocity used as model input. The smallest velocity is 0.8 m/s, where the maximum velocity equals 8 m/s.

Figure 4.5: Boundary conditions for the wave model: wind and wave conditions. The conditions repeat themselves after 31 days.

Flow The offshore boundary uses an astronomical boundary condition. Its constituents with amplitude and phase were given in Table 3.1. Figure 4.6 shows the waterlevel at the open offshore boundary induced by the tidal waterlevel boundary condition. The lateral boundaries are assigned Neumann boundaries, as explained in Section 4.2.
The simplified model setup does not include the land subsidence or any sea level rise, as these are important especially for longer term simulations. This research uses short term (two years) simulations, where land subsidence and sea level rise is not the focus.

Sediment The three open boundaries require a boundary condition for the morphology module, e.g. a SSC. In case of unknown cohesive sediment concentrations at the boundaries, Neumann boundaries can be used where the incoming flow carries the same mud concentration as computed in the inner grid cells, see Section 4.2.3. Currently, it is not possible to combine a prescribed sediment concentration at one boundary and Neumann boundary conditions at other boundaries in one model. Therefore all the boundaries need be either prescribed sediment concentrations or Neumann boundaries.
No accurate data is available to prescribe a SSC on the boundaries of the Demak model. The reference model setup will include Neumann sediment boundary conditions. When spatially constant SSC's are prescribed at the

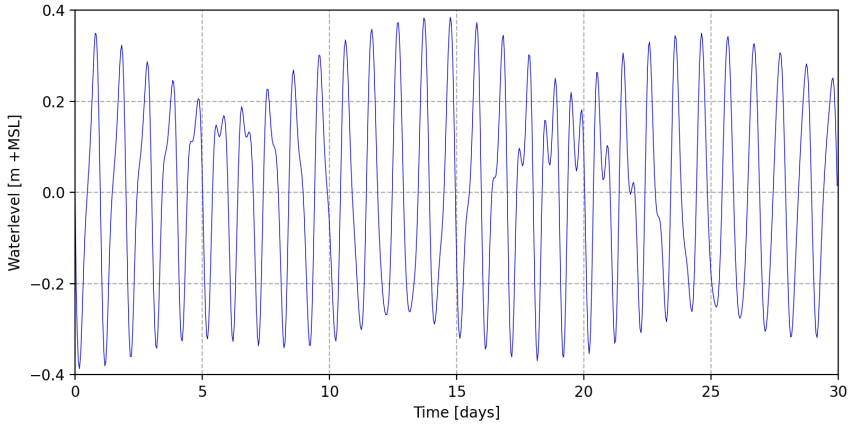

Figure 4.6: The waterlevel for 30 days at the open offshore boundary.

boundaries, they influence the model behaviour too much and inconsistent bedlevel development results. Appendix C (Subsection C.1.1) shows this model behaviour and gives the results for the sensitivity runs with spatially constant sediment boundary conditions.

In order to prescribe a sediment boundary condition the Neumann boundary condition values are mimicked. Accordingly, this pseudo-Neumann SSC boundary condition can be varied to study the influence of the suspended sediment boundary condition on the sedimentation behind the dams. Subsection C.1.1 shows the construction of these spatially varying, time-constant SSC boundary conditions and Subsection 4.5 elaborates on the scenarios of prescribed SSC boundary conditions.

4.3.4 Parameter settings

The parameters settings are based on the modelling study of Smits (2019). The calibration and validation of the model is done in respect to the model of Smits (2019).

The wave model is set to use a JONSWAP spectrum with a constant friction coefficient. The JONSWAP spectrum is used for the growth of waves over a limited fetch and their attenuation in shallow water. Using a Jonswap spectrum for modelling the Java Sea were validated by Smits (2019) and BioManCo (2018). The friction coefficient is 0.019 m^2/s^3, as is normally used for smooth sea floors Smits (2019). Other settings in D-Waves are kept to their default values.

Four variables are set to non-default values. The Manning coefficient for bottom roughness is 0.012 $s/m^{1/3}$, the water density is equal to 1025 kg/m^3 and the horizontal eddy viscosity and eddy diffusivity are equal to 1.0 m^2/s. All other parameters are default D-Flow FM values.

Lastly, the sediment parameters are based on two mud fractions, both have a specific settling velocity (w_s), erosion parameter (M) and a critical shear stress for erosion ($\tau_{erosion}$). Table 4.2 lists the two mud fractions and their sediment characteristics. The critical shear stress for both sediment fractions is set to 1000 N/mm^2 to enable permanent sedimentation. The bed composition is modelled as uniform and does not exhibit different layers. This enables the erosion rate to be proportional to the bed composition.

		Mud fraction 1	**Mud fraction 2**
w_s	$[mm/s]$	0.05	0.1
M	$[kg/m^2s]$	4.3E-06	1.2E-05
$\tau_{erosion}$	$[N/m^2]$	0.1	0.5
$\tau_{sedimentation}$	$[N/m^2]$	1000	1000

Table 4.2: The parameter settings for the sediment module.

4.3.5 Dam setup

The dams are placed at a water depth of 0.10 m relative to MSL, based on the average depth of the permeable dams in the model by Smits (2019). They are located on the tidal flat, 500 meters from the landward boundary. The setup includes three dams of each 50 meters long. A gap of 10 meters divides each dam.

4.4 Model validation: Demak

The lack of a big data collection makes the validation of the model limited. The numerical field study of Smits (2019) is validated by limited available data and expert judgement, so the results of simulations with the idealized model setup for Demak are compared to the sedimentation/erosion patterns and values of the model by Smits (2019). It is not expected that the results of the two models compare exactly, but sedimentation/erosion values should be in the same order of magnitude. The bedlevel after 10 years is compared to the results from Smits (2019).

4.4.1 Bedlevel validation

The area behind the dams is the area of interest for this research. The bedlevel development behind the dams modelled by the simplified model is compared to the bedlevel development behind the dams modelled by Smits (2019). The bedlevel is validated for a timescale of 2 years. Both the baseline simulation and the dam simulation are plotted. The bedlevel results for three dams are reproduced from Smits (2019) and illustrated in Figure 4.8a, 4.8b and 4.8c.
Figure 4.7 shows the bedlevel development in two years and in ten years at approximately 15 meters behind the left dam. The bedlevel development of behind the middle and right dam show similar results and are included in Appendix The location of the modelled bedlevel by Smits (2019) is also 15 meters onshore of the dams.

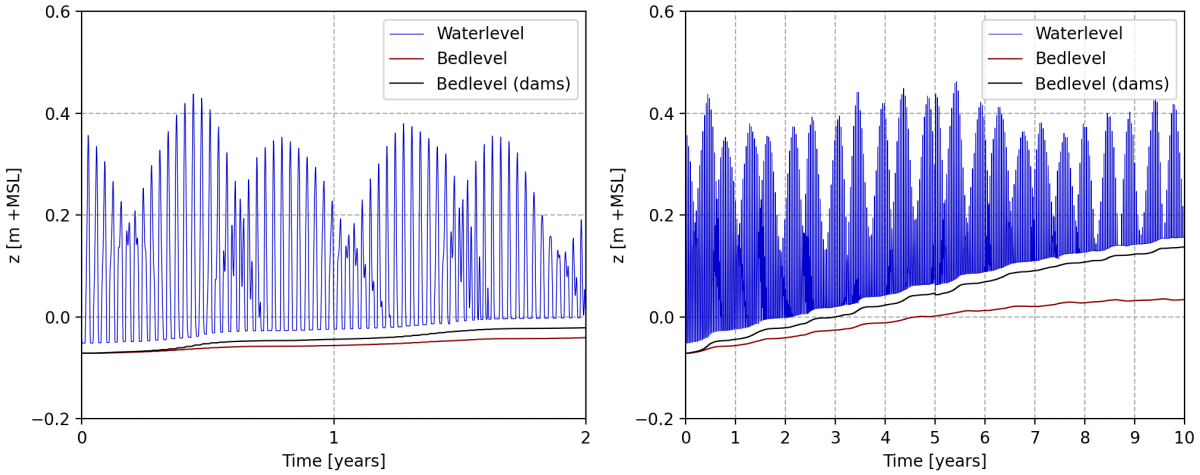

(a) Bedlevel development in two years – Left dam

(b) Bedlevel development in ten years – Left dam

Figure 4.7: The bedlevel in time for the baseline simulation and the dam simulation. The location of the bedlevel development is 15 meters onshore of the left dam.

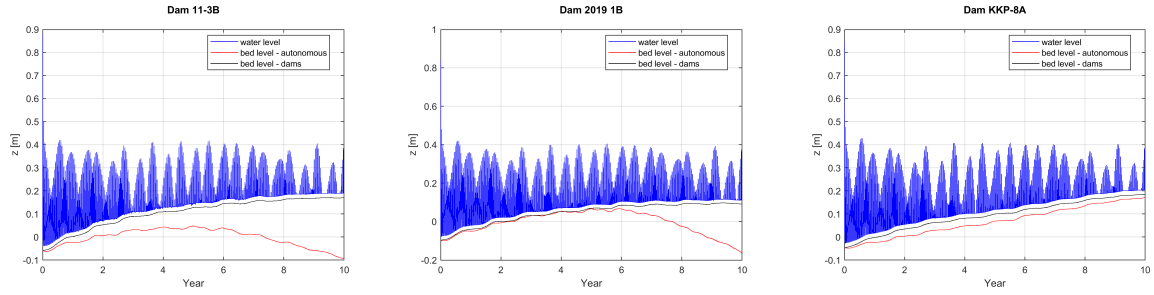

(a) Dam 11-3B

(b) Dam 2019-1B

(c) Dam KKP-8A

Figure 4.8: The bedlevel development in ten years behind three different dams modelled by Smits (2019). The bedlevel development is shown for approximately 15 meters onshore of each dam.

The bedlevel results from the simplified model show an increasing bedlevel in both the baseline simulation and the dam simulation. The bedlevel results from Smits (2019) deviate for each dam. The dam setup in the model by Smits (2019) is also irregular: the dams are placed at various distances from the shore and at various water depths. This explains the different bedlevel development for each dam. The bedlevel behind dam KKP-8A heightens for both the baseline simulation and the dam simulation, similar to the bedlevel results from the simplified model.

The difference between the bedlevel resulting from the baseline simulation and dam simulation ranges between 1.0 to 2.0 cm for the simplified model of Demak, as can be seen in Figure 4.7. The results of Smits (2019) show a difference in bedlevel between the baseline simulation and dam simulation of 1.0 to 5.0 cm after two years. This is in the same order of magnitude and validated by expert judgement.

4.5 Variable forcing parameters: Demak

The model setup as described in the previous subsections, can be validated with the model created by Smits (2019). To explore the influence of different boundary conditions on the sedimentation behind the dams, the forcing parameters vary as described in the following subsections and are compared to the reference simulation explained in the previous section (Section 4.3).

Wave direction The reference simulation has a wave direction perpendicular to the coast. In Suriname the main wave direction is approximately 45 ° and in Vietnam mainly in longshore direction (changes to opposite longshore direction from one monsoon to the other). The wave height (time-varying) is similar in all runs.

Scenario	Wave direction [°]
Reference	0
Scenario 1	45 (315)
Scenario 2	90 (270)

Table 4.3: Scenarios for the wave boundary conditions. The time-varying wave height is modelled using a Rayleigh distribution.

Wave height Varying the wave height between half the reference wave height (time-varying) and double the reference wave height.

Scenario	Wave height [m]
Reference	0.1 - 1.0
01	0.05 - 0.5
02	0.2 - 2.0

Table 4.4: Scenarios for the wave boundary conditions. The time-varying wave height is modelled using a Rayleigh distribution.

Suspended sediment concentration To be able to have prescribed sediment concentrations at the boundaries, the Neumann boundaries are mimicked. The reference model setup is run with Neumann boundary conditions for sediment. The sediment concentration at the boundary is then analysed and averaged in time to result in spatially varying SSC values at the boundaries. These values are used to set up boundary conditions mimicking more realistic SSC's and model behaviour. Appendix C illustrates the construction of the pseudo-Neumann boundary conditions, which comprise the time-averaged, spatially varying values of the SSC at the boundaries from the reference simulation.
Simulations with different prescribed SSC boundary conditions show the influence of the SSC boundary conditions on the dam functioning in Demak. Table 4.5 includes the four scenarios for the SSC boundary conditions.

Scenario	Lateral boundary condition	Offshore boundary condition
Reference	PN	PN
01	0.5 x PN	0.5 x PN
02	2 x PN	2 x PN

Table 4.5: Scenarios for the SSC boundary conditions. PN represents the pseudo-Neumann boundary condition.

5

Sedimentation behind the dams

The state of the mangrove-mud coast of Demak is erosive and mangrove-degrading, i.e. an unsteady profile. The coastline retreats and the nearshore bedlevel profile steepens by erosion. This chapter shows the results of the simulations on this profile state. The modelled effect of a change in boundary conditions on the short-term bedlevel development is shown for the case excluding (baseline) and including dams. The effect of the dams for different boundary conditions is derived from the comparison of the baseline and dam simulations. The varied boundary conditions are the wave height, the wave direction and the suspended sediment concentration. Section 5.1.1 and 5.1.2 show the results for the change in wave height and wave direction respectively. The results for a change in suspended sediment concentration are given in Section 5.1.3.

5.1 Results

For every boundary condition three different scenarios are modelled. A scenario includes two simulations: excluding (baseline) and including dams. The effect of the dams on the bedlevel behind the dams is defined as the difference in bedlevel development between the baseline simulation and the dam simulation. For each boundary condition, the baseline simulations for all three scenarios are evaluated first. Secondly, the simulations including the dams are shown. Comparing these evaluations gives the dam effect under a sudden change of the particular boundary condition. For all simulations a spin up time of 2 morphological years is used, with the forcing related to that scenario. The bedlevel development in two years over both the flow domain and the rectangular area sheltered by the dams is shown for each scenario. An explanation on the processes related to the erosion and deposition of the bed gives an interpretation of the results.

The reference model setup for Demak is used as reference scenario for each boundary condition. For the wave direction and the suspended sediment concentration, the reference scenario is slightly altered. The reference scenario for the wave direction uses a perpendicular wind and wave direction of 0° for both. The wind direction in the model setup of Demak (Section 4.2) has a direction of 340°. The reference scenario for the SSC uses the mimicked Neumann sediment conditions, instead of the Neumann conditions as provided by Delft3D FM.

5.1.1 Wave height

The three scenarios for the wave height include the reference, smaller and larger wave heights. Table 4.4 gives the three scenarios. The baseline simulations (dams excluded) of all scenarios are evaluated first, followed by the dam simulations. A comparison between the baseline and dam simulations enables an evaluation of the dam effect and comes last.

5.1.1.1 Baseline simulation

Figure 5.1 shows the bedlevel change in two years when no dams are present. The reference simulation (Figure 5.1a) shows an increase in bedlevel elevation on the tidal flat. The tidal flat boundary is located 1 km offshore of the landward model boundary. There, a transition between erosion/sedimentation is visible. The bedlevel erodes in front of the tidal flat. Wave dissipation causes the erosion of the nearshore area (Figure 5.1a). The breaking of waves stirs up the sediment. The sediment is then transported by the tide and largely deposited on the tidal flat. As explained in Section 2.2, the wave attack on a mangrove mud coast causes erosion as the waves bring the

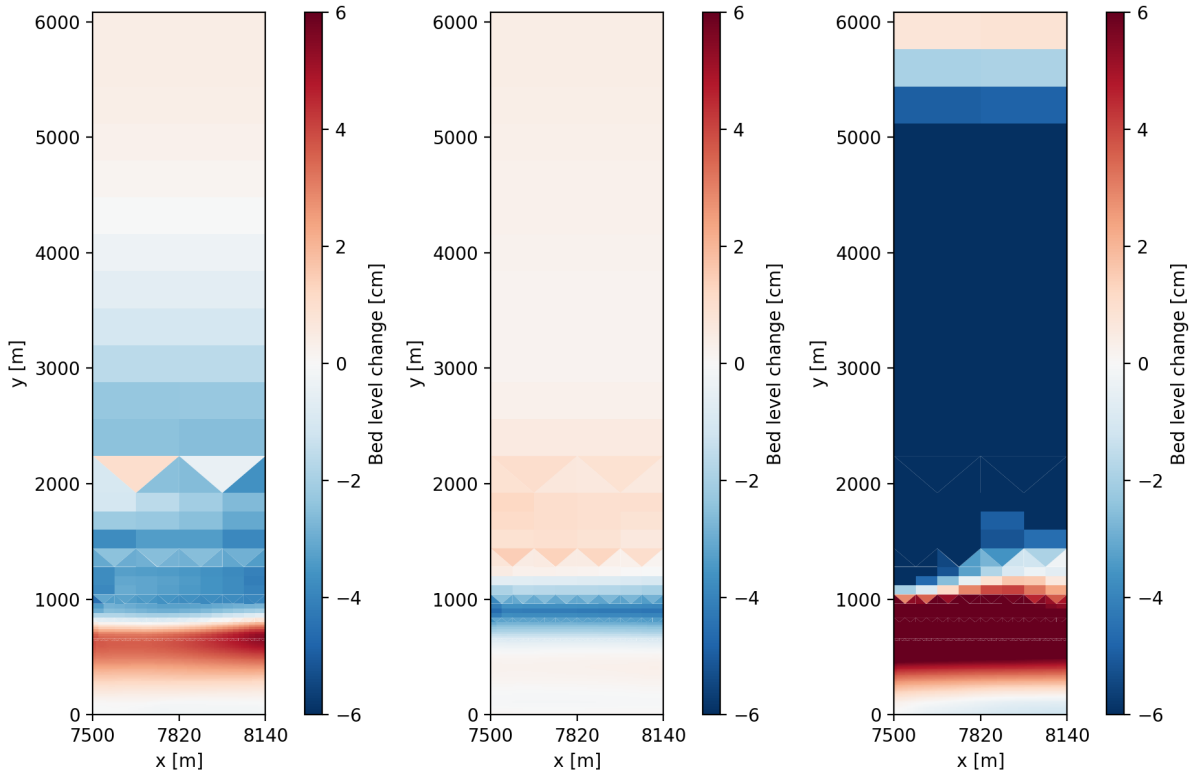

(a) 00-height: reference wave heights **(b)** 01-height: small wave heights **(c)** 02-height: large wave heights

Figure 5.1: The bedlevel change after two years for the baseline simulation of each wave height scenario. The bedlevel development is plotted over the whole flow domain.

fine sediments into suspension. The net sediment flux is directed either onshore or offshore depending on the height of the waves (relative to the tidal range). Larger wave heights erode the foreshore, which is then mostly transported towards the coast by the tide. Smaller wave heights cause more onshore erosion. The sediment is mostly transported in offshore direction by the tide. This influence of wave height on the nearshore of mud coasts can be seen in the small wave scenario and the large wave scenario in Figure 5.1b and 5.1c respectively.
Around the tidal flat boundary in Figure 5.1b, erosion occurs. The re-entrained sediment is mainly deposited just offshore of the tidal flat boundary. The bedlevel development in this scenario creates a more convex profile shape.
The larger wave height scenario shows strong erosion further offshore (relative to the reference scenario) (Figure 5.1c and strong sedimentation on the tidal flat. The larger waves break further offshore, bringing sediment in suspension to be transported onshore by the tide. The profile in this scenario becomes more concave due to the larger dominance of the waves.

5.1.1.2 Dam simulation

Figure 5.2 shows the bedlevel change after two years for the dam simulation. The black lines in the figure indicate the location of the dams. Largely the same cross-shore sedimentation and erosion patterns can be observed for the three baseline simulations (Figure 5.1). The larges difference in bedlevel change appears to be in the area behind the dams. The next subsection evaluates the difference in bedlevel change between the baseline and dam simulation to determine the effect of the dams.

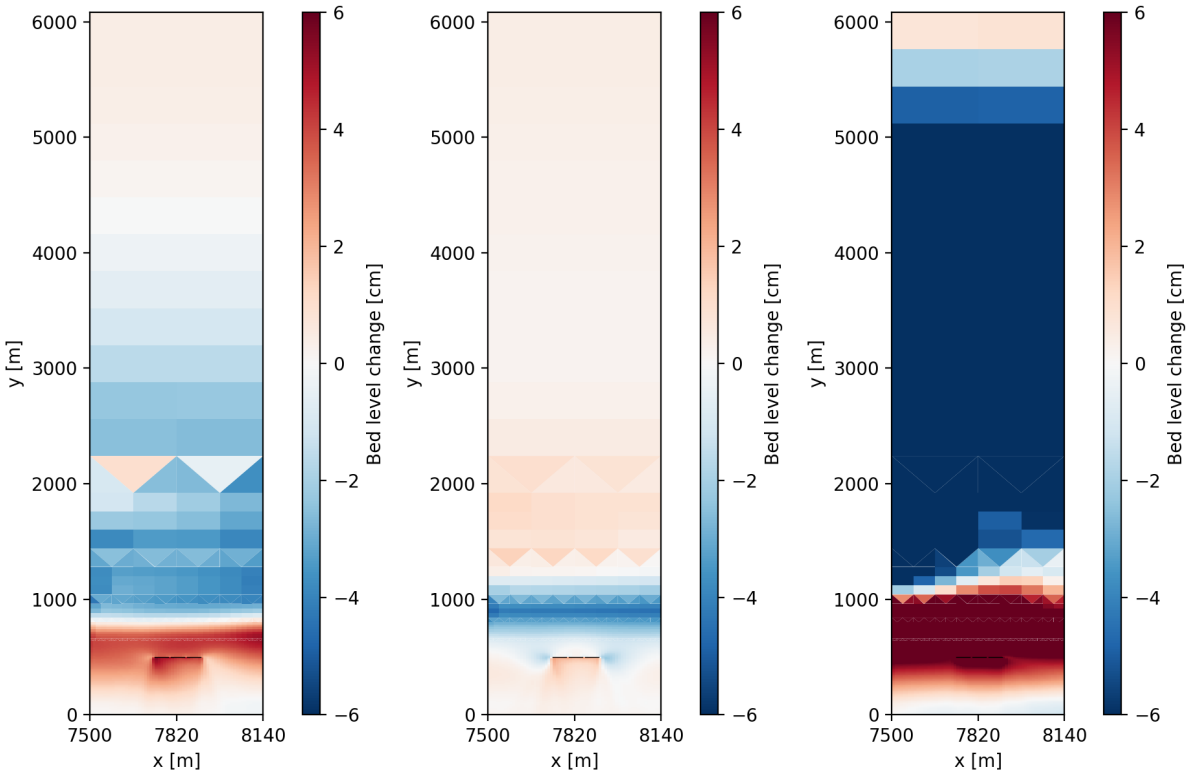

(a) 00-height: reference wave heights **(b)** 01-height: small wave heights **(c)** 02-height: large wave heights

Figure 5.2: The bedlevel change after two years for the dam simulation of each wave height scenario. The bedlevel development is plotted over the whole flow domain. The three black lines indicate the dam locations.

5.1.1.3 Dam effect

To determine the performance of the dams in case of a change in wave height the bedlevel change after two years for the baseline and the dam simulation are compared. Figure 5.1 shows the difference in bedlevel change between the baseline and dam simulation, which is called the 'dam effect'. The reference scenario and the small wave height scenario both show erosion on both sides of the dam setup. The effect of the dams on the bedlevel behind the dams is clearly visible in each scenario. All three scenarios show an increased deposition of fines in the area sheltered by the dams.

To estimate the influence of the change in wave height on the dam effect, the cross-shore (width-averaged) bed profiles behind the dams are plotted and shown in Figure 5.4. The upper plot presents the bedlevel profiles and the lower plot shows the effect of the dams (the difference between the bedlevels in the upper plot). The lower plots in Figure 5.4 show a peak in the dam effect: here the increase in bedlevel is largest. The total sedimentation behind the dams is determined by calculating the area underneath the curve in the lower plot. Table 5.1 gives the maximum value and the total change in bedlevel for each scenario. It can be seen that the dam effect is similar in case of the reference and large wave heights. In both scenarios the baseline simulation shows an increase in bedlevel on the tidal flat (behind the dams) already. The dams induce extra sedimentation behind the dams, for both scenarios similar. The small wave height scenario however shows a less overall bedlevel change.

Scenario	**Maximum change**	**Total change**	**Relative total change**
	$[cm]$	$[m^3/m]$	$[m^3/m]$ [-]
00-height	1.43	4.17	- 1.00
01-height	1.78	3.23	-0.94 0.77
02-height	1.92	4.26	+0.09 1.02

Table 5.1: The effect of the dams on the bedlevel change for each scenario of the wave height. The maximum dam-induced bedlevel change represents the peak of the curve in the lower plot in Figure 5.4. The total change of bedlevel is equal to the area underneath the curve. This is the dam-induced change of bedlevel over the area sheltered by the dams. The last column shows the bedlevel change relative to the reference scenario.

The interaction between erosion and deposition is governed by the bed shear stress (bed shear stresses that are higher than the critical bed shear stress induce erosion) and the sediment concentration (a high sediment concentration at first order means a larger deposition rate) respectively (see Appendix B). The difference between the

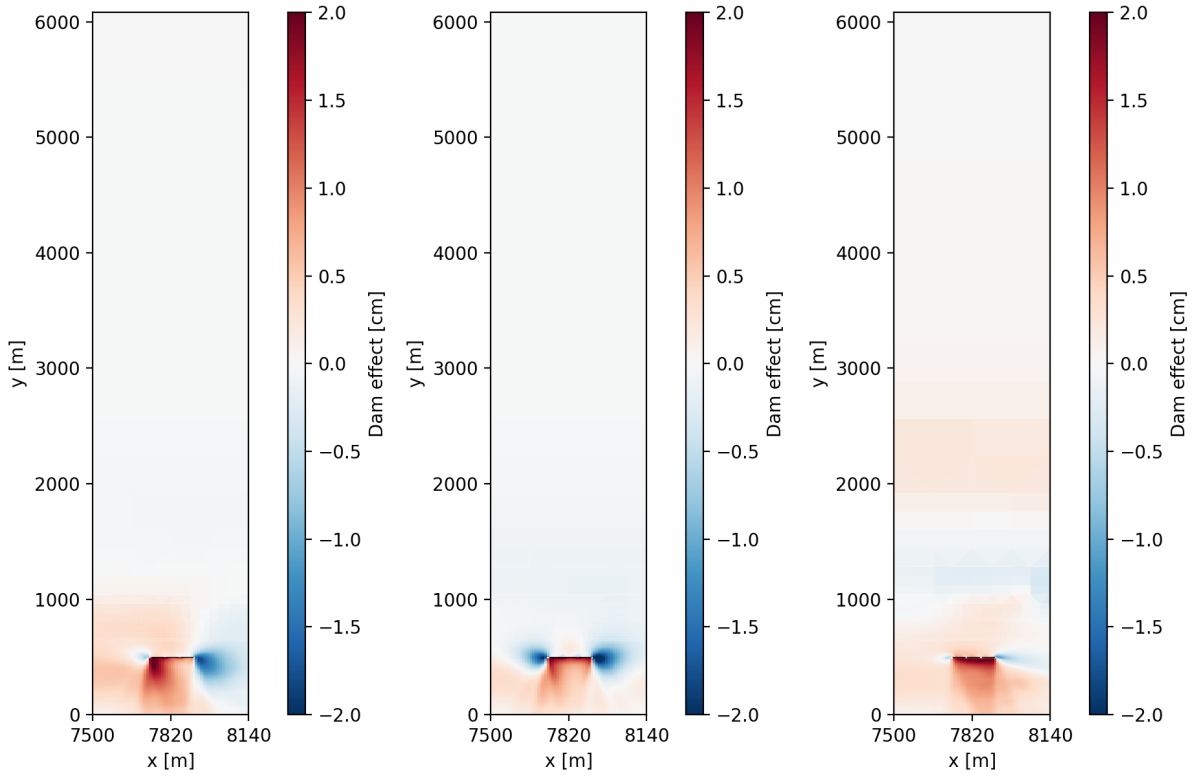

(a) 00-height: reference wave heights **(b)** 01-height: small wave heights **(c)** 02-height: large wave heights

Figure 5.3: The effect of the dams on the bedlevel for each wave height scenario. The dam effect is plotted over the whole flow domain. The three black lines indicate the dam locations.

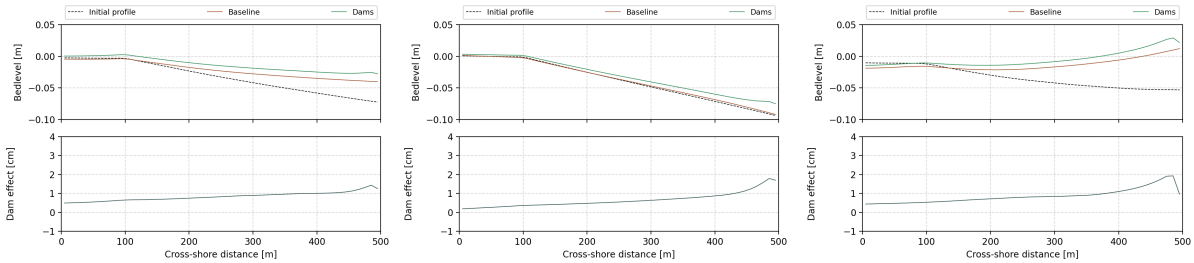

(a) 00-height: reference wave heights **(b)** 01-height: small wave heights **(c)** 02-height: large wave heights

Figure 5.4: Dam effect for each scenario by change in bedlevel. The upper plot includes bedlevel after two years for the baseline and dam simulation. The black dotted line represents the initial profile. The lower plot gives the difference between the bedlevel of the baseline and the dam simulation. The difference in bedlevel is the effect of the dams on the bedlevel development.

erosion flux and deposition flux determines net erosion or sedimentation: a change in bedlevel. Relating rate of bedlevel change to waterlevel, bed shear stress and SSC in Figure 5.6 gives insight in the conditions favourable for a net deposition flux.

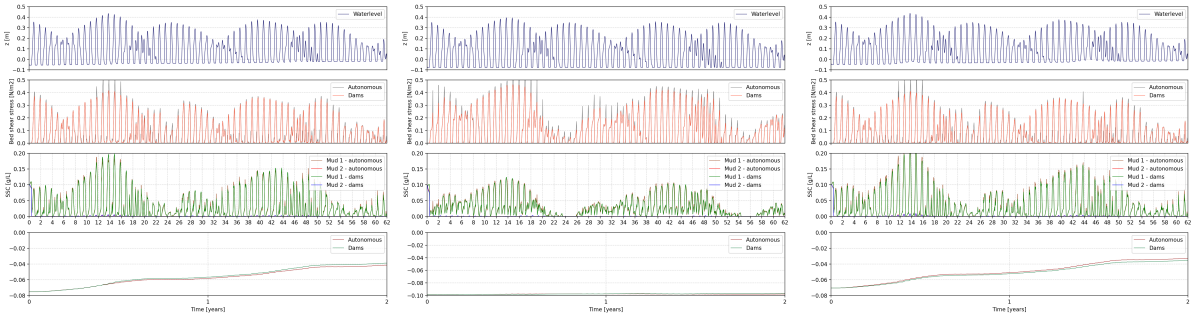

(a) 00-height: reference wave heights **(b)** 01-height: small wave heights **(c)** 02-height: large wave heights

Figure 5.5: The three upper plots show the waterlevel, wave-induced bed shear stress and the sediment concentration of the two mud fraction for each scenario, in front of the dams. The lower plot shows the bedlevel development in two years (morphological) at the same location. Note the y-axis of the bedlevel does deviate in each scenario.

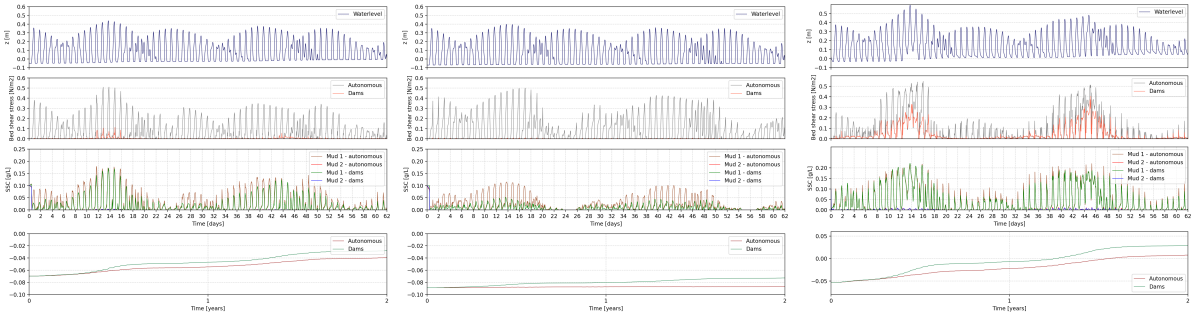

(a) 00-height: reference wave heights **(b)** 01-height: small wave heights **(c)** 02-height: large wave heights

Figure 5.6: The three upper plots show the waterlevel, wave-induced bed shear stress and the sediment concentration of the two mud fraction for each scenario, 20 meters behind the dams. The lower plot shows the bedlevel development in two years (morphological) at the same location behind the dams. Note the y-axis of the bedlevel does deviate in each scenario.

5.1.2 Wave direction

The three scenarios for the wave direction comprise the reference direction (0°), under an 45° angle and an angle of 90°. Table 4.3 gives the three scenarios. The baseline simulations (dams excluded) of all scenarios are evaluated first, followed by the dam simulations. The comparison between the baseline and dam simulation results show the effect of the dams and comes last.

5.1.2.1 Baseline simulation

Figure 5.7 shows the bedlevel change in two years when dams are excluded. The simulation with reference wave direction (shore-normal) (Figure 5.7a) shows an increase in bedlevel on the tidal flat, which is enhanced in case of oblique waves (Figure 5.7b). The third scenario includes waves refracting from 90° to almost shore-normal due to the mild slopes For the third scenario the bedlevel changes are less compared to the reference scenario, both in terms of deposition and erosion.

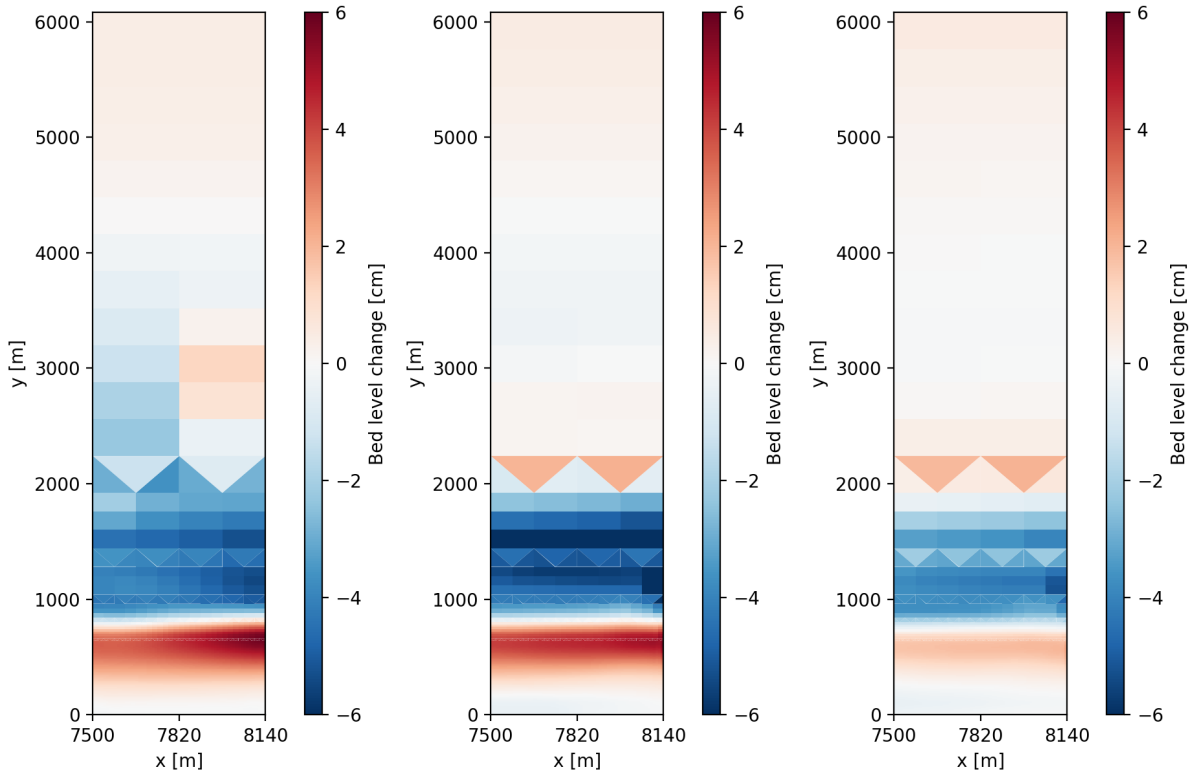

(a) 00-dir: reference wave direction **(b)** 01-dir: 45° wave angle **(c)** 02-dir: 90° wave angle

Figure 5.7: The bedlevel change after two years for the baseline simulation of each wave direction scenario. The bedlevel development is plotted over the whole flow domain.

5.1.2.2 Dam simulation

All three scenarios show a heightening of the bedlevel behind the dams in Figure 5.8. The pattern of sedimentation behind the dams differ, which is shown in Figure 5.9. The bedlevel change in the area behind the dams is given for each scenario. The reference scenario shows a more or less symmetric change in bedlevel, whereas the other incidence wave angles result in slightly more sedimentation behind the right dam; the direction of wave incidence.

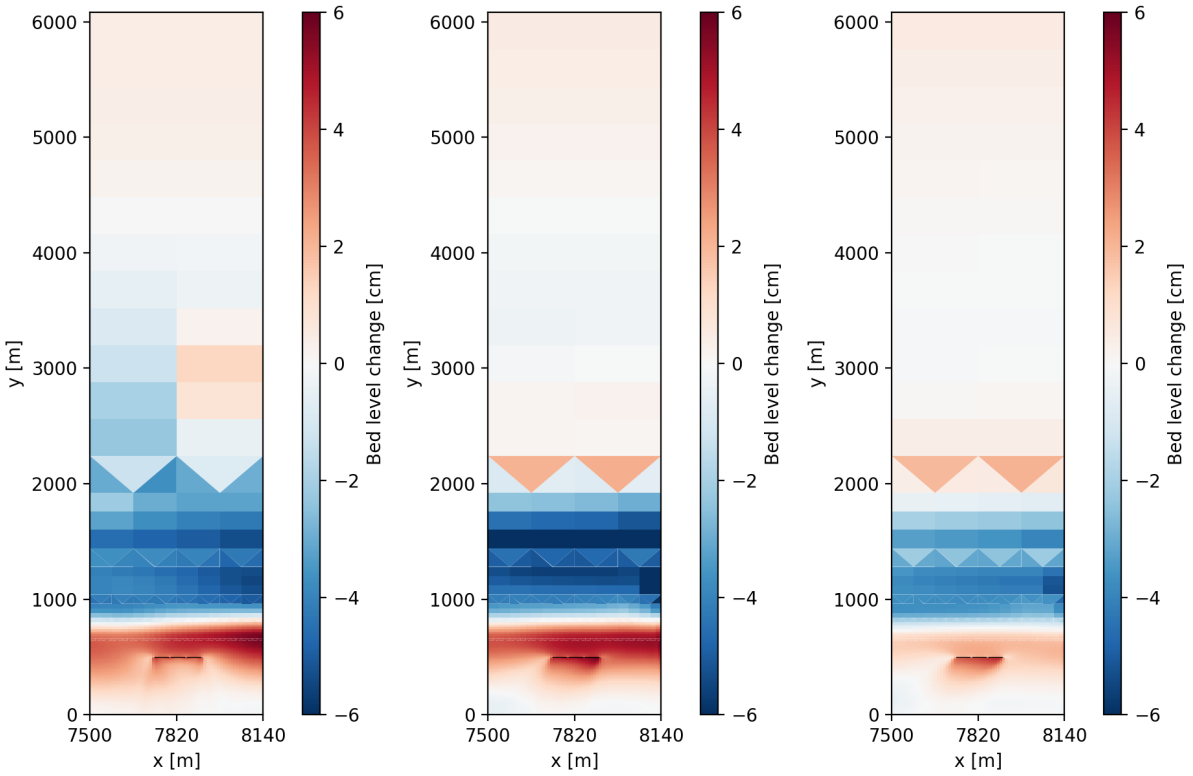

(a) 00-dir: reference wave direction **(b)** 01-dir: 45° wave angle **(c)** 02-dir: 90° wave angle

Figure 5.8: The bedlevel change after two years for the dam simulation of each wave direction scenario. The bedlevel development is plotted over the whole flow domain. The three black lines indicate the dam locations.

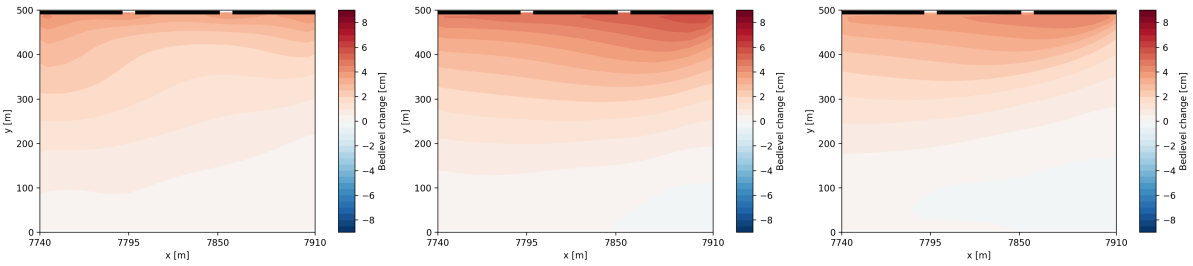

(a) 00-dir: reference wave direction **(b)** 01-dir: 45° wave angle **(c)** 02-dir: 90° wave angle

Figure 5.9: The bedlevel change behind the dams after two years for the dam simulation of each wave direction scenario. The bedlevel development is plotted for the area sheltered by the dams. The three black lines indicate the dam locations.

5.1.2.3 Dam effect

Figure 5.10 includes the effect of the dams in two years. The reference scenario shows approximately zero bedlevel change behind the dams, see Figure 5.10a. Figure 5.11a shows net erosion in the area right behind the dams, which transitions after 250 meters landwards to sedimentation. Erosion and sedimentation are balanced and total change of bedlevel behind the dams is approximately zero, see **??** for the calculation of total change of bedlevel. The explanation of a decrease in bedlevel is decreased suspended sediment transport due to the dams. Figure 5.13a shows dam-induced decrease of bed shear stress and SSC behind the dams. The lower SSC governs a net erosion flux. The reference wave height scenario simulates a shore-normal wave incidence but a 340° wind direction. This difference in wind direction results in larger dam-induced bedlevel change. Figure 5.6a shows around similar reductions in bed shear stresses, however during high water levels the dam-induced reduction in SSC is less than for wave direction reference scenario. This indicates a reduced sediment supply from offshore, transported by the tide, due to a reduced sediment transport around the structures if sediment transport direction is more perpendicular to the dams. Figure 5.12a shows the sediment concentration in front of the dams. Comparing the sediment concentration in front of the dams (Figure 5.12a) to the location behind the dams (Figure 5.13a) shows a decrease in SSC due to the dams. Since dam permeability is not considered in this model setup, higher dam-induced sedimentation is expected in reality. The permeability then allows for a sediment transport through

the dams.

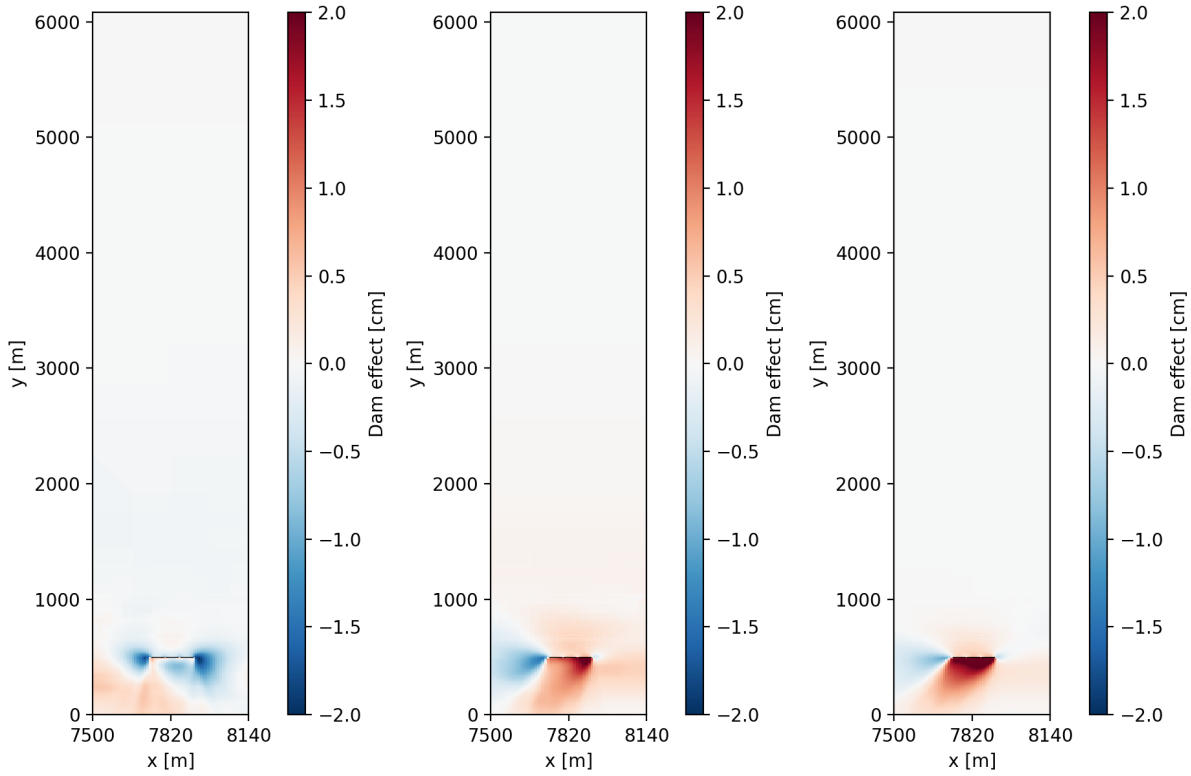

(a) 00-dir: reference wave direction **(b)** 01-dir: 45° wave angle **(c)** 02-dir: 90° wave angle

Figure 5.10: The effect of the dams on the bedlevel for each wave direction scenario. The dam effect is plotted over the whole flow domain. The three black lines indicate the dam locations.

Figure 5.10 shows an increase of dam effect for increasing wave angles. Baseline bedlevel change in the reference scenario (Figure 5.11a) is highest compared to bedlevel change for the baseline simulation in the other two scenarios. The bedlevel change behind the dams in two years for the baseline simulation decreases for an increasing wave angle. However, the effect of the dams increases for an increasing wave angle. Comparing the differences in dam-induced reduction of sediment concentration at the location in Figure 5.13, shows the largest dam-induced decrease of SSC for the reference scenario. In case of oblique waves (Figure 5.13b) the dam-induced reduction of SSC is less than for the reference scenario and the for 90° angle waves, there is almost no difference in SSC with and without dams. The 90° angle waves scenario shows a smaller reduction in bed shear stress due to the dams than in the reference and oblique waves scenario. The dams dissipate less wave energy, but also allow for a higher sediment flux relative to the baseline simulation. The dams are more effective for increasing wave angles if modelled with impermeable dams.

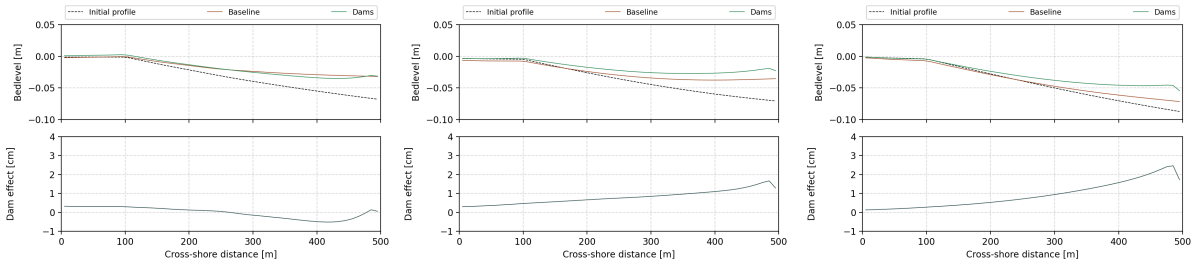

(a) 00-dir: reference wave direction **(b)** 01-dir: 45° wave angle **(c)** 02-dir: 90° wave angle

Figure 5.11: Dam effect for each wave direction scenario by change in bedlevel. The upper plot includes bedlevel after two years for the baseline and dam simulation. The black dotted line represents the initial profile. The lower plot gives the difference between the bedlevel of the baseline and the dam simulation. The difference in bedlevel is the effect of the dams on the bedlevel development.

Scenario	Maximum change $[cm]$	Total change $[m^3/m]$	$[m^3/m]$	Relative total change [-]
00-height	0.32	-0.07	-	1.00
01-height	1.66	3.98	+1.34	5.19
02-height	2.46	4.52	+2.14	7.69

Table 5.2: The effect of the dams on the bedlevel change for each scenario of the wave direction. The maximum dam-induced bedlevel change represents the peak in curve in the lower plot of Figure 5.11. The total change of bedlevel is equal to the area underneath the curve in the lower plot. This is the dam-induced change of bedlevel over the area sheltered by the dams. The last column shows the bedlevel change relative to the reference scenario.

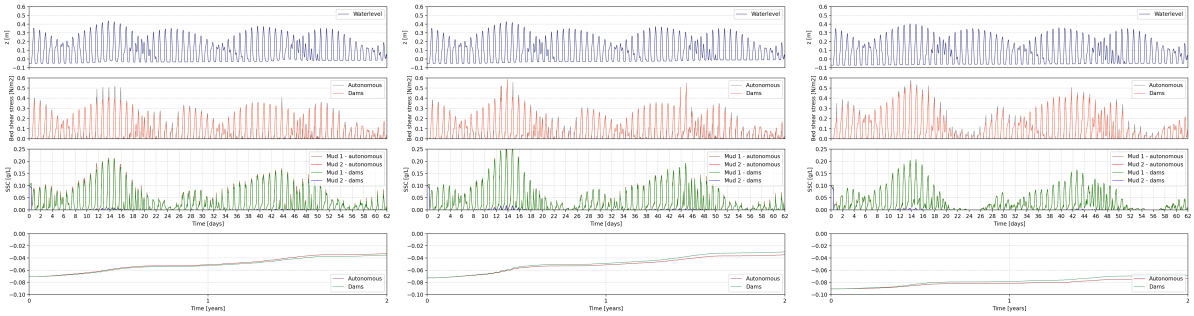

(a) 00-dir: reference wave direction **(b)** 01-dir: 45° wave angle **(c)** 02-dir: 90° wave angle

Figure 5.12: The three upper plots show the waterlevel, wave-induced bed shear stress and the sediment concentration of the two mud fraction for each wave direction scenario, in front of the dams. The lower plot shows the bedlevel development in two years (morphological) at the same location. Note the y-axis of the bedlevel does deviate in each scenario.

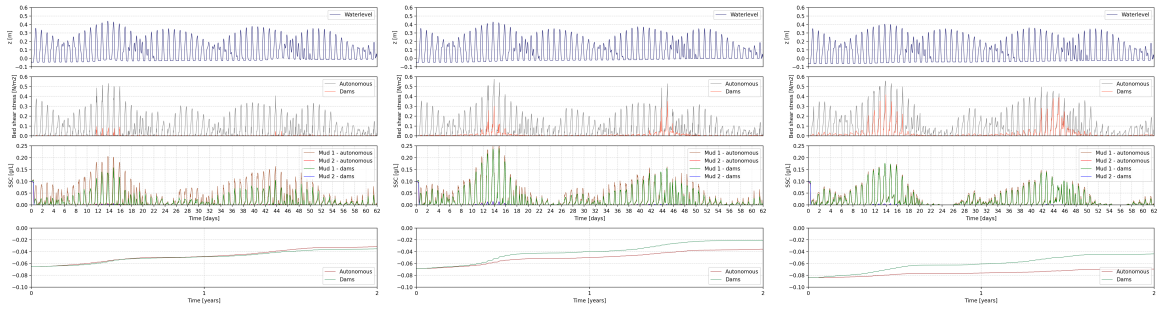

(a) 00-dir: reference wave direction **(b)** 01-dir: 45° wave angle **(c)** 02-dir: 90° wave angle

Figure 5.13: The three upper plots show the waterlevel, wave-induced bed shear stress and the sediment concentration of the two mud fraction for each wave direction scenario, 20 meters behind the dams. The lower plot shows the bedlevel development in two years (morphological) at the same location behind the dams.

5.1.3 Sediment input

The three scenarios for the suspended sediment input comprise the reference SSC (Pseudo-Neumann boundaries), half the PN SSC values and twice these values. Table 4.5 gives the three scenarios. The baseline simulations (dams excluded) of all scenarios are evaluated first, followed by the dam simulations. The comparison between the baseline and dam simulation results show the effect of the dams and comes last. The prescribed SSC boundaries are described in C.1 and are constant in time. Though the boundary condition varies along the lateral boundary, having a maximum around 1.2 km offshore.

5.1.3.1 Baseline simulation

The bedlevel change for each scenario is shown in Figure 5.14. The use of the pseudo-Neumann sediment conditions creates a stronger asymmetry about the y-axis in the bedlevel change than for the use of the normal Neumann sediment conditions. Figure 5.1a showed the bedlevel change resulting from the baseline simulation in the reference wave height scenario. This simulation is equal in forcing and parameters as the SSC reference scenario except here Neumann sediment boundary conditions are used. The bedlevel change resulting from the simulations using normal Neumann sediment boundary conditions are more or less symmetric about the y-axis. Section 4.3.3 described the Neumann sediment boundary conditions and its functioning. They can vary in time and are based on the sediment concentration in the inner grid cells. This way the Neumann conditions allow for some asymmetry in the sediment concentration. The same SSC values on both lateral boundaries does not allow for

longshore sediment transport, causing asymmetry about the y-axis if a longshore transport occurs.

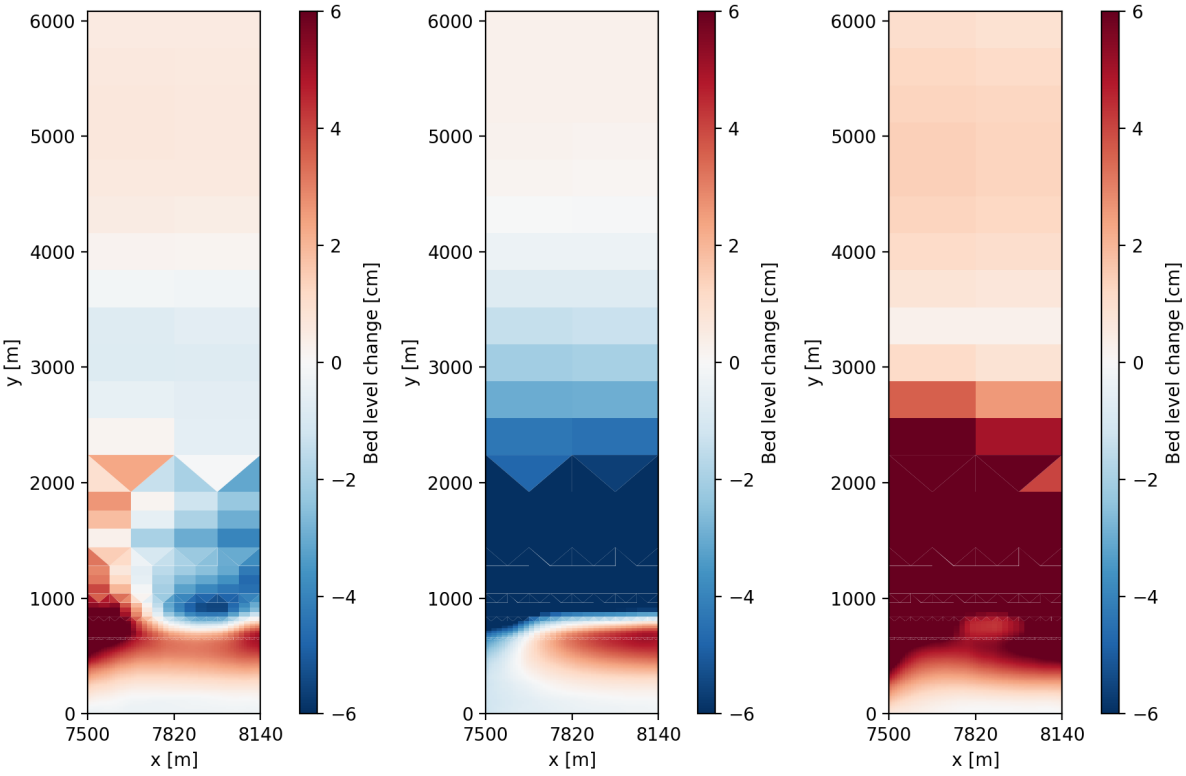

(a) 00-SSC: PN **(b)** 01-SSC: low sediment input **(c)** 02-SSC: high sediment input

Figure 5.14: The bedlevel change after two years for the baseline simulation of each SSC input scenario. The bedlevel development is plotted over the whole flow domain.

Lowering the sediment input results in stronger erosion around and in the breaker zone (Figure 5.14b), compared to the reference simulation (Figure 5.14a). Figure 5.15 shows the bedlevel, waterlevel, bed shear stress and sediment concentration at the western boundary (1.5 km offshore) for the reference scenario (Figure 5.15a) and the low SSC input scenario (Figure 5.15b). The spin up of both scenarios creates the difference in bedlevel at the start; the low SSC input scenario shows a lower bedlevel than the reference simulation, indicating erosion already occurred there. The bed shear stresses for the low input scenario are larger and exceed 0.1 and 0.5 N/m^2 more often than in the reference simulation. The sediment concentrations are lower, indicating less sediment supply to this region or an outgoing flux of re-entrained sediment. The combination of higher shear stresses and lower sediment concentration increases the erosion flux and decreases the deposition flux, causing net erosion. The profile steepens and becomes more concave: a retreating profile.
A higher sediment input causes sedimentation, especially in the area where wave dissipation is largest (between 500 and 2000 m from the land boundary). Figure 5.16 shows the waterlevel, bed shear stress and sediment concentration at the same location on the western boundary (1.5 km offshore) for high sediment input scenario. Comparing the high sediment input scenario with the reference scenario gives much higher sediment concentrations at this location for the higher sediment input scenario. The SSC settles when the water level and bed shear stress decrease. The bedlevel development reduces the water depth and the wave attack even more, allowing the high sediment input from the boundary to settle.

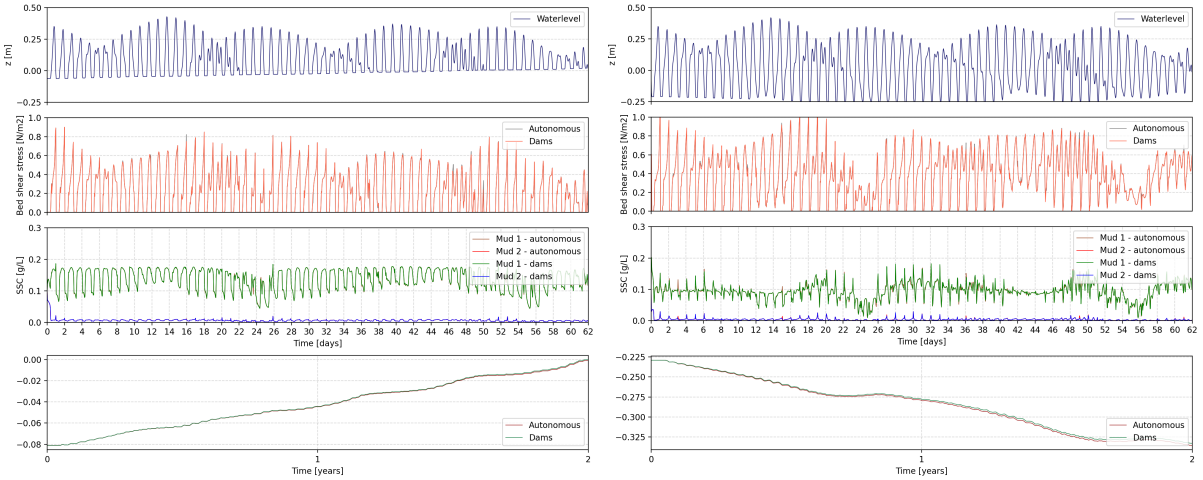

(a) 00-SSC: PN **(b)** 01-SSC: low sediment input

Figure 5.15: The three upper plots show the waterlevel, wave-induced bed shear stress and the sediment concentration of the two mud fraction for the reference and low sediment input scenario, 1.5 km offshore. The lower plot shows the bedlevel development in two years (morphological)

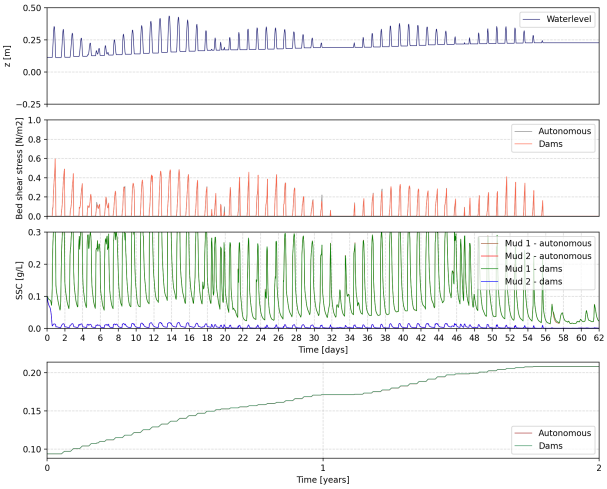

Figure 5.16: The three upper plots show the waterlevel, wave-induced bed shear stress and the sediment concentration of the two mud fraction for high sediment input scenario, 1.5 km offshore. The lower plot shows the bedlevel development in two years (morphological)

5.1.3.2 Dam simulation

Figure 5.17 shows the bedlevel development for each sediment input scenario when dams are included. In all three scenarios sedimentation occurs behind the dams. The next subsection will elaborate on the effect of the dams.

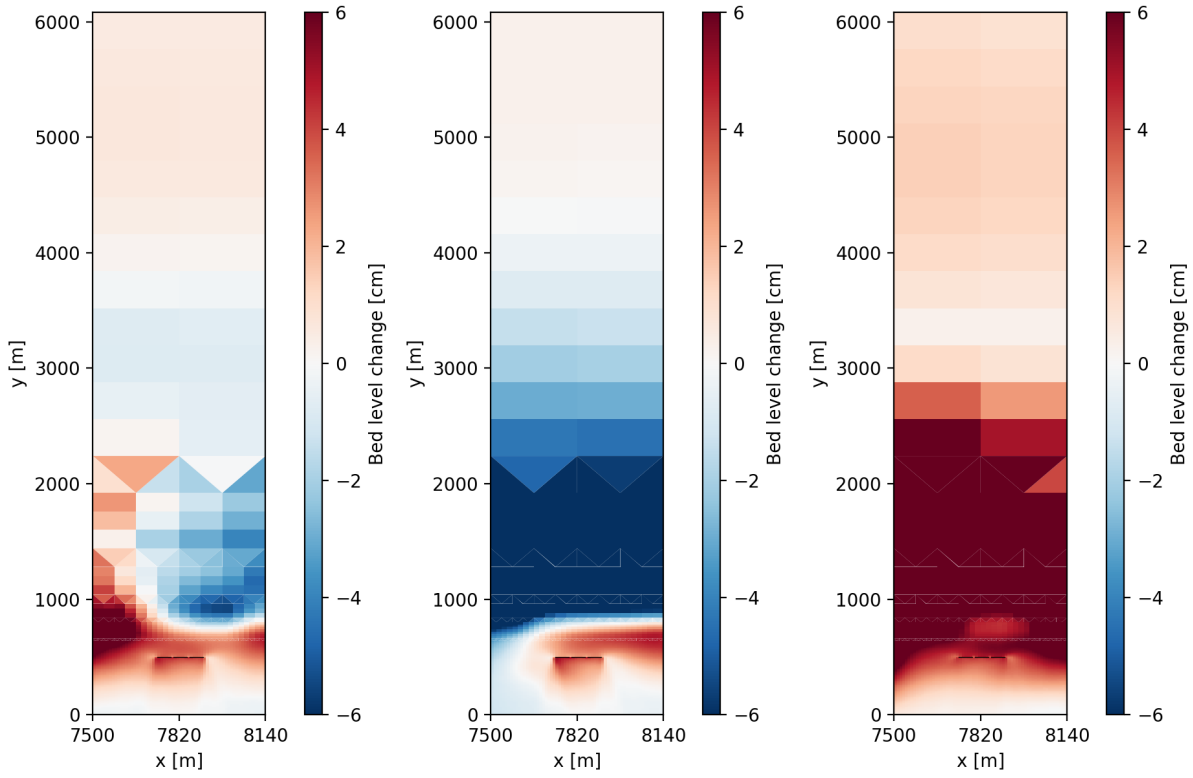

(a) 00-SSC: PN **(b)** 01-SSC: low sediment input **(c)** 02-SSC: high sediment input

Figure 5.17: The bedlevel change after two years for the dam simulation of each SSC input scenario. The bedlevel development is plotted over the whole flow domain. The three black lines indicate the dam locations.

5.1.3.3 Dam effect

The difference in bedlevel development between the baseline and the dam simulation is given in Figure 5.18 and represents the effect of the dams. Stronger dam-induced sedimentation occurs in case of low sediment input compared to the reference scenario, whereas the dams show almost no effect for a high sediment input. Figure 5.19 gives the bedlevels after two years for each scenario in the upper plot. The lower plot includes the effect of the dams. Evaluating the upper plots and comparing the baseline bedlevel (red curve), indicates that an increase in sediment supply already causes the bedlevel to increase. The effect of the dam becomes negligible since the profile is already restoring due to the higher sediment supply. Figure 5.21c shows the decrease in bed shear stress over time and the high sediment concentration at 20 m behind the middle dam for the baseline simulation. The dams influence the bed shear stress and a decrease in bed shear stress due to the dams can be seen. However, a decrease in sediment concentration can be seen. When the sediment supply suddenly decreases (e.g. a nearby mouthing river is dammed), represented by the low sediment input scenario, the baseline bedlevel lowers compared to the reference sediment input. The efficacy of the dams then increases.

The bed shear stress over time for is decreased by the dams in each scenario (Figures 5.21a, 5.21b and 5.21c). However, relatively the dams decrease the bed shear stress for the low sediment input scenario the most and for the high sediment input scenario the least. The high sediment input scenario (Figure 5.21c) shows an decrease in bedlevel while the dams decrease the bed shear stress favoring deposition at that location. The decrease of sediment concentration due to the dams determines the bedlevel development. The lower sediment concentration can be the result of a decreased sediment flux onshore or less re-entrainment of sediment due to a decrease in bed shear stress.

Scenario	**Maximum change**	**Total change**	**Relative total change**
	$[cm]$	$[m^3/m]$	$[m^3/m]$ [-]
00-SSC	1.53	3.46	- 1.00
01-SSC	2.02	4.92	+1.46 1.42
02-SSC	0.29	0.03	-3.43 0.01

Table 5.3: The effect of the dams on the bedlevel change for each SSC input scenario. The maximum dam-induced bedlevel change represents the peak in Figure **??**. The total change of bedlevel is equal to the area underneath the curve in Figure **??**. This is the dam-induced change of bedlevel over the area sheltered by the dams. The last column shows the bedlevel change relative to the reference scenario.

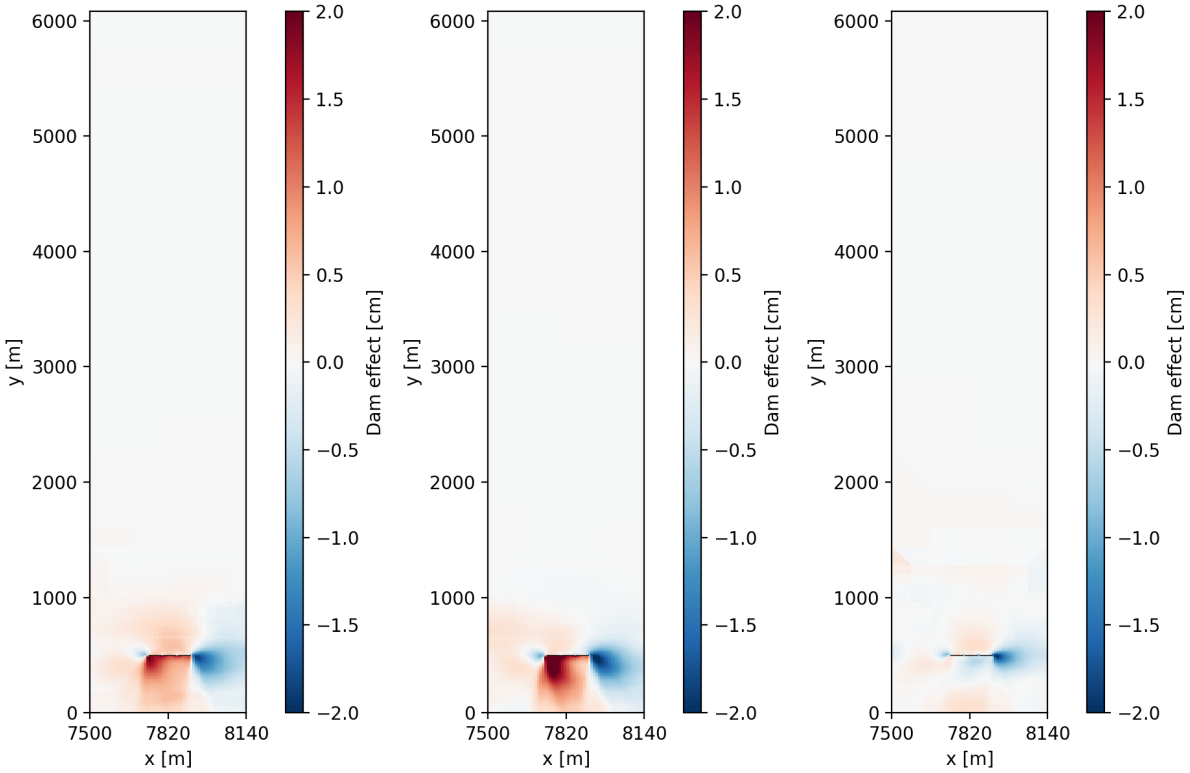

(a) 00-SSC: PN **(b)** 01-SSC: low sediment input **(c)** 02-SSC: high sediment input

Figure 5.18: The effect of the dams on the bedlevel for each SSC input scenario. The dam effect is plotted over the whole flow domain. The three black lines indicate the dam locations.

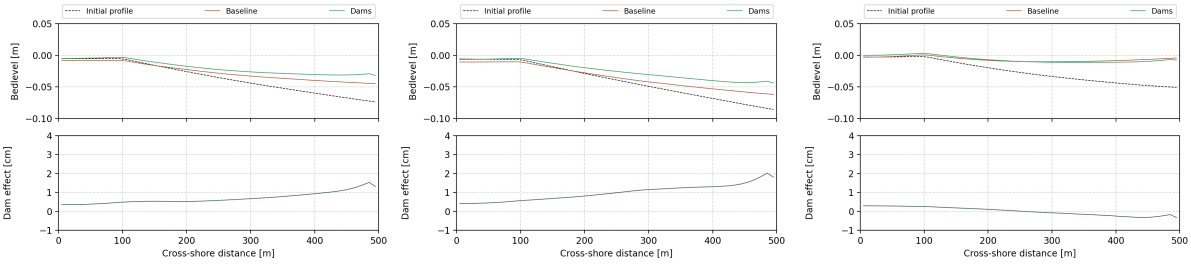

(a) 00-SSC: PN **(b)** 01-SSC: low sediment input **(c)** 02-SSC: high sediment input

Figure 5.19: Dam effect for each SSC input scenario by change in bedlevel. The upper plot includes bedlevel after two years for the baseline and dam simulation. The black dotted line represents the initial profile. The lower plot gives the difference between the bedlevel of the baseline and the dam simulation. The difference in bedlevel is the effect of the dams on the bedlevel development.

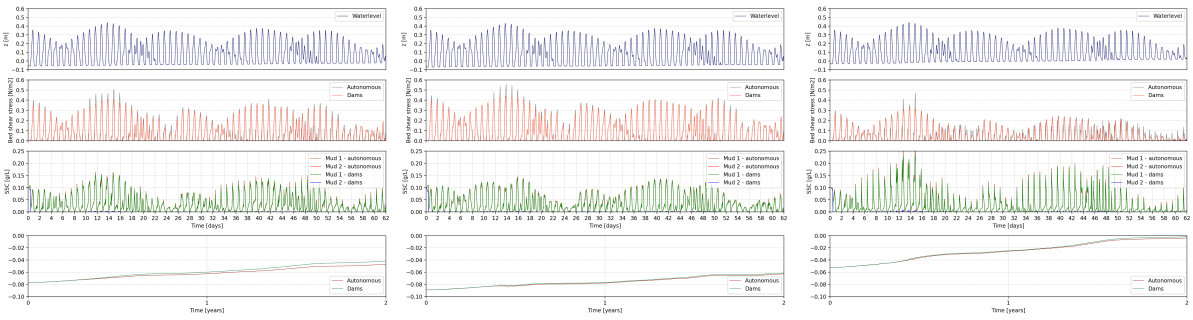

(a) 00-SSC: PN **(b)** 01-SSC: low sediment input **(c)** 02-SSC: high sediment input

Figure 5.20: The three upper plots show the waterlevel, wave-induced bed shear stress and the sediment concentration of the two mud fraction for each sediment input scenario, in front of the dams. The lower plot shows the bedlevel development in two years (morphological) at the same location. Note the y-axis of the bedlevel does deviate in each scenario.

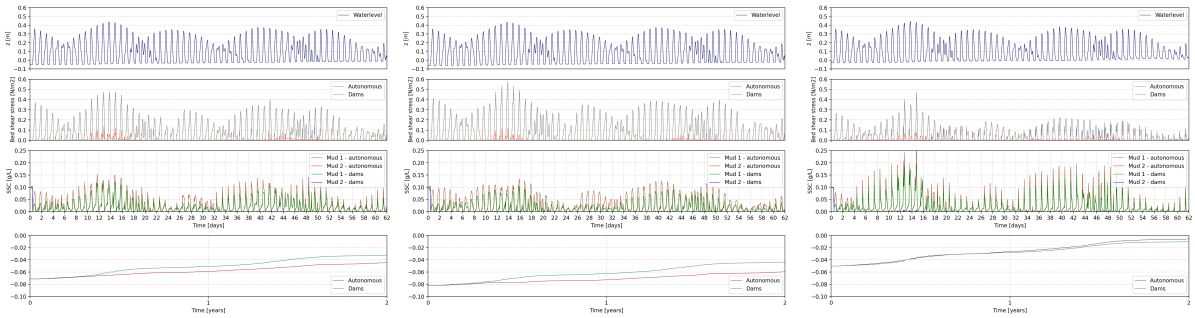

(a) 00-SSC: PN **(b)** 01-SSC: low sediment input **(c)** 02-SSC: high sediment input

Figure 5.21: The three upper plots show the waterlevel, wave-induced bed shear stress and the sediment concentration of the two mud fraction for each SSC scenario, 20 meters behind the dams. The lower plot shows the bedlevel development in two years (morphological) at the same location behind the dams.

6

Discussion

This chapter discusses the results described in Chapter 5. It includes an interpretation of the results and defines the limitations of the model. Section 6.1 includes the model limitations, followed by Section 6.2.1 which describes the influence of a change in physical parameters on the dam performance. Section 6.2.2 introduces practical implications for future dam designs. Improvements on the modelling approach to upscale the approach to different case studies are discussed in Section **??**. The last section, Section **??** evaluates possible long term impacts of the dams.

6.1 Limitations of the model

6.1.1 Data

As mentioned in earlier modelling or field studies (Borsje, 2017; Smits, 2019) the scarcity of the data in the coastal region of Demak makes the calibration and validation of numerical models setup for analysis of the coastal region of Demak complex. Model outcomes cannot be completely verified by accurate and extensive datasets and often outcomes are validated by expert judgement. This study uses the data from the field modelling study of Smits (2019) to setup and validate the simplified model setup of Demak. Due to data scarcity in the coastal area of Demak, the modelling study by Smits (2019) is also validated by expert judgement and limited available data.

6.1.2 Model simplifications

In order to quickly assess the performance of structures on any coastal site the model setup requires many simplifications.

SSC boundary conditions To run model simulations with prescribed SSC boundary conditions they should replace the Neumann sediment boundary conditions. However, since the lateral boundaries of the flow domain are really close to the area of interest to reduce computation time the prescribed SSC boundary conditions influence the sedimentation/erosion pattern in the area of interest significantly. When no data is available on the spatial variety of the SSC in the area there is no information on the values for the SSC boundary conditions either. For the case study in Demak the Neumann sediment boundary conditions deemed to give realistic outcomes, as it is assumed that the prominent source of sediment in the coastal area of Demak is from locally stirred up sediments from the bed by waves. (Smits, 2019). However, in case of high sediment inputs from rivers, such as in Vietnam or Suriname, a sediment input needs to be prescribed. In this study the sediment input was simulated by multiplying the PN boundary conditions by a certain value. Some limitations arise related to this PN boundary condition though. Firstly, the Neumann sediment boundary condition for the left flow boundary shows different time-average SSC values than for the right boundary. The PN boundary condition, however, results from averaging the SSC values of the right and left boundary and is applied to both boundaries. Figure 5.1a shows an almost symmetrical cumulative sedimentation/erosion pattern over the longshore direction, while Figure 5.14a shows an asymmetrical cumulative sedimentation/erosion pattern in the longshore direction. The left PN boundary condition should include somewhat lower SSC values and the right PN boundary condition somewhat higher SSC values, to approach the Neumann sediment boundary conditions better. Although the sedimentation/erosion pattern is deviating from symmetrical in the longshore direction due to the estimated PN boundary conditions,

the longshore-average profile of the flow domain for both scenarios are approximately equal and the performance of the dams also shows around the same results. In order to reduce the impact of the inaccuracies due to the PN boundary conditions they could be made different from each other or to reduce the sensitivity of the model to the SSC boundary conditions the lateral boundaries could be chosen further away from the area of interest. Though, extending the flow domain in the lateral direction will increase the computation.

Equilibrium profile Section C.2 describes the modelling of an the equilibrium bedlevel profile using the conditions for Demak (Section 4.3). A stable profile was found after 30 hydrological months. Modelling stable spin up profiles for each scenario would therefore require a lot of computation time. Since permeable dams are supposed to restore erosive coastlines which are not in equilibrium, a non-equilibrium spin up profile was used. The initial non-equilibrium profile is concave and includes a tidal flat, based on the equilibrium profile derived in section C.2 and the current morphological conditions in Demak (Section 3.2). Modelling different boundary conditions (e.g. sediment input, wave height) with a non-equilibrium profile represents a sudden change of the boundary conditions in a real coastline situation. The short term results derived with this modelling approach do not directly describe dam performance on different coastlines. The results of the modelling in Demak can be extrapolated to changes in boundary conditions at other coastlines. This is discussed in Section 6.2.

Thin dams The flow module of Delft3D-FM does not have an option to include permeable structures, so the permeable dams were modelled as thin dams. Thin dams are impermeable and force the flow to go around the structures while blocking any sediment transport through the dams. Borsje (2017) states that permeability of the dams is certainly influential on the flow pattern around the dams. However, exact influence of the permeability of the dams on the flow is still largely unknown and needs future investigation. Current research involving permeable dams modelled by thin dams show realistic results related to sedimentation behind the structures (Smits, 2016, 2019). In this research permeable structures were modelled as thin dams. It showed realistic values for the dam effect.
The results in dam effect for varying incoming wave angles show an increase in dam effect for increasing wave angles. Although the dams showed a larger reduction in bed shear stress for shore-normal waves than in case of a 90° wave angle, a larger reduction in suspended sediment concentration was found too. This indicates influence of impermeability of the thin dams in the model results.

6.1.3 Model performance

Despite limited possibility for validation due to scarcity of data in the region of interest and a strongly idealised model setup, the model outcomes show bedlevel developments behind the dams in the same order of magnitude as for the model by Smits (2019).
However, asymmetrical patterns of sedimentation and erosion occur around the y-axis (cross-shore), even with forcing directed perpendicular to the coast (waves with shore-normal incidence, wind direction perpendicular to the coast and an offshore uniform tidal boundary with parallel orientation to the coast) and an alongshore uniform bedlevel. This asymmetry in sedimentation/erosion is caused by asymmetry in the current direction. The quality of the computational grid determines to great extend the quality of the model and an explanation for the deflecting flow velocity could be found herein. In the offshore part of the flow domain (between the offshore boundary and 2000 m from the landward boundary) the width comprises two grid cells of 320 x 320 m. The grid refines towards the coast to a cell size of 10 x 10 m (Figure 4.2b). The current deflection arises around transitions between grid cell sizes, especially the transition from 320 m to 160 m grid cell size. The smoothness of the grid at transitions is 2.0 at the cell edges, while maximum smoothness values should be 1.4 (Luijendijk, 2011). Another reason for the flow velocity to be longshore directed could be the presence of just one cell edge between the two lateral boundaries in the offshore zone. As D-FLOW FM uses an first order interpolation scheme for the discretization of the convective terms, inaccuracies due to numerical diffusion can happen if the computational grid is too coarse. A small deviation in the direction of the flow perpendicular to the coast can cause inaccurate longshore flow directions due to only one transition between the two lateral flow boundaries. Refining the grid in the offshore part of the flow domain (where only two grid cells are apparent for this research) could decrease the inaccuracies due to numerical diffusion. The computation time, however, must be considered too and is limited due to the application of the model to quickly assess dam efficacy for different coastal sites. Considering the limited computation time, the flow domain could be reshaped and be extended in width while made smaller in cross-shore direction.

6.2 Upscaling to other mangrove-mud coasts

The intention behind the strongly idealised model is to investigate possibilities of permeable dam implementation at other erosive coastlines. This section evaluates the results from Chapter 5 in terms of dam performance in

case of changing boundary conditions and to find practical implications for the dam design. It concludes with a description of model improvements to use in future upscaling assessments.

6.2.1 Influence of physical parameters on dam performance

The wave height, wave direction and sediment input at the boundary were varied independently to study effects of a change in individual boundary conditions on the efficacy of permeable dams. The three dams are located on a tidal flat 500 m offshore of the land boundary. Chapter 5 includes the model outcomes on dam-induced bedlevel development.

An increased wave height results in stronger net deposition at the tidal flat (Figure 5.4c). Sediment is brought in suspension at offshore locations by waves and transported by flood tidal currents towards the coast. It settles at the tidal flat due to a low water depth during high tide. Deposition at the tidal flat in the baseline simulation occurs for each wave height scenario, but deposition increases in case of higher wave heights and decreases for lower wave heights. The effect of the dams for different wave heights is more or less the same. Dams more effectively decrease the bed shear stress for the low wave height scenario, but also reduce the sediment concentration (Figure 5.5b and Figure 5.6b). In case of high wave heights the dams are less effective in decreasing the bed shear stress. However, they allow for a larger onshore sediment transport. So, a change in wave height won't affect the dam performance significantly. Larger wave heights induce a larger sediment transport towards the coast, where it is partly trapped behind the dams. Lower wave heights reduce bed shear stresses more effectively, but reduces the sediment transport towards the coast. Table 5.1 indicates approximately equal dam effects for either low or high wave heights (or reference heights). This means that in case of a change in wave climate (height), the dams do not necessarily perform worse or better. Following a different line of reasoning; placing the dams in a situation where the wave height is decreased or increased is equally effective. So, decreasing the wave height in a coastal area and placing dams would offer good support to restore a convex profile.

In the wave direction scenarios the dam effect increases for increasing wave angles (shore-normal to shore-parallel). Shore-normal waves reduce the bed shear stress effectively, but reduce the sediment transport towards the coast at the same time. The dam effect shows a decreased bedlevel directly behind the dams and an increased bedlevel further onshore. The net change in bedlevel is zero. When the wave angle increases, reduction of bed shear stress by the dams is less effective, but the sediment concentrations show less reduction due to the dams. Bedlevel change in the baseline simulation of the reference scenario is largest and decreases for increasing wave angles. The dams show a higher efficacy when the wave direction is least favourable in the baseline simulation.

Reducing the nearshore sediment supply induces erosion in the breaker zone and a more concave profile shape. Sedimentation on the tidal flat keeps occurring, but reduces. The profile offshore of the tidal flat boundary steepens and an increase in bed shear stress at the location of the dams is found (baseline simulation). The effect of the dams, however, increases. The reduction in bed shear stress is larger for the low sediment input scenario compared to the reference scenario. When the sediment supply is increased the results show an increase in bedlevel in the breaker zone. The bedlevel profile becomes more convex. The high sediment input is already efficient enough to restore the coastal profile and the dam performance reduces to almost zero. Installing the dams in these conditions would not have much effect.

To study seasonal effects in Demak or other coastal areas the boundary conditions should be varied simultaneously. For example, the wave height should be altered together with the sediment input to simulate wet or dry season more accurately.

6.2.2 Practical implications for design

The dam location in the simplified model setup is on the tidal flat, 500 m offshore of the land boundary. Around 1000 m offshore of the land boundary a tidal flat boundary is characterized; the profile slope increases from 1:4000 to 1:550 at this location. The profile shape is shown in Figure 4.4. The results from Chapter 5 can be used to suggest design implications for permeable dams. Note that the implications are based on the initial profile used for this model setup.

Wave height Increased wave heights favour a concave profile shape. Figure 5.1c shows the increase in bedlevel at the tidal flat and in erosion offshore, causing the profile to steepen in case of large wave heights. Placing the dams at the tidal flat will induce extra bedlevel development, but will not reduce erosion offshore. This enhances the concave profile shape. Placing the dams more offshore of the tidal boundary, would reduce bed shear stresses where wave dissipation is higher. It should be noted however, that the wave heights could be too large and the dams loose their efficiency in reducing bed shear stresses. This depends on the erosion state of the profile and the wave heights at that site.

Tide-dominance enhances convex profile shapes and a smaller wave height favours this. The bedlevel change in the baseline simulation for the small wave height scenario in Figure 5.1b shows the erosion at the tidal flat boundary and the deposition onshore and offshore of this boundary. This creates a more convex profile shape.

In this scenario, the dams showed a great efficiency in reducing bed shear stresses, but also reduced the onshore sediment transport flux. Favouring the redistribution of the sediment that creates a more convex profile, the dams should be placed relatively close to the coastline. The erosion of the tidal boundary will create a smoother (convex) profile and thus this area of wave dissipation is not useful for dam placement. Closer to the coast the dams can efficiently reduce the bed shear stress while at the same time allowing the sedimentation offshore of the tidal boundary to smoothen the profile.

6.2.3 Model improvements

The simplified model setup is based on quick assessment of dam performance at different coastal regions globally. This requires simplifications as explained in Chapter 4 to control computation times. However, improvements are necessary for model use in different muddy areas as Vietnam and Surinam. The first paragraph elaborates on these improvements. The paragraphs that follow include physical processes or features which could give a more complete assessment of the dam performance. These improvements will increase computation time.

Computational grid Large differences between coastal sites as Demak and other sites like Vietnam or Surinam are, amongst others, sediment input and wind/wave direction. Since the computational grid for the flow domain is rather small in width, the morphology is really sensitive to lateral SSC boundary conditions. Using the simplified model setup for regions in Vietnam and Surinam requires improvement of the flow grid. Widening the flow domain reduces the sensitivity to the prescribed lateral SSC boundary conditions. To avoid a larger grid with long computation times, the length of the flow domain can be reduced. If more accurate data on the spatially varying suspended sediment concentration is available, the flow domain can be kept small in width.

Fluid mud Wave dissipation over fluid mud is not included in the simplified model setup. Following Winterwerp et al. (2007), dissipation due to fluid mud can be extensive and an important factor in the energy decrease of incoming waves. The wave input used for this model setup is based on the wave data analysis by Smits (2016); BioManCo (2018) and involves offshore wave data. There is no validation on the wave height at the location of the dams. Modelling wave propagation at Demak including the influence of fluid mud could increase accuracy in wave modelling (Smits, 2020).

Cheniers Section 3.2 includes an explanation on cheniers and their presence in the coastal area of Demak. These small strokes of sand along the coast causes part of the incoming wave to break, dissipating part of the wave energy before these waves reach the coast. This shelters part of the coast from higher wave attack (Smits, 2019; Muskananfola et al., 2017; van Domburg, 2018). The simplified model setup does not include cheniers in the bathymetry. Including the cheniers will improve the quality of the bathymetry.

Vegetation The current model setup does not account for the influence of vegetation on the hydrodynamics and sediment dynamics. Section 2.1.1 explains the ability of vegetation to increase flood protection and bedlevel elevation. Since the coasts to be modelled with the simplified model are erosive and involve degraded mangrove forests a bare mudflat is assumed. However, modelling the development of vegetation on the mudflat would increase knowledge on the ability of permeable dams to restore mangrove forests.

7

Conclusions and Recommendations

This research studied the effect of a change in boundary conditions on the dam performance. Section 7.1 answers the sub-research question in order to conclude to the main research question, which is restated below. To study these effects, a simplified 2DH process-based model was set up. The model setup can easily be adapted to include the broad spectrum of boundary conditions of different coastal sites. Recommendations on model improvements and extensions for future use at different coastal sites are given in Section 7.2.

Which erosive mangrove-mud coasts could benefit from permeable coastal structures?

7.1 Conclusions

This section describes the conclusions on the research outcomes based on each sub-research question.

Which mangrove coasts qualify for the assessment on dam functioning, based on the local boundary conditions and the pilot project in Demak?

Various erosive mangrove-mud coasts were analyzed to formulate the coastal systems that could benefit from permeable dam implementation to rehabilitate mangrove forests and restabilize the coastline. The developed model in this research aimed for assessment on sites where mangroves had degraded or were degrading and where the coastline was in a prolonged erosive state. The three pilot projects in Demak (Indonesia), Soc Trang (Vietnam) and Weg naar Zee (Suriname) offer insight in conditions related to erosive mangrove-mud coasts. Large differences between these sites can be found in tidal regime, wave climate and sediment supply.

How can the coastal characteristics of Demak and other evaluated sites be schematized in a general model setup?

Several aspects determined the requirements for the model setup. Firstly, the modelling of the permeable dams required a 2D model setup as the dams can only be modelled as thin dams in Delft3D-FM. Thin dams are impermeable and water flows around the structures. Also, the longshore currents and wave directions in Vinh Tan (Vietnam) and Weg naar Zee (Suriname) cannot be captured in a 1D model setup. Modelling the permeable dams as vegetation in 1D would cancel out the option of modelling longshore transports. Three dams are placed along side each other, having a length of 50 m and a gap between each dam of 10 m, representing the dam setup in the field in Demak. Secondly, the aim of the simplified model is to study the short-term effects of a change in boundary conditions on the dam performance. The model setup is created based on the extension to apply the setup for other coastline characteristics too. This increases involvement of a broad spectrum of boundary conditions and coastal site properties. As the variety of model input is large, the model setup must be simplified in order to reduce computation times. Process-based models tend to increase heavily in computation time with complexity of the model. Ideally simplicity would be obtained by a 1D model setup, but the permeable dams and the longshore transports require a 2DH model. Simplifying the bathymetry is done with an alongshore uniform bedlevel. The computational grids of the flow domain and the wave domain are refined in the area of interest

(area behind the dams) to model the sedimentation behind the dams and the gap of 10 m between the dams, but become coarser further away from the dam location. The flow domain has a width of 640 m, to enable free flow around the dams, and from the coastline extends 6000 m offshore. The wave domain is 20 by 20 km to ensure the waves at the boundary are still unaffected by the water depth and that errors due to inconsistent wave boundary conditions are not travelling into the flow domain.
Thirdly, the research on different coastal sites, covering the first sub-research question, led to requirements for the model setup especially related to boundary conditions. The sediment availability in Demak is from locally stirred sediment by waves and Neumann boundary conditions for the mud fractions suffice. However, at the coastal sites in Vietnam and Suriname high concentrations of sediment are transported along the coast. This requires a prescribed sediment concentration at the boundaries to ensure inflow of suspended sediment. Due to the small width of the flow domain the model showed a high sensitivity to the lateral SSC boundary conditions. This means that accurate data of sediment supply data will be necessary for modelling sites with other sediment sources than locally stirred up sediment.
The simplified model setup is tested and validated for Demak. Improvements on the model setup for application at other coastal sites is given in Section 7.2.

How does a change in boundary conditions influence sedimentation rates behind the dams?
Three boundary conditions were varied independently for a concave profile including three dams located 500 meters away from the land boundary. The profile is not in equilibrium state. Changing a boundary condition implies the sudden change of a boundary condition and its effect on the dam performance at a real coastline situation.
A change in wave height does not affect the dam performance significantly. Larger wave heights increase the tidal flat elevation and steepen the foreshore, enhancing a concave profile. The dams will enhance the tidal flat elevation and likely a more concave profile on the long term. Small wave heights decrease the tidal flat elevation but smoothen the foreshore, inducing a more convex profile. The dams increase bedlevel elevation in case of small wave heights to the same extend as for the large wave heights. However, in case of small wave heights the dams are likely to enhance the convex profile shape, which is favourable for mangrove rehabilitation and coastline stabilization. The dams should be placed more onshore for small wave heights and around somewhat offshore of the tidal flat boundary for large wave heights.
In the wave direction scenarios the dam effect increases for increasing wave angles (shore-normal to shore-parallel). The dams show a higher efficacy when the wave direction is least favourable in the baseline simulation. The effect of the dams related to a change in sediment supply is larger for the low sediment input scenario and lower for the high sediment input scenario. The high sediment input scenario showed the capability of the profile to restore by itself and the dams become unnecessary in that situation. The dam efficacy increases for the lower sediment input scenarios (low and reference sediment input scenario). Here the dams induce a reduction in erosion of the upper tidal favourable for mangrove rehabilitation. However, they do not mitigate erosion of the foreshore and likely cannot prevent the profile from becoming more concave. In case of reduced sediment supply, the dams are a good short-term solution, but for are likely not preventing a concave profile shape in a long-term scenario.

7.2 Recommendations

This research concludes in several recommendations related to improvements for the simplified model and possibilities for future research.

7.2.0.1 Improvements of the model

As discussed in Section 6.1.3 and 6.2.3 the computational grid is likely to cause strange current patterns for low flow velocities. Since the flow velocities are low, the sediment transport is not affected significantly on small time scales. However, as the bathymetry changes due to these inconsistent flows, the errors can accumulate in time. This limits the current model setup to short term modelling. Improving the grid quality has a large effect on the quality of the model. The grid size in longshore direction should be increased or refinement of the offshore grid cells is recommended in order to increase the number of grid cells in longshore direction. This also improves the grid smoothness.
Currently there is no option for modelling structures as permeable in Delft3D FM. They are modelled as “thin dams” with an infinite height and zero permeability. Modelling permeable structures would give a more realistic outcome on the sediment transport through the dams.
The model does not account for consolidation, which would in reality strengthen the bedlevel behind the dams over time. When deposition behind the dams occurs, consolidation improves the shear strength of the bed. A consolidation model could be implemented when made available. Delft3D FM includes the possibility for modelling flocculation, but this is not considered in the current model setup. For simplicity, two fractions with constant settling velocity are used, which decreases computation time.

Another process related to sediment dynamics is the dissipation of waves over fluid mud. For example in Suriname or Guyana, fluid mud is of major importance to the wave dissipation at the coast (Winterwerp et al., 2007). Modelling wave damping by fluid mud increases the accuracy of the model and the extension SWAN-mud could be used for future modelling (Kranenburg et al., 2011). Also, the inclusion of cheniers can give more accuracy on wave dissipation in the model (van Domburg, 2018).

Future application and research

The simplified model setup is based on the possibility of generating model setups for various coastlines to investigate dam performance at different sites. Since the setup for Demak is validated, it is interesting to test whether other coastal sites could be modelled correctly with this model setup. The model improvements in the previous section can be implemented to increase the applicability of the model. The two sites in Vietnam and Surinam, given in Figure 3.7 and 3.8, could be tested first. Some data is available in relation to dam performance at these coastlines. This could give more insight into the influence of different boundary conditions on the dam performance, giving more knowledge on prediction of dam effects.

To examine the effect of the dams on the equilibrium profile, larger time scales should be modelled. It could be possible that the dams induce a change of shape of the equilibrium profile or they could only alter the bedlevel profile on the short term. Modelling for longer time scales would require an increase in MORFAC as long computation times can be expected for a MORFAC 3.

When long term bedlevel development is modelled, including development of vegetation would give a more complete view on the restoration of the mangrove-mud coast. It is expected that mangroves will rehabilitate on the bedlevel restored by the dams, and will increase the stability of the coastline. Modelling longer term scenarios including vegetation could give more insights in the performance of dams in restoring the coastline in cooperation with the mangroves.

Also related to long term modelling, is the relative sea level rise. This will become an important factor for longer timescales. The modelling study by Smits (2019) includes relative sea level rise and predicts lower dam-induced sedimentation rates than RSLR rates. This suggests the need for other solutions besides the permeable dams too. The Building with Nature philosophy involves more than just solving a problem with an engineered solution. The BwN project in Demak includes construction of permeable dams for coastal restoration, but also the reformation of the former fish ponds, river restorations and other small-scale engineering. These restorations and measures are meant to restore the ecosystem so that it can regain its old scale and function. Future research could be done on combinations of solutions involving the permeable dams. Increasing the tidal prism by removing the fish ponds and increasing the sediment supply by removing upstream dams in rivers could increase or decrease the efficacy of the dams.

The effect of the dams is modelled at a concave initial profile. This profile represents an erosive non-equilibrium state. Changing the boundary conditions on a non-equilibrium profile gives results on the dam performance on a coastline where a change in boundary condition occurs, such as a decreased sediment supply or an increase in wave height. Using an equilibrium profile to change boundary conditions would imply dam performance on different coastal sites (sites with different coastal parameters as tidal range or wind direction). The use of an equilibrium profile would enable testing the dam efficacy influenced by boundary conditions at different coastal sites.

This research suggested some cross-shore dam locations could be more successful than others for the varied boundary conditions. Future research can model the dams at different elevations on the tidal flat or offshore of the tidal flat while the boundary conditions are varied. This gives an indication on an more ideal dam setup for different boundary conditions. The variation in location could well be combined with the initial profile variation to see what dam setups work best on different coastal profiles.

References

Albers, T., Dinh Cong San, and Schmitt, K. (2013). Coastal Protection in the Lower Mekong Delta. page 124.

Albers, T. and Von Lieberman, N. (2011). Current and Erosion Modelling Survey. Technical report.

Ali, A. (2016). Assessing Change and Vulnerability of the GuyanaCoastline with Multi-Temporal Landsat Imageryand Survey Data. Master's thesis, University of Windsor.

Anthony, E. and Gratiot, N. (2012). Coastal engineering and large-scale mangrove destruction in Guyana, South America: Averting in an environmental catastrophe in the making. *Ecological Engineering*, pages 268–273.

Bakker, J., Esselink, P., Dijkema, K., van Duin, W., and de Jong, D. (2002). Restoration of salt marshes in the Netherlands.

Balke, T., Bouma, T., Horstman, E., Webb, E., Erftemeijer, P., and Herman, P. (2011). Windows of opportunity: thresholds to man- grove seedling establishment on tidal flats.

BioManCo (2018). Bio-morphodynamic modeling of mangrove-mud coasts. PhD research project.

Booij, N., Ris, R. C., and Holthuijsen, L. H. (1999). A third-generation wave model for coastal regions 1. Model description and validation. *Journal of Geophysical Research: Oceans*, 104(C4):7649–7666.

Borsje, R. (2017). Assessing current patterns behind hybrid dams. Master's thesis, Delft University of Technology.

Bosboom, J. and Stive, M. (2015). Coastal Dynamics I. Lecture Notes CIE-4305.

Braat, L., Van Kessel, T., Leuven, J. R., and Kleinhans, M. G. (2017). Effects of mud supply on large-scale estuary morphology and development over centuries to millennia. *Earth Surface Dynamics*, 5(4):617–652.

Burke, L. and Ding, H. (2016). Valuation of Coastal Protection near Paramaribo, Suriname. page 54.

Daniel, J. (1989). The chenier plain coastal system of Guyana. *Marine Geology*, pages 283–287.

Dankers, P. and Winterwerp, J. (2007). Hindered settling of mud flocs: theory and validation. *Continental Shelf Research*.

Davis, R. A. and Hayes, M. O. (1984). What is a Wave-Dominated Coast? *Developments in Sedimentology*, 39:313–329.

de Vriend, H., van Koningsveld, M., Aarninkhof, S., de Vries, M., and Baptist, M. (2015). Sustainable hydraulic engineering through building with nature. *Journal of Hydro-environment Research*.

Delft University of Technology (2020). *SWAN User Manual*, 41.31a edition. User Manual.

Deltares (2020a). *D-Flow Flexible Mesh*, 0.9.1 edition. User Manual.

Deltares (2020b). *D-Morphology, 1D/2D/3D*, 1.5 edition. User Manual.

Deltares (2020c). *D-Waves. Simulation of short-crested waves with SWAN*, 1.2 edition. User Manual.

Deltares and TU Delft (2018). Long-term Shoreline Changes.

Dijkema, K. S., van Duin, W. E., Dijkman, E. M., and van Leeuwen, P. W. (2007). Monitoring van kwelders in de Waddenzee: rapport in het kader van het WOT programma Informatievoorziening Natuur i.o. (WOT IN). *Alterra-rapport 1574*, page 63.

Ecoshape (2015). Building with Nature in Indonesia; Securing Eroding Delta Coastlines. Technical report, Ecoshape.

Erban, L. E., Gorelick, S. M., and Zebker, H. A. (2014). Groundwater extraction, land subsidence, and sea-level rise in the Mekong Delta, Vietnam. *Environmental Research Letters*, 9.

Ewel, K., Twilley, R., and Ong, J. E. (1998). Different kinds of mangrove forests provide different goods and services. *Global Ecology and Biogeography Letters*.

Fagherazzi, S., Carniello, L., D'Alpaos, L., and Defina, A. (2006). Critical bifurcation of shallow microtidal landforms in tidal flats and salt marshes. *Proceedings of the National Academy of Sciences of the United States of America*.

Friedrichs, C. T. (2012). *Tidal Flat Morphodynamics: A Synthesis*, volume 3. Elsevier Inc.

Furukawa, K. and Wolanski, E. (1996). Sedimentation in mangrove forests. *Mangroves and Salt Marshes*, pages 3–10.

Giri, C., Ochieng, E., Tieszen, L., Zhu, Z., Singh, A., Loveland, T., Masek, J., and Duke, N. (2011). Status and distribution of mangrove forests of the world using observation satellite data. *Global Ecology and Biogeography*.

Hamilton, S. E. and Casey, D. (2016). Creation of a high spatio-temporal resolution global database of continuous mangrove forest cover for the 21st century (CGMFC-21). Research Paper.

Hu, Z., Suzuki, T., Zitman, T., Uittewaal, W., and Stive, M. (2014). Laboratory study on wave dissipation by vegetation in combined current-wave flow. *Coastal Engineering*.

J.C. Winterwerp, B. v. P. (2015a). Chapter 10: erosion of mangrove-mud coasts. Lecture notes of TU Delft.

J.C. Winterwerp, B. v. P. (2015b). Chapter 8: Net transport of fine sediments - Barotropic effects. Lecture notes of TU Delft.

Kathiresan, K. (2015). *Ecology of mangroves*, chapter 8, pages 169–207. Jodhpur.

Kathiresan, K. and Rajendran, N. (2005). Coastal mangrove forests mitigated tsunami. *Estuarine Coastal and Shelf Science*.

Kranenburg, W. M., Winterwerp, J. C., de Boer, G. J., Cornelisse, J. M., and Zijlema, M. (2011). SWAN-Mud: Engineering model for mud-induced wave damping. *Journal of Hydraulic Engineering*, 137(9):959–975.

Laboratory, D. H. (1962). Demerara coastal investigation.

Lewis, R. R. (2005). Ecological engineering for successful management and restoration of mangrove forests. *Ecological Engineering*, 24:403–418.

Longuet-Higgins, M. and Stewart, R. (1964). Radiation stresses in water waves: a physical discussion with applications.

Luijendijk, A. (2011).

Luijendijk, A., Aarninkhof, S., Hagenaars, G., Ranasinghe, R., Baart, F., and Donchyts, G. (2018). The State of the World's Beaches. *Nature*.

Luther, D. A. and Greenberg, R. (2009). Mangroves: A global perspective on the evolution and conservation of their terrestrial vertebrates. *BioScience*, 59(7):602–612.

Maan, D., van Prooijen, B., Wang, Z., and de Vriend, H. (2015). Do intertidal flats ever reach equilibrium? *Journal of Geophysical Research: Earth Surface*.

Maggi, F. (2005). *Flocculation dynamics of cohesive sediment*. PhD thesis.

Masselink, G. and Hughes, M. (2003). Hodder Arnold.

McIvor, A., Möller, I., Spencer, T., and Spalding, M. (2012). Reduction of Wind and Swell Waves by Mangroves.

McIvor, A., Möller, I., Spencer, T., and Spalding, M. (2013). The response of mangrove soil surface elevation to sea level rise.

Mehta, A. (1986). *Characterisation of cohesive sediment properties and transport processes in estuaries*. Springer.

Miche, R. (1944). Mouvements ondulatoires de la mers en profundeur constante on decroisante.

Mietta, F., C. C. M. A. and Winterwerp, J. (2009). Influence of shear rate, organic matter content, PH and salinity on mud flocculation. *Ocean Dynamics*, 59:751–763.

Mitra, A. (2013). *Sensitivity of Mangrove Ecosystems to Changing Climate*. Springer India.

Montserrat, F., Van Colen, C., Degraer, S., Ysebaert, T., and Herman, P. M. (2008). Benthic community-mediated sediment dynamics. *Marine Ecology Progress Series*, 372(1):43–59.

Muskananfola, M., Haeruddin, Purnomo, P., and Sulardiono, B. (2017). Erosion and transport rates of sediments at degraded coastal waters in Bedono Village, SayungDemak, Central Java. *Proceeding of the 15th International Conference on QiR (Quality in Research)*.

Nguyen, T. (2009). Surface sediment characteristics and sediment transport from Bassac River mouths to Ca Mau Peninsula (Mekong Delta).

Nguyen, T., Statteger, K., Unverricht, D., Nittrouer, C., Phach, P. V., Liu, P., DeMaster, D., Dung, B. V., Anh, L. D., and Dong, M. D. (2014). Surface sediment grain-size distribution and sediment transport in the subaqueous Mekong Delta, Vietnam. *Vietnam Journal of Earth Sciences*.

NOAA (2020). Tidal current predictions and data.

Ogston, A. S., Allison, M. A., Mullarney, J. C., and Nittrouer, C. A. (2017). Sediment- and hydro-dynamics of the Mekong Delta: From tidal river to continental shelf.

Persaud, E. (2014). Sea Level Rise and the Coastline of Guyana. University of Guyana.

Persaud, S., Flynn, D., and Fox, B. (1999). Potential for wind generation on the Guyana coastlands. *Renewable Energy*, pages 175–189.

Pham, T. (2011). Mangroves of soc trang.

Phan, H. M., Ye, Q., Reniers, A. J., and Stive, M. J. (2019). Tidal wave propagation along The Mekong deltaic coast. *Estuarine, Coastal and Shelf Science*, 220:73–98.

Polidoro, B. A., Carpenter, K. E., Collins, L., Duke, N. C., Ellison, A. M., Ellison, J. C., Farnsworth, E. J., Fernando, E. S., Kathiresan, K., Koedam, N. E., Livingstone, S. R., Miyagi, T., Moore, G. E., Nam, V. N., Ong, J. E., Primavera, J. H., Salmo, S. G., Sanciangco, J. C., Sukardjo, S., Wang, Y., and Yong, J. W. H. (2010). The loss of species: Mangrove extinction risk and geographic areas of global concern. *PLoS ONE*, 5(4).

R.J. Reimold, W. Q. (1974). *Ecology of halophytes*. Academic Press.

Ruitenbeek, H. (1992). *Mangrove Management: An Economic Analysis of Management Options with a Focus on Bintuni Bay, Irian Jaya*. Dalhousie University.

Schleiss, E. P. A. (2006). Communication 24 Efficiency of brushwood fences in shore protection against wind-wave induced erosion Selim Sayah. *Communication*.

Scoffin, T. (1970). The trapping and binding of subtidal carbonate sediments by marine vegetation in Bimini Lagoon, Bahamas.

Shrestha, P. and Blumberg, A. (2005). *Cohesive Sediment Transport*. Springer.

Smits, B. (2016). Morphodynamic optimisation study of the design of semi-permeable dams for rehabilitation of a mangrove-mud coast. Master's thesis, Delft University of Technology.

Smits, B. (2019). Functionality of ecosystem-based interventions to sea level rise and land subsidence: Modelling report of IKI project in Demak, Indonesia. Unpublished report.

Smits, B. (2020). Pers. comm.

Spencer, T. and Möller, I. (2013). *Mangrove Systems*. Academic Press San Diego.

Tu, L. X., Thanh, V. Q., Reyns, J., Van, S. P., Anh, D. T., Dang, T. D., and Roelvink, D. (2019). Sediment transport and morphodynamical modeling on the estuaries and coastal zone of the Vietnamese Mekong Delta. *Continental Shelf Research*.

Twilley, R. and Rivera-Monroy, V. (2009). Ecogeomorphic Models of Nutrient Biogeochemistry for Mangrove Wetlands. In *Coastal Wetlands: An Integrated Ecosystem Approach*, volume 8, chapter 23, pages 641–675. Elsevier.

Unverricht, D., Szczuciński, W., Stattegger, K., Jagodziński, R., Le, X. T., and Kwong, L. L. W. (2013). Modern sedimentation and morphology of the subaqueous Mekong Delta, Southern Vietnam. *Global and Planetary Change*, 110:223–235.

van Domburg, T. (2018). Identifying Windows of Opportunity for Mangrove Establishment on a Mud Coast. Master's thesis, Delft University of Technology.

Van Maren, D. S. and Winterwerp, J. C. (2013). The role of flow asymmetry and mud properties on tidal flat sedimentation. *Continental Shelf Research*, 60:S71–S84.

Vermaat, J. and Thampanya, U. (2006). Mangroves mitigate tsunami damage: A further response. *Estuarine Coastal and Shelf Science*.

Wells, J. and Kemp, G. (1986). Interaction of surface waves and cohesive sediments: field observations and geologic significance. Lecture notes on Coastal and Estuarine Studies.

Wilms, T., Prusina, I., van der Goot, F., Tonneijc, F., and van Wesenbeeck, B. (2019). Building With Nature: Restoring Mangrove Coast. *38th IAHR World Congress - "Water: Connecting the World"*, 38(1):3137–3142.

Winterwerp, J., de Graaf, R., Groeneweg, J., and Luijendijk, A. (2007). Modelling of wave damping at Guyana mud coast. *Coastal Engineering*, pages 249–261.

Winterwerp, J., Erftemeijer, P., Suryadiputra, N., Eijk, P. V., and Zhang, L. (2013). Defining eco-morphodynamic requirements for rehabilitating eroding mangrove-mud coasts. *Wetlands*, pages 515–526.

Winterwerp, J. and van Kesteren, W. (2004). *Introduction to the Physics of Cohesive Sediment Dynamics in a Marine Environment*. Elsevier.

Winterwerp, J., Wesenbeeck, B., van Dalfsen, J., Tonneijck, F., Astra, A., Verschure, S., and van Eijk, P. (2014). A sustainable solution for massive coastal erosion in central java. Discussion paper.

Winterwerp, J. C., Borst, W. G., and De Vries, M. B. (2005). Pilot study on the erosion and rehabilitation of a mangrove mud coast. *Journal of Coastal Research*, 21(2):223–230.

Wyrtki, K. (1961). Physical Oceanography of the Southeast Asian waters. Technical report, UC San Diego.

A

Coastal systems

The three selected coastal sites in Indonesia, Vietnam and Surinam exhibit mangroves in their very different coastal systems. The various system characteristics affect the mangrove ecosystem all in their own way, which makes a thorough understanding of the coastal system one of the most crucial points in the dam modelling.
The coastal system near Demak has been described in Chapter **??**, leaving Vietnam and Surinam still open to be defined in this Appendix. Section A.1 and A.2 respectively describe the coastal system characteristics of Vietnam and Surinam, concluding on them with a schematised overview of the appointed coastal systems in Section 3.3. This will help to get a grip on the similarities and differences of the three coastal systems more quickly.

A.1 Vietnam

A.1.1 Meteorology

As in Demak, Vietnam experiences two monsoon seasons as well. This seasonal variability is an important driver for the coastal dynamics of the Southern coast of Vietnam. From November to early March, the northeastern winds are dominant and determine the period of the Northeast (NE) monsoon. In April the wind changes to an opposite direction and southwestern winds prevail. Until mid October this covers the Southwest (SW) monsoon. Similar maximum wind speeds occur in both monsoons, when in stormy conditions can reach 20/30 m/s. The annual average wind speeds equals 6 to 8 m/s, which has been recorded in a station in Bac Lieu from 1999 to 2008. (Nguyen et al., 2014). Figure A.1 clearly shows the abrupt change in wind direction in between the two monsoon periods.

Northeast monsoon

During the NE monsoon the wind blows from northeast direction along the shoreline of Soc Trang. This season is also referred by as the dry season, as only 15% of the annual rainfall occurs during these winter months. When the flood season ends at the start of the NE monsoon, large plumes of sediment are observed in the lower Mekong Delta. (Ogston et al., 2017)

Southwest monsoon

The southwestern winds bring most of the precipitation to the southern coast of Vietnam and these wet months make up for 85% of the annual rainfall. According to Unverricht et al. (2013) the annual rainfall is around 1600 to 2000 mm in southern Vietnam.

A.1.2 Hydrodynamics

Tide

A numerical modelling study from Phan et al. (2019) provides a lot of information about the tidal influence at the southeast coastline of Vietnam. Along this part of the coastline the tide has a mixed but mainly semi-diurnal character, contradictory to the rest of the Vietnamese coastline which has a mainly diurnal character. Three main constituents and their phase and amplitude observed at a station in My Thanh (close to Vinh Tan) are given in Table A.1.

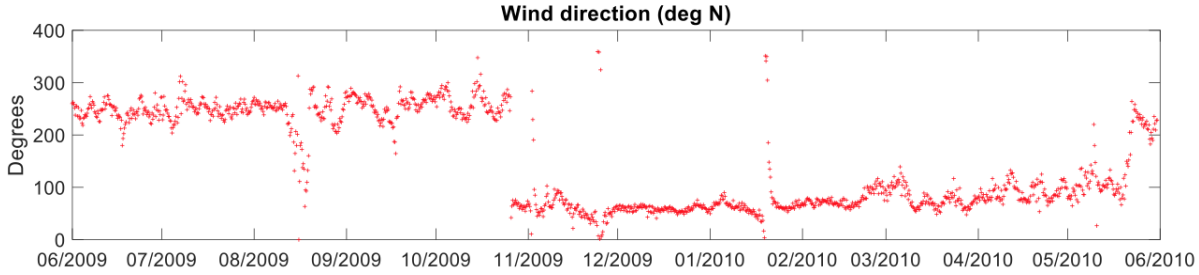

Figure A.1: Wind direction along the southern Vietnam coast, Tu et al. (2019).

From Phan et al. (2019), the waterlevel at the Condao station, offshore of Vinh Tan, gives insight in the waterlevel variations due to the tides. The tidal range ranges between 1.2 m during neap tide and 3.8 m during spring tide, causing significant tidal currents with a net tidal current in flood direction, parallel to the coastline.

Tidal constituents	**Amplitude [cm]**	**Phase [°]**
S_2	37	141
K_1	64	342
O_1	45.1	293

Table A.1: Tidal constituents at My Thanh, Phan et al. (2019).

Wave climate

The wave climate shows a strong seasonal variability with waves coming mainly from the northeast in the NE monsoon and waves coming from the southwest in the SW monsoon. During the more dynamic NE monsoon significant wave heights appear to be larger and reach offshore values of around 1 - 2 m with a peak wave period of 6 - 9 seconds. Figure A.2a shows the significant wave height from 2009 to 2010, 120 km offshore of the southern coastline. (Tu et al., 2019). Somewhat lower significant wave height of 0.5 - 1.5 m are experienced when the opposed southwestern winds prevail during the SW monsoon, with corresponding peak wave periods of 5 - 6 seconds. Another offshore station in Con Dao which collected wave data shows, in Figure A.2b, the same wave climate as shown previously in Figure A.2a.
Towards the shoreline dissipation processes cause the waves heights to decrease. According to field measurements addressed by Albers and Von Lieberman (2011), nearshore significant wave heights (300 m from the dyke at Vinh Tan) in between the two monsoon periods were around 0.2 - 0.3 m. During the NE monsoon the significant wave heights measured around 0.4 - 1.0 m.

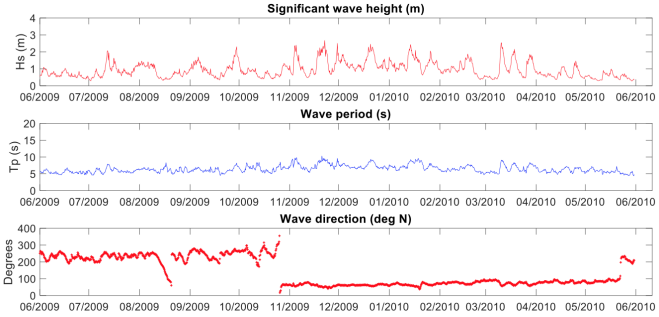

(a) Wave boundary condition. (Tu et al., 2019).

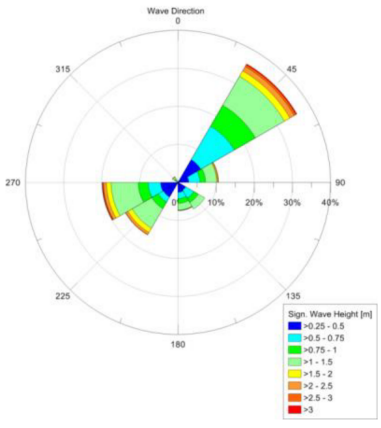

(b) Wave rose for Con Dao. (Albers and Von Lieberman, 2011).

Figure A.2: Offshore wave data.

Currents

The flood tide runs parallel to the coastline, as illustrated in Figure A.3, with magnitudes in the order of 0.2 to 0.5 m/s in the nearshore during the NE monsoon (Albers and Von Lieberman, 2011). The NE monsoon wind-driven

currents increase the longshore tidal currents as they run in a similar direction, again referring to Figure A.3. The opposite appears in the SW monsoon, when the longshore wind-driven current enhances the ebb-currents and runs parallel to the shoreline from southwest direction.

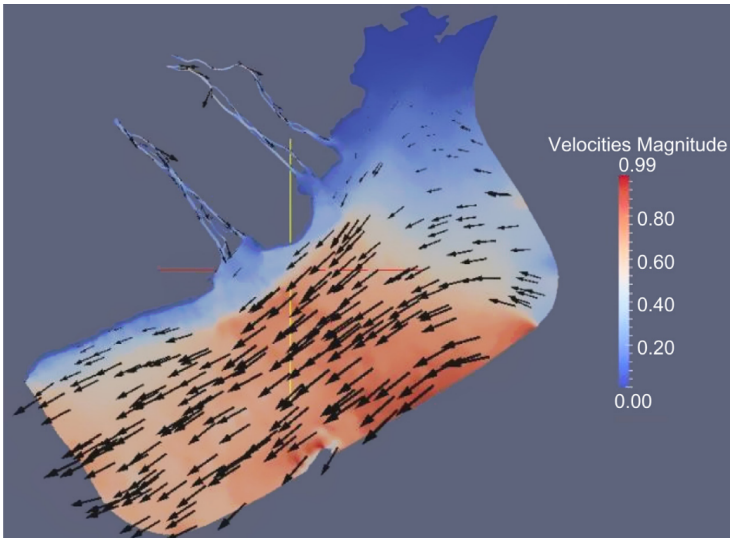

Figure A.3: Computed tidal currents during flood tide in the NE monsoon. (Albers and Von Lieberman, 2011)

A.1.3 Morphology

Bathymetry

The bathymetry varies along the southern coast with a multiple channel system in front of the coastline. Figure A.4a and A.4b give an overview of the bathymetry along the southern coast. Starting around Vinh Tan and aligned parallel to the coast the channels spread out towards the most southern point of Vietnam. The southern coastal slope varies between 1:900 and 1:2000, but near Vinh Tan, where channels are not occurring yet and erosion is a local problem, the slope ranges more towards steeper values.

Nguyen (2009) also gives some bathymetric profiles at the southern coast of Vietnam, of which Figure A.5 gives a coastal profile near Vinh Tan. Here the average slope of of the non-horizontal profile is around 1:900.

In front of the coast cheniers are found, just as in Demak. Sand originating from the Mekong River creates sandbars which attenuate incoming waves, enabling a smaller design dam height.

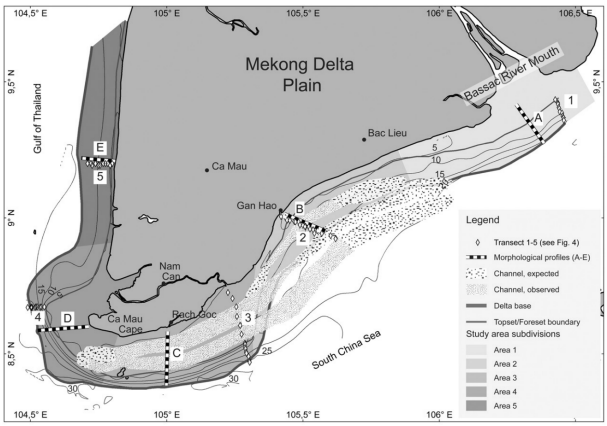

(a) Overview of the bathymetry.

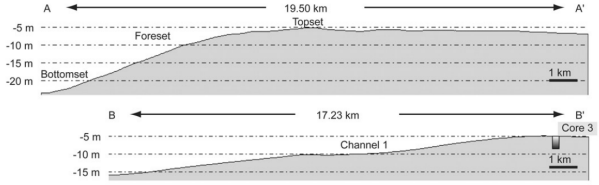

(b) Profiles for two transects.

Figure A.4: Bathymetry along the southern coast of Vietnam. (Unverricht et al., 2013).

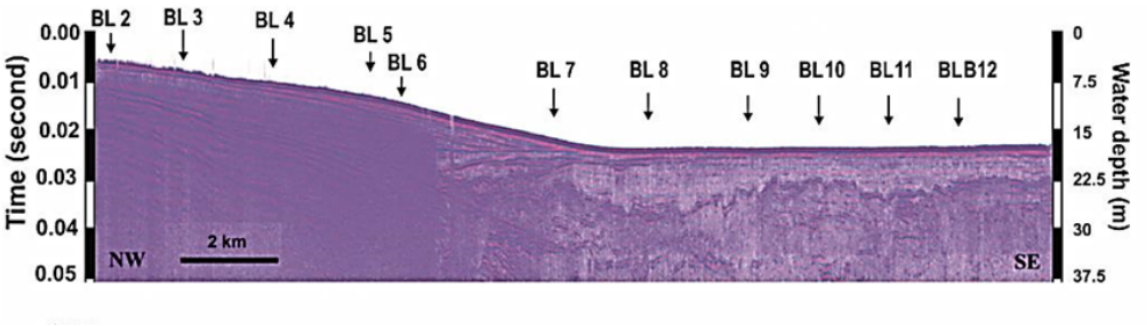

Figure A.5: Coastal profile near Vinh Tan. (Nguyen, 2009).

Sediment composition

Mostly sandy and clayey silt is found near the coast at Vinh Tan, as shown in Figure A.6a. Figure A.6b shows the grain size distribution at the coast of Vinh Tan, where the median grain size is 0.0065 mm. Around 90% of the sediment consists of mud and 10% of the sediment is fine sand. Measurements on the (dry) bulk density of mud at the coast of Vinh Tan were carried out by (Albers et al., 2013) and showed a bulk density of 1.2/1.3 g/cm^3 and a dry density of 0.4/0.5 g/cm^3.

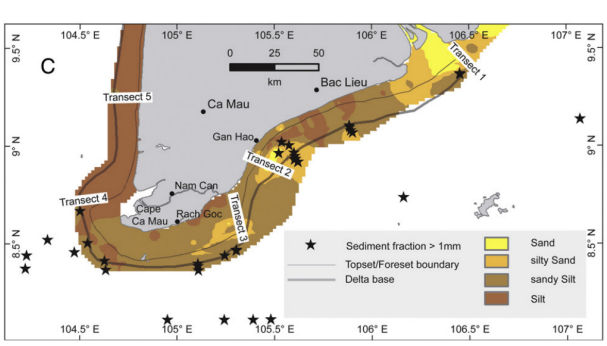

(a) Surface sediment map. (Unverricht et al., 2013).

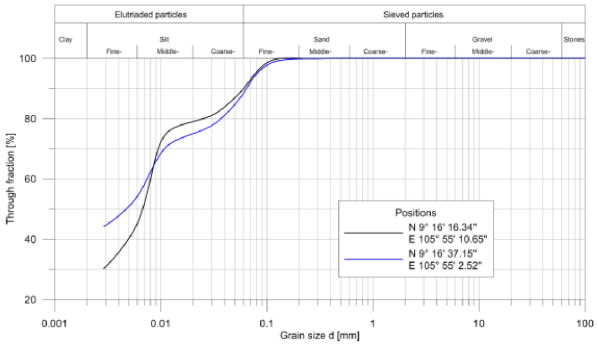

(b) Grain size distribution at the coast of Vinh Tan. (Albers and Von Lieberman, 2011).

Figure A.6: Sediment distribution Vinh Tan.

Sediment sources/sinks

A major sediment source for the southern coast of Vietnam is the Mekong River. When in May/June, during the SW monsoon, the wet season begins, large amounts of rainfall causes the Mekong to distribute a lot of sediment to its river mouth. Parts of it end up along the southern coast. During the NE monsoon, when it is dry season and less sediment is available, the more energetic conditions can cause erosion along the south coast.

As the monsoon changes the sediment availability, the suspended sediment concentrations will also differ during the year. Measurements from Albers and Von Lieberman (2011) show a suspended concentration between 0.4 and 1.5 g/L in the nearshore area of Vinh Tan. It follows the significant wave height and water levels during this period of inter-monsoon. During the SW monsoon measurements showed SSC values of 0.1 to 1.0 g/L. Also, Nguyen et al. (2014) studied the SSC in different areas around the Mekong Delta during the inter-monsoon season. Along the transect near Vinh Tan, Figure A.7 shows the higher SSC close to the coastline and the decrease in SSC further offshore.

A.1.4 Mangroves

Avicennia communities of *Avicennia alba* are found along the coastal stretches of Soc Trang. Especially on the accreted soft mudflats which are inundated by the semi-diurnal tide. When sedimentation occurs and the soft mud consolidates to a more dense state forming harder ground, the *Avicennia* is slowly displaced and *Rizophora* makes ground. (Pham, 2011).

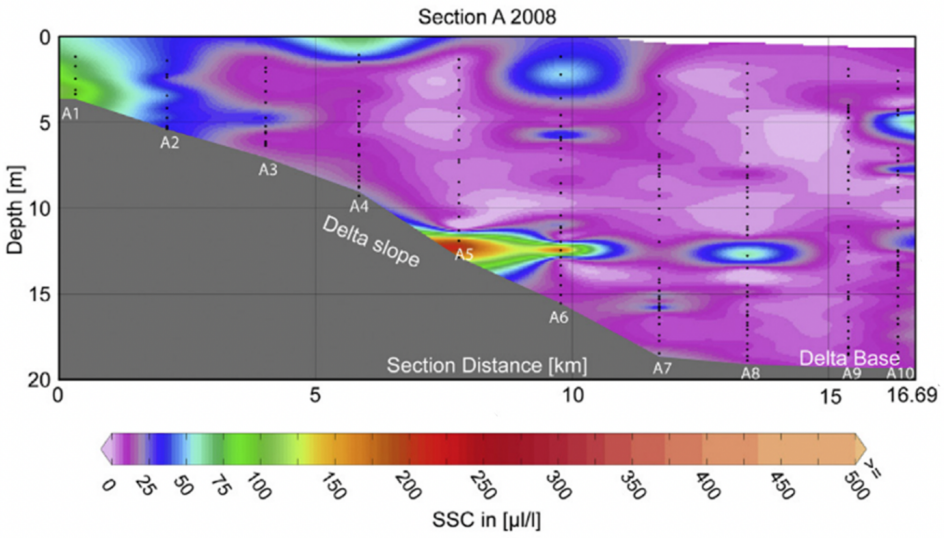

Figure A.7: SSC along the transect at Vinh Tan. (Nguyen et al., 2014).

A.1.5 Human activities

Cutting trees and exploiting important ecosystems of their resources. Again, in Vietnam we show the same behaviour. Even though Vietnam is a country really vulnerable to floods, storms and sea level rise. Especially the Mekong Delta due to its low-lying nature.

Sea level rise predictions for the Soc Tran (southern Vietnam) Province are at least one meter for 2100. For the coming years the sea level rise is estimated on 0.2 - 0.4 cm/yr. (Erban et al., 2014). Besides the rise of sea level, the frequency of floods and storms is also likely to increase, together with a shift in even more rainfall during the wet season less during the dry season.

As groundwater pumping is causing significant land subsidence rates for southern Vietnam, they do not compare to the rates near Demak. According to a study by Erban et al. (2014) rates of land subsidence equal 1 - 4 cm per year.

A.2 Suriname

A paper on the Suriname mud coast by Burke and Ding (2016) demonstrates the problem Surinam is facing associated with its erosive coastline. The cause of the mangrove degradation can be found in the agricultural land use at the coastline and accompanying hard coastal structures, e.g. concrete sea walls, replacing much of the previous mangroves.

Guyana is located in the Northern part of South America and its 1600 km-long coastline is characterized by huge mud banks migrating alongshore from the mouth of the Amazon river (Brazil) to Venezuela and its extensive colonisation of mangrove forests. According to Anthony and Gratiot (2012) the cyclic mud-bank phases play a dominant role in mangrove colonisation by regulating their regeneration. Though, the sediment trapping by mangroves is, also in this mud bank-mangrove system, still important for coastal safety.

A short overview of the coastal system is given in the next subsections.

A.2.1 Meteorology

Two predominant weather zones influence Surinam, the North East Trade Winds and the Inter Tropical Convergence Zone (ITCZ) (Persaud et al., 1999). The northeast trade winds are stronger and predominant at the shoreline. In winter (northern winter) the higher wind speeds (5.5 - 7 m/s) are experienced and the summer is characterized by low mean wind speeds (4.5 - 5.5 m/s).

A.2.2 Hydrodynamics

Tide

According to Ali (2016) the mean tidal range at the coastline is around 1.55 - 1.8 m, dependent on the alongshore location. It experiences a semi-diurnal tide.

Wave climate

The coastline experiences a low to medium energy wave climate. Wave spectra have been established by Wells and Kemp (1986) at three locations in the Suriname coastal waters. Figure A.8 shows the results of the measurements where it is clearly visible that waves are strongly attenuated. The viscous dissipation in the liquefied seabed causes this strong attenuation. As waves approach the mangroves their height has been decreased to approximately 32 to 19 cm (RMS wave heigt). The larger, offshore wave height is around 1 meter.

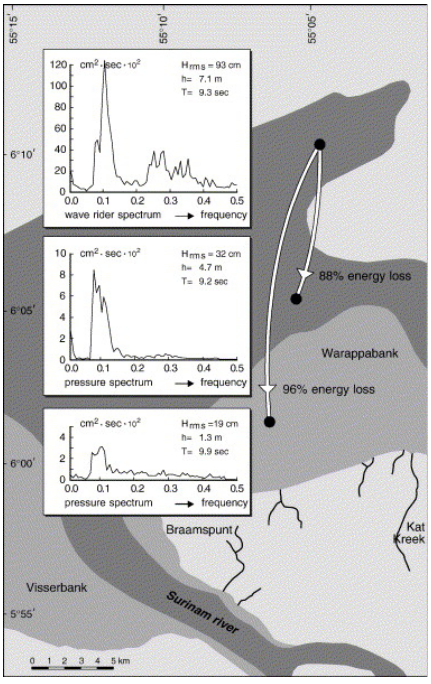

Figure A.8: Wave spectra at three locations by Wells and Kemp (1986)

Currents

The Guiana current and Equatorial currents transport the sediment from the Amazon river towards the Northwest to Venezuela. This is the governing alongshore transport direction, but alongshore currents on the nearshore could be far less due to the really mild slope. Ali (2016) describes the mud flats that will develop on the landward edge when mud banks are stationary.

A.2.3 Morphology

Bathymetry

The slope in the nearshore of Suriname ranged between 1:800 and 1:1500 in 1989, estimated by Daniel (1989). This is an even milder slope than in Demak, but alterations of the slope are very likely to have occurred in time. According to Burke and Ding (2016), the coastal slope is around 0.03 to 0.04 °.

Sediment sources/sinks

Winterwerp et al. (2007) describes the Guyana coastal system by its "*thick deposits of Amazon mud and high mud concentrations in its coastal waters*". The Amazon river is considered a major sediment source as sediment input from local rivers is small. Trade Winds and cross-shore salinity gradients keep the sediment near the coast and prevent the plume from drifting to deeper water. According to a what older study of Laboratory (1962), the surface-water suspended sediment concentrations in the nearshore muddy coastal waters vary between minimum of 5 g/L to a maximum of 2625 g/L.

A.2.4 Human activities

As described earlier many mangrove forests have been demolished for agricultural land use. Moreover, mangroves were replaced by concrete sea walls, not fulfilling a proper flood protection where the reason for failure is explained by Winterwerp et al. (2013). The sea walls also block any propagules from flowing to the mud banks disturbing the mud bank-mangrove dynamic in this area.
Sea level rise will also affect the Surinam coastline, but land subsidence rates are much smaller than in Demak. Persaud (2014) stated a land subsidence of 4 cm in the period of 1970 to 2008. This would mean a general subsidence rate of 0.1 cm/year.

B

Delft3D Flexible Mesh

This appendix explains the processes and their governing equations included in the model setup to model the morphodynamic effect of the permeable dams. Section B.1 includes the relevant processes that are used in the flow module for this model setup, Section B.2 gives the relevant processes in the wave module and Section B.3 the relevant processes in the sediment module. Each section is based on the information extracted from the User Manuals by Deltares (2020a,c,b).

B.1 D-Flow FM

The flow module solves the unsteady shallow water equations in two or three dimensions under assumption of incompressible free surface flow. In this research a 2DH field is used so the equations only need to be solved for two dimensions. That means that the 2DH shallow water equations describe the conservation of mass by a time-dependent continuity equation and the conservation of momentum by two time-dependent momentum equations. The shallow water equations are derived through averaging the Navier-Stokes equations over a characteristic time scale and over the vertical.
The continuity equation for three dimensions is given in Eq. B.1.

$$\frac{\delta\eta}{\delta t} + \frac{\delta hu}{\delta x} + \frac{\delta hv}{\delta y} + \frac{\delta hw}{\delta z} = 0 \tag{B.1}$$

Where:

η	=	the waterlevel
u, v, w	=	flow velocity for x, y, z direction
h	=	water depth

Secondary to the continuity equation, the momentum equations for each direction x, y and z are given in Eq. B.2, B.3 and B.4, respectively.

$$\frac{\delta u}{\delta t} + u\frac{\delta u}{\delta x} + v\frac{\delta u}{\delta y} + w\frac{\delta u}{\delta z} = -\frac{1}{\rho}\frac{\delta p}{\delta x} + \frac{\delta}{\delta x}\left(\nu_H\frac{\delta u}{\delta x}\right) + \frac{\delta}{\delta y}\left(\nu_H\frac{\delta u}{\delta y}\right) + \frac{\delta}{\delta z}\left(\nu_V\frac{\delta u}{\delta z}\right) + f_v + M_x \tag{B.2}$$

$$\frac{\delta v}{\delta t} + u\frac{\delta v}{\delta x} + v\frac{\delta v}{\delta y} + w\frac{\delta v}{\delta z} = -\frac{1}{\rho}\frac{\delta p}{\delta y} + \frac{\delta}{\delta x}\left(\nu_H\frac{\delta v}{\delta x}\right) + \frac{\delta}{\delta y}\left(\nu_H\frac{\delta v}{\delta y}\right) + \frac{\delta}{\delta z}\left(\nu_V\frac{\delta v}{\delta z}\right) - f_u + M_y \tag{B.3}$$

$$\frac{\delta w}{\delta t} + u\frac{\delta w}{\delta x} + v\frac{\delta w}{\delta y} + w\frac{\delta w}{\delta z} = -\frac{1}{\rho}\frac{\delta p}{\delta z} + \frac{\delta}{\delta x}\left(\nu_H\frac{\delta w}{\delta x}\right) + \frac{\delta}{\delta y}\left(\nu_H\frac{\delta w}{\delta y}\right) + \frac{\delta}{\delta z}\left(\nu_V\frac{\delta w}{\delta z}\right) - g + M_z \tag{B.4}$$

Where:

u, v, w	=	flow velocity for x, y, z direction
ρ	=	water density
p	=	pressure
ν_H, ν_V	=	horizontal and vertical eddy viscosity coefficients
$f_{x,y}$	=	Coriolis parameter
g	=	gravitational acceleration
$M_{x,y,z}$	=	external sources or sinks of momentum (e.g. wave stresses)

The third momentum equation (Eq. B.4) reduces to a hydrostatic pressure equation (Eq. B.5) if vertical accelerations are neglected in order to obtain a 2DH field.

$$\frac{\delta p}{\delta z} = -\rho g \tag{B.5}$$

When Eq. B.5 is substituted in Eq. B.2 and B.3, the two momentum equations for x and y direction reduce to Eq. B.7 and B.8. Depth-averaging Eq. B.1 leads to Eq. B.6. The derived set of partial differential equations is used in D-Flow to solve the flow.

$$\frac{\delta \eta}{\delta t} + \frac{\delta hu}{\delta x} + \frac{\delta hv}{\delta y} = 0 \tag{B.6}$$

$$\frac{\delta u}{\delta t} + u\frac{\delta u}{\delta x} + v\frac{\delta u}{\delta y} + g\frac{\delta \eta}{\delta x} - \frac{1}{\rho}\left(\frac{\delta \tau_{xx}}{\delta x} + \frac{\delta \tau_{xy}}{\delta y} + \frac{\delta \tau_{bx}}{\delta h}\right) - f_v - M_x = 0 \tag{B.7}$$

$$\frac{\delta v}{\delta t} + u\frac{\delta v}{\delta x} + v\frac{\delta v}{\delta y} + g\frac{\delta \eta}{\delta y} - \frac{1}{\rho}\left(\frac{\delta \tau_{yx}}{\delta x} + \frac{\delta \tau_{yy}}{\delta y} + \frac{\delta \tau_{by}}{\delta h}\right) + f_u - M_y = 0 \tag{B.8}$$

B.1.1 Online coupling to D-Waves

The wave module attributes to the flow module by wave-induced forces, Stokes drift or mass fluxes and by enhancement of the bed shear stress by waves. The flow module communicates the flow velocities and water levels back to D-Waves. The following three attributions are elaborated for 2DH.

Wave-induced forces Wave-induced forcing terms can be substituted (as part of the source terms M_x and M_y) in the two momentum equations. The wave-induced forces can be determined by applying the radiation stresses or the dissipation rate. In this case the dissipation rate is applied. Eq. B.9 includes the wave-induced forcing term for x and y direction based on the dissipation rate. SWAN determines the dissipaion rate due to bottom friction, white-capping and depth-induced breaking.

$$F_i = D\frac{k_i}{\omega} \tag{B.9}$$

Where:

F_i	=	wave-induced forcing in i-direction
D	=	dissipation rate
k_i	=	wave number in i-direction
ω	=	wave frequency

Stokes drift The Stokes drift is a wave-induced drift velocity which leads to additional fluxes in the wave-averaged continuity equation and is given in Eq. B.10 and B.11 for the x and y direction.

$$U^S = \frac{M_x^S}{\rho h} \tag{B.10}$$

$$V^S = \frac{M_y^S}{\rho h} \tag{B.11}$$

The wave-induced mass flux M_i^S in i-direction is given in Eq. B.12. The wave energy E is given in Eq. B.17 and uses the root-mean-square wave height H_{rms} (or converted to the significant wave height).

$$M_i^S = \frac{E}{\omega}k_i \tag{B.12}$$

$$E = \frac{1}{8}\rho g H_{rms}^2 \tag{B.13}$$

Bed shear stress for combined wave current The last attribution is the magnitude of the bed shear stress by combined wave current, which is calculated with Eq. B.14. Here the effective bed shear stress τ_b is computed which corrects for the Stokes drift.

$$\tau_b = \frac{|\tau_m|}{|U|}(U - U^S) \tag{B.14}$$

Where τ_b is the effective bed shear stress, τ_m the magnitude of bed shear stress by combined wave current and U^S is the depth-averaged Stokes drift. The friction model that is used determines the ratio of bed shear stress by waves alone and bed shear stress by current alone to derive the magnitude of the bed shear stress by combined wave current τ_m. The bed shear stress due to current alone τ_c is is computed with Eq. B.15, in which Manning's formulation for the 2D-Chézy coefficient C_{2D} was used.

$$\tau_c = \frac{g\rho U|U|}{C_{2D}^2} \tag{B.15}$$

The bed shear stress due to waves alone τ_w is dependent on the orbital velocity u_{orb} and the friction factor f_w, presented in Eq. B.16. The orbital velocity u_{orb} is a function of the root-mean-square wave height H_{rms}, the wave period T and the wave number k. The wave friction factor f_w is a function of the orbital velocity u_{orb}, the wave angular frequency ω (i.e. the wave period T) and the Nikuradse roughness length-scale k_s.

$$|\tau_w| = \frac{1}{2}\rho f_w u_{orb}^2 \tag{B.16}$$

B.2 D-Waves

To calculate the wave parameters for short-crested wind-generated gravity waves Delft3D FM uses the spectral model SWAN, developed by Delft University of Technology (Booij et al., 1999). SWAN defines the waves by a wave action density spectrum $N(\sigma,\theta)$ and does not describe them by an energy density spectrum $E(\sigma,\theta)$. Eq. B.17 shows the relation between the action density and the energy density where σ is the relative frequency (relative to the current velocity) and the θ is the relative direction (normal to the wave crest). The spectrum can vary in space and time.

$$N(\sigma,\theta) = \frac{E(\sigma,\theta)}{\sigma} \tag{B.17}$$

Eq. B.18 gives the spectral action balance which describes the evolution of the wave spectrum.

$$\frac{\delta}{\delta t}N + \frac{\delta}{\delta x}c_x N + \frac{\delta}{\delta y}c_y N + \frac{\delta}{\delta\sigma}c_\sigma N + \frac{\delta}{\delta\theta}c_\theta N + = \frac{S}{\sigma} \tag{B.18}$$

The left hand side of Eq. B.18 involves the changing of action in time and space, the shifting of the relative frequency and the depth-induced and current-induced refraction. The source term on the right hand side is the sum of the processes wave generation, dissipation of waves and non-linear wave-wave interactions. The waves are generated by wind. Wave dissipation happens through bottom friction, white-capping and depth-induced breaking. Both quadruplet and triad non-linear wave-wave interactions are accounted for in SWAN. The full equations for each source term can be found in the User Manual D-Waves by Deltares (2020c).

B.3 D-Morphology

In the sediment module the two type of sediments "mud" and "sand" represent the respectively cohesive and non-cohesive sediment. This model setup uses two "mud" fractions and therefore only sediment transport of cohesive sediments is modelled which means there is only suspended sediment transport. The suspended sediment transport is modelled using an advection-diffusion (mass-balance) equation as in Eq. B.19 where the advection-diffusion equation is given for three dimensions x, y and z. The results of the hydrodynamic computations in D-Flow are used to derive the local flow velocities and the eddy diffusivities that are substituted into Eq. B.19.

$$\frac{\delta c^{(l)}}{\delta t} + \frac{\delta u c^{(l)}}{\delta x} + \frac{\delta v c^{(l)}}{\delta y} + \frac{\delta (w - w_s^{(l)}) c^{(l)}}{\delta z} - \frac{\delta}{\delta x}\left(\varepsilon_{s,x}^{(l)}\frac{c^{(l)}}{\delta x}\right) - \frac{\delta}{\delta y}\left(\varepsilon_{s,y}^{(l)}\frac{c^{(l)}}{\delta y}\right) - \frac{\delta}{\delta z}\left(\varepsilon_{s,z}^{(l)}\frac{c^{(l)}}{\delta z}\right) = 0 \tag{B.19}$$

Where:

$c^{(l)}$	=	mass concentration of sediment fraction (l)	$[kg/m^3]$
u, v, w	=	flow velocity in x, y and z direction	$[m/s]$
$\varepsilon_{s,x}^{(l)}, \varepsilon_{s,y}^{(l)}, \varepsilon_{s,z}^{(l)}$	=	eddy diffusivities of the sediment fraction (l)	$[m^2/s]$
w_s	=	(hindered) settling velocity of sediment fraction (l)	$[m/s]$

Cohesive sediment is modelled differently than non-cohesive sediment by different formulations for the settling velocity, the dispersive transport and the boundary conditions for Eq. B.19. The following three paragraphs describe these the modelling approach for these three aspects in case of cohesive sediment (two "mud" fractions). Lastly the influence of applying multiple sediment fractions is explained.

Settling velocity In case of high sediment concentrations in the water column the presence of the particles affects the settling velocity of individual/flocculated particles, called hindered settling. To account for the hindered settling a (hindered) settling velocity w_s is calculated with Eq. B.20 for each sediment fraction l, by means of the total mass concentration c_s^{tot} and the non-hindered settling velocity $w_{s,0}$.

$$w_s^{(l)} = \left(1 - \frac{c_s^{tot}}{C_{soil}}\right)^5 w_{s,0}^{(l)} \tag{B.20}$$

C_{soil} is the reference density (input parameter) and the mass concentrations of both sediment fraction is summed up to derive the total mass concentration c_s^{tot}.
A constant non-hindered settling velocity for both mud fractions is used to neglect the effect of flocculation on the settling velocity. In this way the model does not account for the dependency of the settling velocity on the flocculation process. Flocculation itself would be dependent on the residence time, SSC, salinity, organic matter content, PH and turbulence (Mietta and Winterwerp, 2009; Braat et al., 2017).

Dispersive transport A turbulence closure model calculates the eddy viscosity at each layer interface and converts this to the vertical fluid mixing coefficient, which is, in case of cohesive sediment, equal to the vertical mixing coefficient. The simplified model setup uses the k-ε turbulence closure model. In the k-ε turbulence closure model the turbulent kinetic energy k and the energy dissipation ε are solved.

Boundary conditions There are two boundary conditions for each sediment fraction in the advection-diffusion equation (Eq. B.19); the water surface boundary and the bed boundary condition. The water surface boundary condition prescribes the zero vertical diffusive flux through the free surface, given in Eq. B.21.

$$-w_s^{(l)} c^{(l)} - \varepsilon_{s,z} \frac{\delta c_{(l)}}{\delta z} = 0, \qquad z = \eta \tag{B.21}$$

The boundary condition for the bed involves the exchange of the suspended sediment and the bed by erosion and deposition. The Partheniades-Krone formulations solve the sediment fluxes for each sediment fraction by calculating the erosion flux E in Eq. and the deposition flux D in Eq. .

$$E^{(l)} = \begin{cases} M^{(l)}\left(\frac{\tau_{cw}}{\tau_{cr,e}^{(l)}} - 1\right), & \text{when } \tau_{cw} > \tau_{cr,e}^{(l)}. \\ 0, & \text{when } \tau_{cw} \leq \tau_{cr,e}^{(l)}. \end{cases} \tag{B.22}$$

$$D^{(l)} = \begin{cases} w_s^{(l)} c_b^{(l)}\left(1 - \frac{\tau_{cw}}{\tau_{cr,d}^{(l)}}\right), & \text{when } \tau_{cw} < \tau_{cr,d}^{(l)}. \\ 0, & \text{when } \tau_{cw} \geq \tau_{cr,d}^{(l)}. \end{cases} \tag{B.23}$$

Sediment fractions The model setup involves two sediment fractions with different characteristics. However, the stratigraphy of the bed is not explicitly included and the bed composition is assumed to be uniform. This causes the erosion rate to be proportional to the bed composition again.

C

Model setup Demak: Sensitivity analysis

C.1 Boundary conditions

C.1.1 Sediment boundary condition

Spatially constant boundary conditions To study the effect of a constant, in time and space, SSC boundary condition two concentrations are prescribed at the boundaries; 50 mg/L and 100 mg/L. Figure C.1 and C.2 show the bedlevel development relative to the reference simulation for 50 mg/L and 100 mg/L respectively.

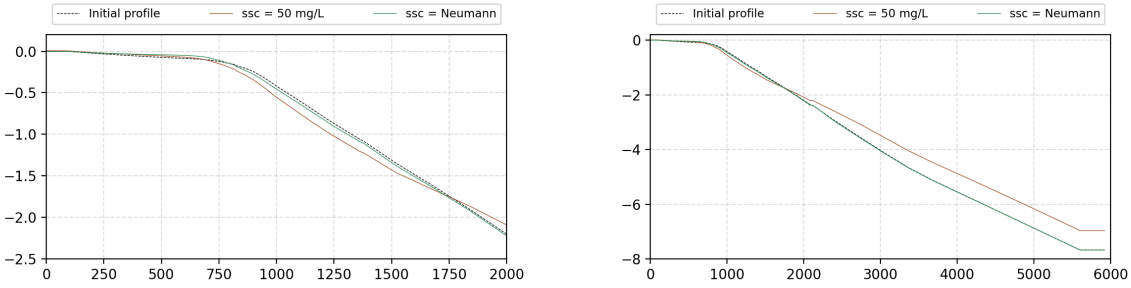

(a) 2 km stretch.

(b) 6 km stretch.

Figure C.1: Bedlevel development in 2 years. Difference between a constant sediment concentration on the boundary of 50 mg/L and Neumann boundaries.

Neumann-mimicked boundary conditions Figure C.3 shows the maximum, time-averaged and minimum values of the SSC at both the eastern and western lateral boundaries for the reference simulation, with Neumann boundary conditions. The offshore boundary is shown in Figure C.4. The figures show both the sediment fractions.
The time-averaged values are used to create spatially varying sediment boundary conditions for each lateral boundary and for the offshore boundary, as a first iteration, see Figure C.5. These time-averaged SSC boundary conditions result in a bedlevel development illustrated in Figure C.6. The offshore (appr. > 3000 m from the coastline) bedlevel development resulting from the time-averaged SSC values at the boundaries is hardly deviating from the offshore bedlevel development resulting from the reference simulation with Neumann sediment boundaries. However, the development of the bedlevel deviates between 1000 to 3000 m (from the coastline) more.
After some iterations the final factor to multiply the simplified (lateral and offshore) boundary condition from Figure C.5a and Figure C.5b appears to be 1.5. Figure **??** and Figure **??** show the obtained pseudo-Neumann boundary condition for the lateral and offshore boundary respectively. Prescribing these sediment boundary conditions results in an equal bedlevel development as with the reference simulation, see Figure **??**.

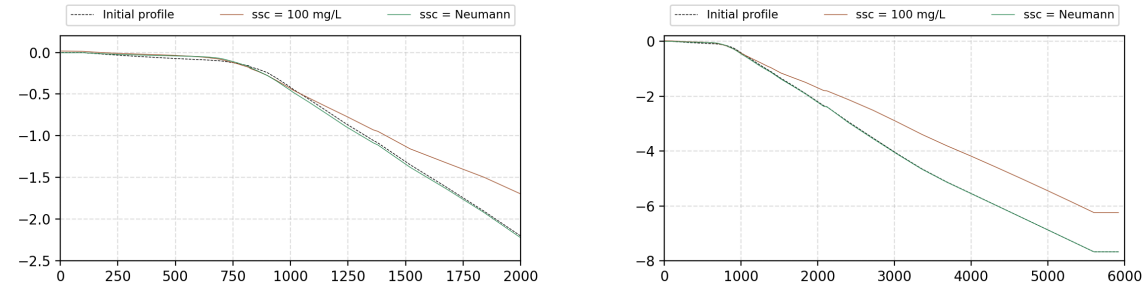

(a) 2 km stretch.

(b) 6 km stretch.

Figure C.2: Bedlevel development in 2 years. Difference between a constant sediment concentration on the boundary of 100 mg/L and Neumann boundaries.

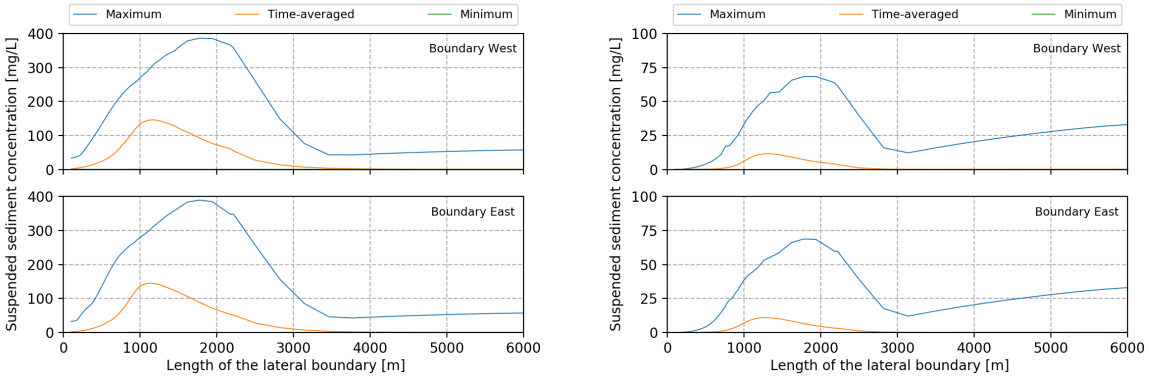

(a) Mud fraction 1.

(b) Mud fraction 2.

Figure C.3: Maximum, time-averaged and minimum values of the SSC at the lateral boundaries resulting from the reference simulation (Neumann boundary conditions). Both the lateral boundaries are represented by the western and the eastern boundary.

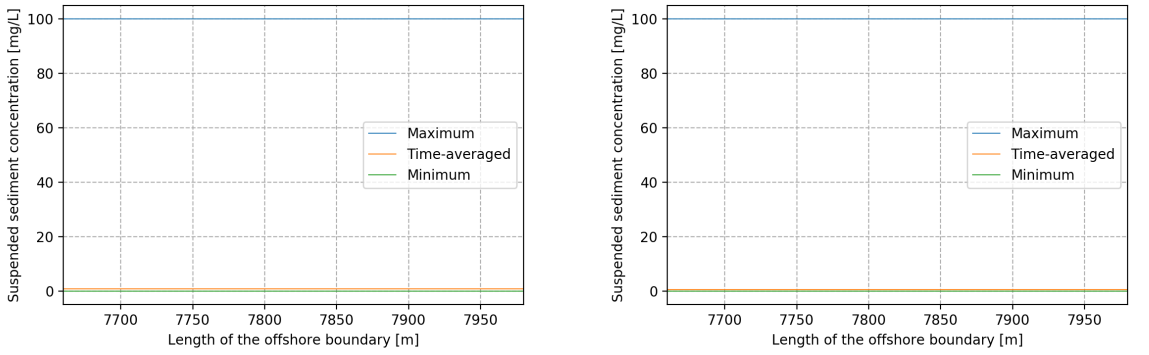

(a) Mud fraction 1.

(b) Mud fraction 2.

Figure C.4: Maximum, time-averaged and minimum values of the SSC at the offshore boundary resulting from the reference simulation (Neumann boundary conditions).

C.2 Equilibrium profile

C.2.1 Steady state

Following Maan et al. (2015), intertidal systems that are dominated by cross-shore tidal currents can reach a horizontally migrating 'steady state'. The cross-shore profile shape does not change as the profile migrates in horizontal direction. Wave-dominated areas are found to reach a stationary equilibrium state, according to Fagherazzi et al. (2006).

With a mean tidal range of 0.3 m and a mean wave height around 0.45 m, the coastal system of Demak is considered a wave-dominated or mixed-energy system, according to Davis and Hayes (1984). This will more likely result in a stationary equilibrium profile.

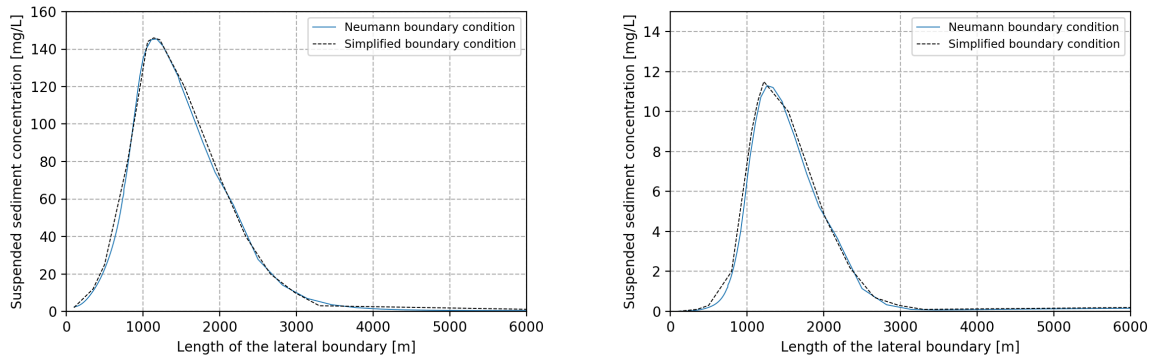

(a) Mud fraction 1.

(b) Mud fraction 2.

Figure C.5: The spatially varying SSCs along the boundaries for the two fractions. The blue line represents the time-averaged sediment concentration along the boundary during the reference simulation which is used for a simplified boundary condition for other simulations.

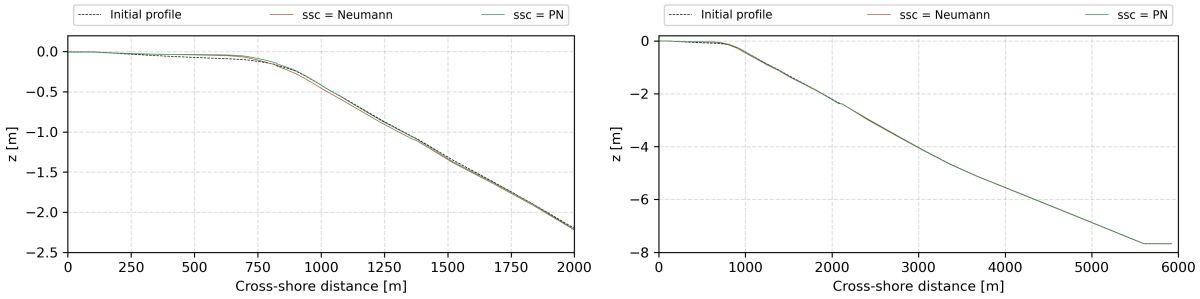

(a) Stretch of 2 km.

(b) Stretch of 6 km.

Figure C.6: Time-averaged sediment concentrations are used as prescribed boundary conditions.

Figure C.7 shows the cross-shore profile development (averaged over the model width) through time for Demak with model settings described as in Section **??**, but a MORFAC of 10 to speed up the computation. The cross-shore profile reaches a stable profile around 100 years (morphological), equal to 30 hydrological months.

C.2.2 MORFAC comparison

To investigate long-term profile development a 100-year run with a MORFAC 10 was done. The MORFAC equal to 10 will reduce the computation time by 3.33 in comparison to a run with a MORFAC equal to 3. The results of Maan et al. (2015) are based on MORFACs of 10 or higher, however, the forcing is lower than for the model of Demak and the sediment parameters simulate a bed that is harder to erode (larger settling velocity). Therefore, a MORFAC higher than 10 seems not suitable and the MORFAC equal to 10 is compared to the run with a MORFAC equal to 3, to check the usability of a MORFAC 10. Figure C.8 includes the bedlevel after a 30 year run for both MORFAC 10 and MORFAC 3. The averaged bedlevel profile differs 0.1 m in the upper part of the profile, showing a significant difference between the runs. Therefore a MORFAC 10 is not suitable for this model setup, the equilibrium profile in Section **??** is not considered valuable to use as a spin up profile.
The shape of the two profiles are equal. This suggests the equilibrium profile using MORFAC 10 or 3 will be similar.

C.2.3 Spin up time

Reaching an equilibrium profile with a MORFAC equal to 3 uses a lot of computation time. Therefore, a smaller spin up time is picked which represents an averaged, cross-shore profile which does not show any unrelated bedlevel changes. Figure C.9 shows the width-averaged, cross-shore profile for 20 years and 10 years, using a MORFAC of 3. A spin up time of 2 years is chosen, enabling a shorter computation time before runs.

C.3 Bedlevel validation

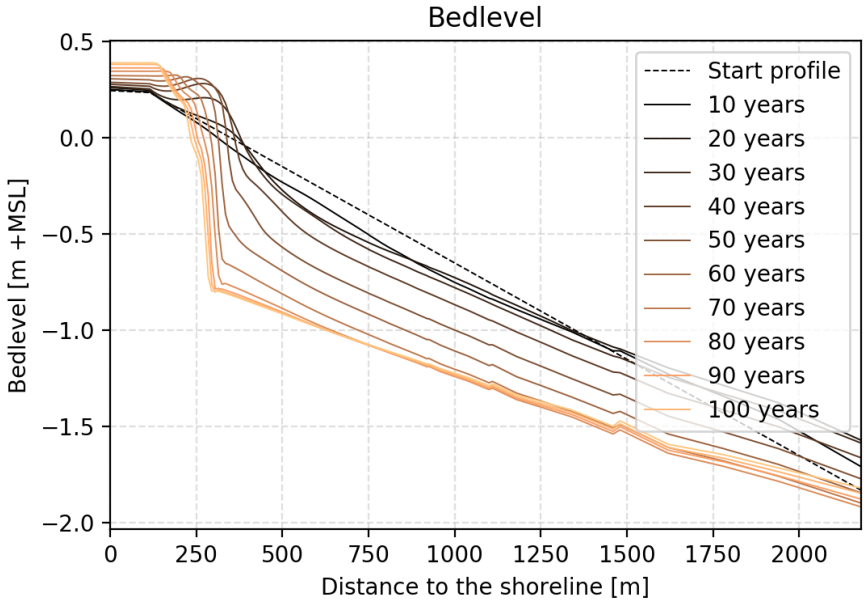

Figure C.7: The averaged cross-shore profile evolution in 100 years using a MORFAC = 10. The profile shape converges to a steady state, where the cross-shore profile is largely maintained after 100 years.

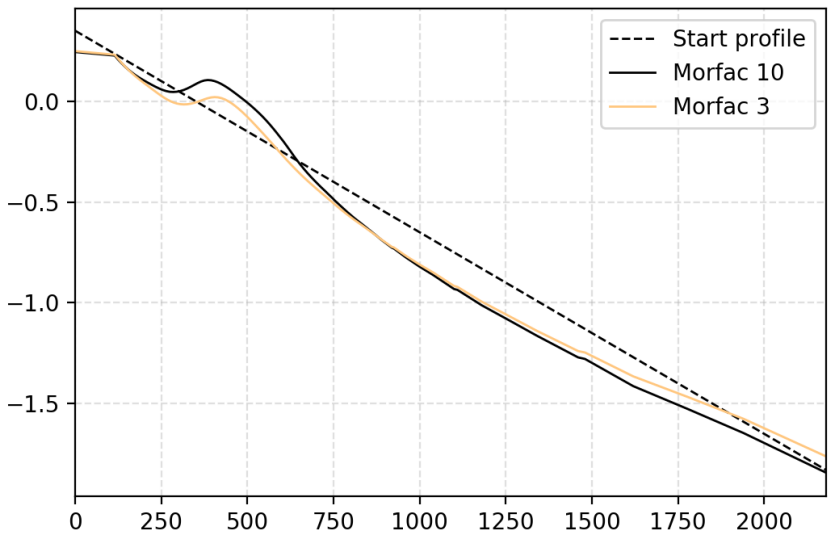

Figure C.8: The width-averaged cross-shore profile evolution in 30 years.

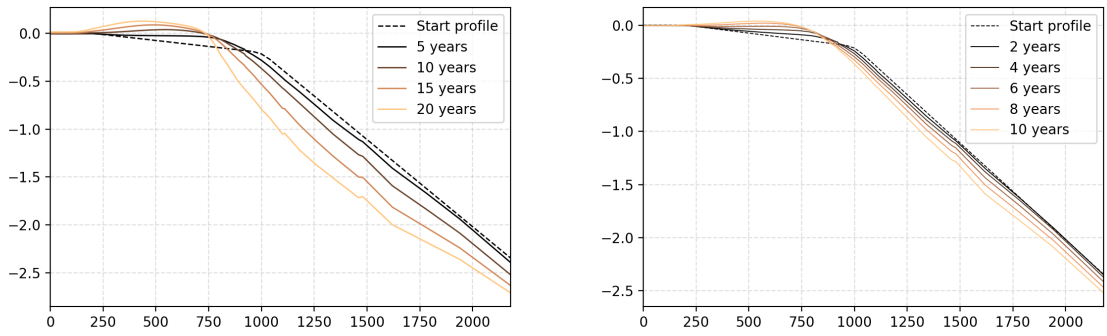

Figure C.9: Averaged, cross-shore profile for 20 years and 10 years, using a MORFAC equal to 3.

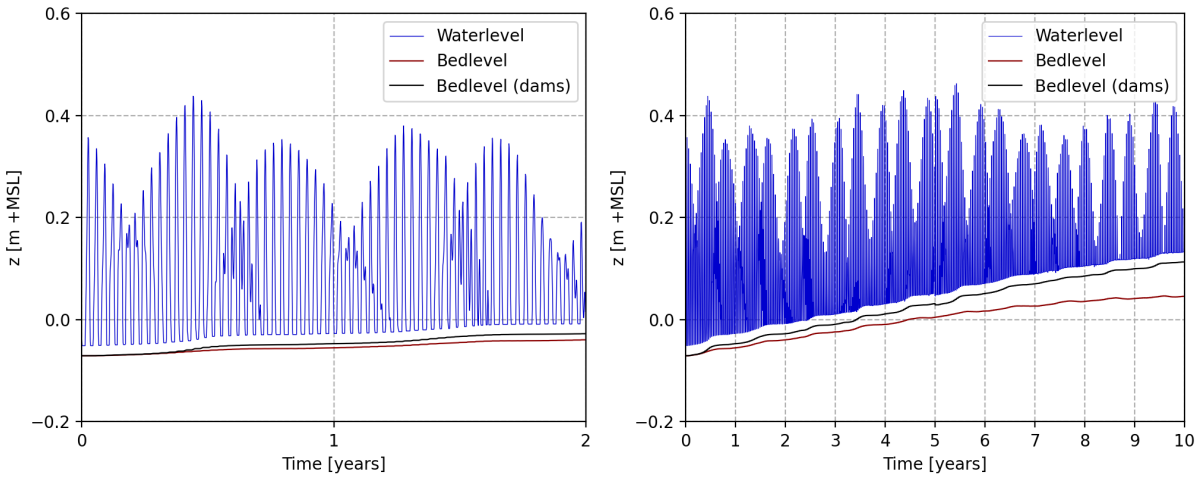

(a) Bedlevel development in two years – Middle dam

(b) Bedlevel development in ten years – Middle dam

Figure C.10: The bedlevel in time for the baseline simulation and the simulation including dams. The location of the bedlevel development is 15 meters onshore of the middle dam.

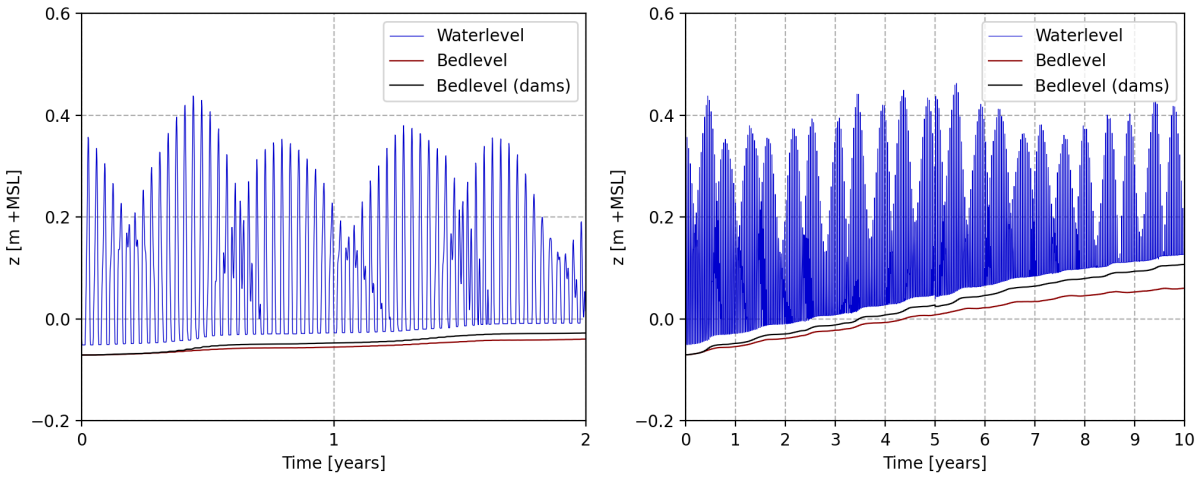

(a) Bedlevel development in two years – Right dam

(b) Bedlevel development in ten years – Right dam

Figure C.11: The bedlevel in time for the baseline simulation and the dam simulation. The location of the bedlevel development is 15 meters onshore of the right dam.

D

Results

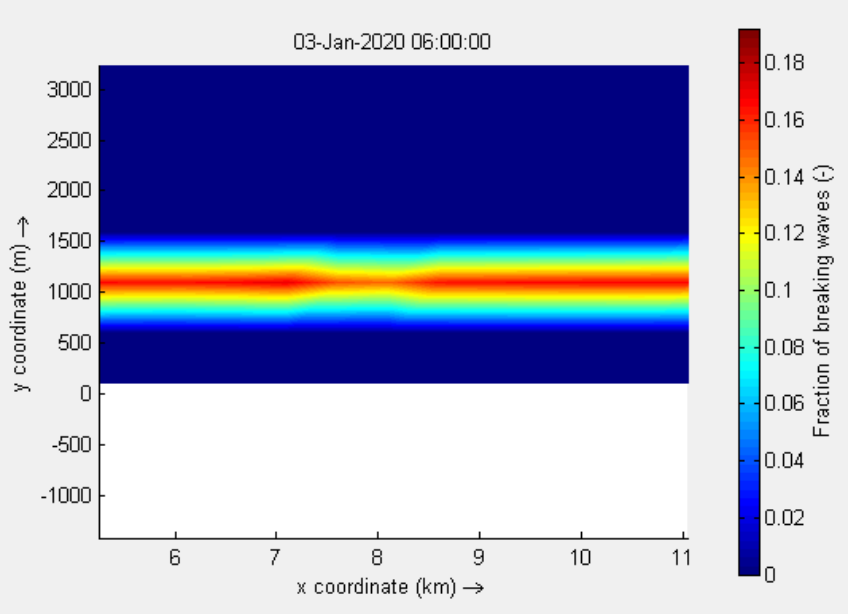

Figure D.1: Fraction of breaking waves in the wave domain for shore-normal incidence. The flow domain lies within the wave domain (from x = 7500 to x = 8140 m). The breaker zone extends from 800 m to 1500 meters offshore of the land boundary.

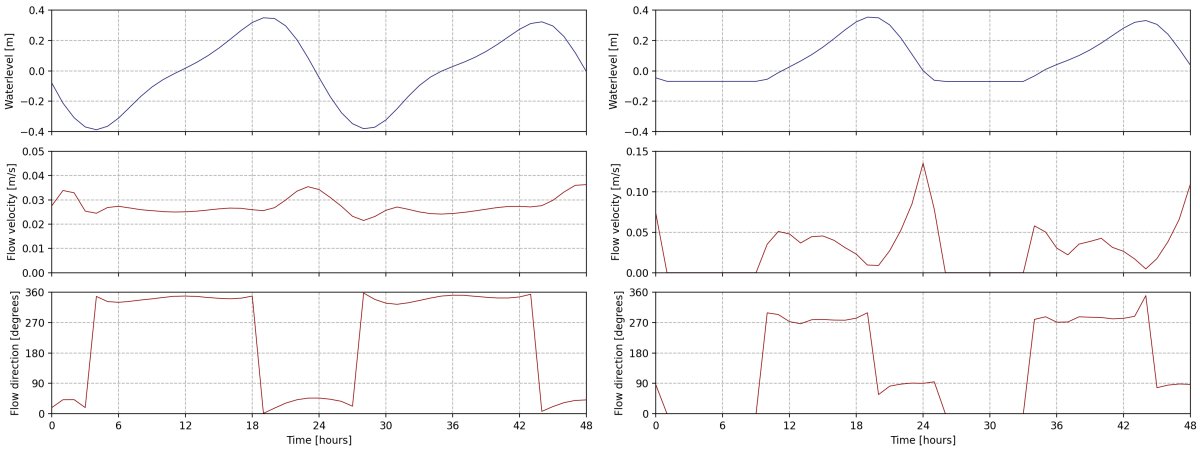

(a) At the offshore boundary

(b) 715 m offshore from the land boundary

Figure D.2: Tidal signal (two tidal cycles) with the waterlevel and flow velocity (magnitude and direction) for the offshore boundary and on the tidal flat.